L.C. Alfaro Monge

Assessment of a Lagrangian 1DV Modelling Approach for Turbidity Currents Generated by Water Injection Dredging

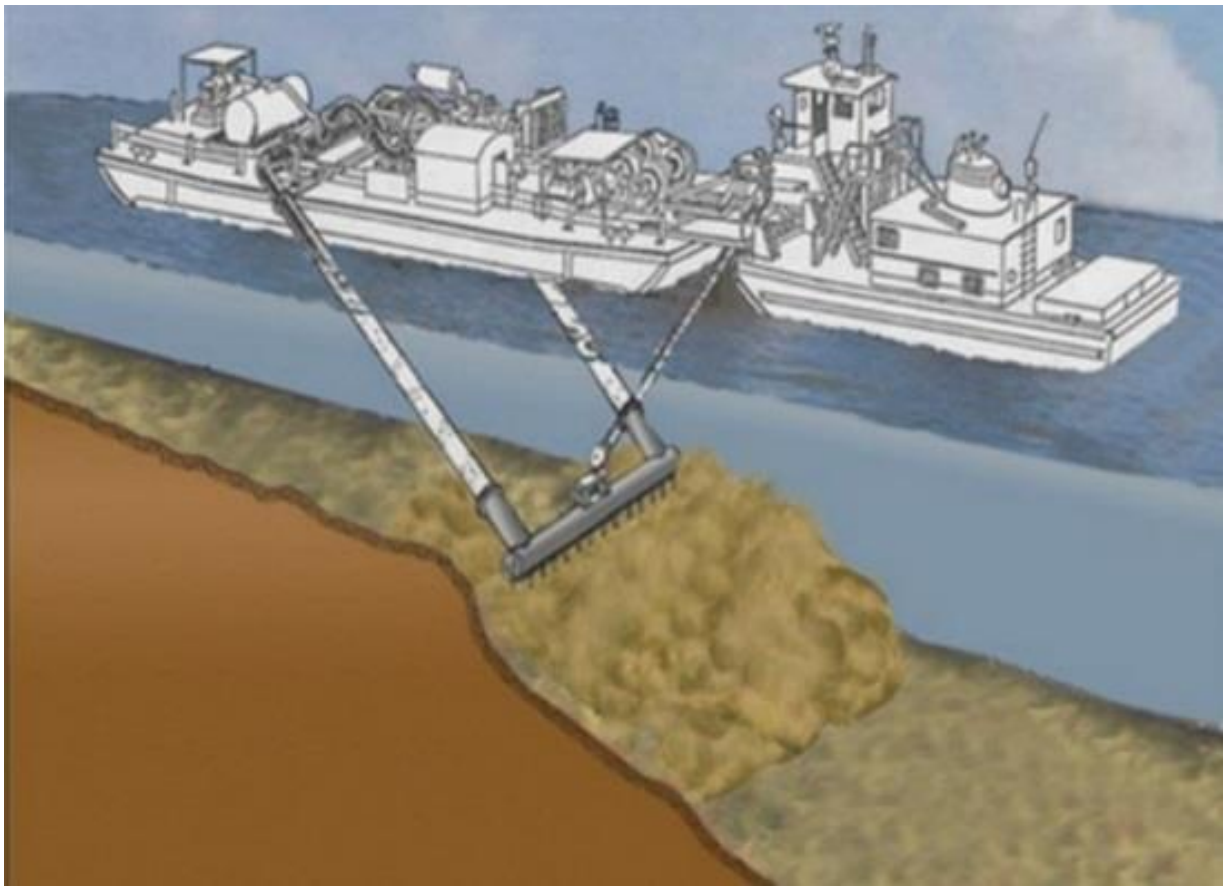

Image source: USACE, 2017

TU Delft Boskalis

Assessment of a Lagrangian 1DV Modelling Approach for Turbidity Currents Generated by Water Injection Dredging

By

L.C. Alfaro Monge

in partial fulfilment of the requirements for the degree of

Master of Science
in Civil Engineering

at the Delft University of Technology,
to be defended publicly on Monday, January 27th , 2020 at 15:00 hrs.

Thesis committee:
Prof. dr. ir. W.S.J. Uijttewaal (TU Delft)
Dr. ir. R.J. Labeur (TU Delft)
Ir. H.C.M. Hendriks (TU Delft / Deltares)
Prof. dr. ir. H. Winterwerp (Advisor)
Ir. T. Vijverberg (Royal Boskalis Westminster NV)

This thesis is confidential and cannot be made public until January 21st, 2022.

TU Delft Boskalis

Summary

Siltation affects navigation in harbors and waterways by reducing the water depth. To regain depth and safeguard navigation, dredging is required. Water Injection Dredging (WID) is one of the available hydrodynamic dredging techniques, in which pumps on a vessel inject water at high flow velocities and low pressure into the bed and fluidize the bed material into a mixture of water and suspended sediment. The fluidized material travels as a turbidity current to deeper areas, driven by natural processes. Sediment transport is then less controlled and the final destination of the dredged material is more difficult to estimate than for other dredging techniques.

The passage of a WID-induced turbidity current produces an increase in suspended sediment concentration (SSC) in the water column that increases turbidity. Turbidity increase may have a negative environmental impact. Therefore, to evaluate and mitigate the environmental impact of WID, the increase in SSC should be estimated. Additionally, from an operational perspective, the sedimentation footprint of the turbidity current should be determined.

Deltares developed with Boskalis a numerical tool named “Lagrangian 1DV model” (Deltares, 2019). The Lagrangian 1DV model can calculate the thickness and density of the WID-induced turbidity current at a distance from the dredger, as well as the deposition rate. It provides the information to estimate the increase in SSC in the water column and the sedimentation footprint. The tool was defined to be a rapid assessment tool, as it is necessary at the early stages of WID projects when there is usually a limitation of time and available data. Such a tool is useful to analyze different dredging strategies and different solutions to mitigate environmental impact.

As its name indicates, it follows a Lagrangian 1DV (**1-D**imensional **V**ertical) approach. This approach follows the turbidity current in space as it moves away from the dredger. It is an innovative approach that requires less computational effort than a 3D or a 2DV (**2**-**D**imensions in the **V**ertical plane) approach.

Three main steps were followed by Deltares (2019) for the conceptual and mathematical modelling:

- Step 1: assume that the turbidity current is a 2DV process, thus neglecting lateral gradients
- Step 2: schematize the 2DV process as a Lagrangian 1DV approach.
- Step 3: select the 1DV Point Model (Uittenbogaard and Winterwerp, 1997) as the basis to solve velocity and concentration profiles over the vertical.

In order to schematize the 2DV process as a Lagrangian 1DV approach (Step 2), two main points were assumed:

- Uniformity of the 1DV Point Model (in the Eulerian frame of reference) was assumed as stationarity in the Lagrangian frame of reference
- The Lagrangian velocity was defined as a concentration-weighted velocity over the water column (u_c), expressed as the ratio between the mass flux and sediment load.

The validity of these assumptions to estimate sediment transport was analyzed in this report. For that purpose, the Lagrangian 1DV model (Lagrangian 1DV approach) was compared to a 2DV computation in Delft3D-FLOW (called Delft3D model) in four sets of numerical experiments.

In Experiments Set 1, the results of the Lagrangian 1DV model were compared to the Delft3D model in uniform flow conditions in a channel. By satisfying the uniformity assumption in the Delft3D model, it was expected that the difference with the Lagrangian 1DV model was not significant. The results agreed with the expected result. Then, Experiments Set 1 confirmed the validity of the Lagrangian 1DV approach for uniform flow.

Experiments Set 2 examined if non-uniform conditions in a channel (same geometry as Experiments Set 1) lead to differences between the models. It consisted of six experiments combining three different initial concentration profiles (upstream boundary profiles in the Delft3D model) and two types

of models (uncoupled and coupled). In uncoupled models, the concentration did not influence the density of the fluid, and the solution of the sediment transport equation had no effect on the momentum equation. In coupled models, concentration was considered in the density of the fluid.

For uncoupled models, no important differences were observed between the Lagrangian 1DV model and the Delft3D model, which means that the Lagrangian 1DV approach is as valid as the Eulerian 2DV approach to represent sediment transport in non-uniform flow when density differences are negligible.

Differences between the Lagrangian 1DV model and the Delft3D model in velocity, concentration and, consequently, in the concentration-weighted velocity u_c (calculated in the Delft3D model as the ratio between mass flux and sediment load), arose when density differences became significant, in the coupled models. The initial concentration profile shape influenced the magnitude of the difference.

The results of the coupled models in non-uniform flow indicated that the origin of the differences between the Lagrangian 1DV model and the Delft3D model in u_c relies on the expression of the advective transport term of the sediment transport equation. In the Lagrangian 1DV model, sediment is transported at a velocity u_c at all levels, while the Delft3D model uses the velocity u at every particular level. This affects the horizontal concentration gradient and, consequently, produces differences between the concentration profiles and, accordingly, differences in u_c between the models. This was shown to be valid for the relatively low baroclinic pressure gradient of Experiments Set 2 (concentration in the order of 10 kg/m^3 and very small bed slope).

In Experiments Set 3 and Set 4, the numerical models were based on laboratory experiments on turbidity currents by Parker et al. (1987) and van Kessel and Kranenburg (1996), respectively. The baroclinic pressure gradient was higher for these experiments (and closer to the order of magnitude of the gradient for the typical parameters of a WID-induced turbidity current). Thus, differences in the baroclinic pressure gradient between the models produced important differences in velocity.

In the case of Experiments Set 3, based on Run 13 of Parker et al. (1987), u_c was lower for the Lagrangian 1DV model along the analyzed reach. Both models presented an initial deceleration of the sediment mass (decrease in u_c). This deceleration was related to an increase in sediment load in the Delft3D model, which was also observed in the measured concentration profiles. The sediment load was higher in the Delft3D model than in the Lagrangian 1DV model. Then, a possible explanation for the difference in u_c is that a larger concentration (due to a larger sediment load) generated a larger baroclinic forcing in the Delft3D model. This produced higher velocities, which yielded a higher value of u_c for the Delft3D model. The analysis of the decrease of sediment load along the channel, when considering deposition, showed that sediment was transported further for the Delft3D model.

Experiments Set 4, based on Run 2 of van Kessel and Kranenburg (1996) presented the opposite behaviour: a higher u_c value for the Lagrangian 1DV model. Also opposite to Experiments Set 3, there was an acceleration of the sediment mass (increase in u_c) in both models at the first meters from the source. This acceleration was clearly related to a decrease in sediment load in the Delft3D model, which was also suggested by the measurements. Following the same reasoning as for Experiments Set 3, the decrease in sediment load may have produced a lower value of u_c for the Delft3D model.

In order to analyze possible implications of the observed differences when the model parameters are in the range of WID application, the variation of u_c was calculated in the Lagrangian 1DV model for a typical case of WID. The trend of the variation of u_c along the reach was similar to the case of Experiments Set 3, showing a deceleration of the sediment mass from the beginning. In analogy with Set 3, the results suggest that the estimated u_c in the Lagrangian 1DV model may be lower than the result for the 2DV approach. Additionally, the travelling distance of the turbidity current may be shorter. If the calculation of the travelling distance is for a case in which the sediment should be transported as far as possible, the estimation may be conservative (the actual travelling distance may be longer than the calculated distance). If the travelling distance is restricted for environmental reasons, the estimation may be unsafe (sediment could reach a longer distance than estimated, affecting the sensitive area). More specific cases can be addressed by comparing the Lagrangian 1DV model and the Delft3D model, following the methodology presented in this report.

Preface

To my family: for being extremely supportive during my academic and non-academic projects.

To my friends in Costa Rica: for always motivating me and not forgetting about me during these two years.

To the new friends I met in TU Delft and Boskalis: for making this a nice cultural and social experience.

To the Committee: for the interest and enthusiasm about this topic, for the high-level constructive comments to produce this document and for the guidance during this modelling experience.

L.C. Alfaro Monge

Delft, 2020.

Contents

1 Introduction

1.1 Background

Siltation is a continuous process that affects navigation in harbors and waterways by reducing the water depth. Dredging is required to keep the needed water depths and safeguard navigation. As an example, more than 11 million m^3 of sediment were dredged in the Port of Rotterdam in 2017 to keep accessibility to ports and waterways. The dredged volume doubled from 2011 to 2017 (Kirichek et al, 2018).

Water Injection Dredging (WID) is one of the available dredging techniques. This section presents an overview of this dredging technique and a description of the "Lagrangian 1DV model", a rapid assessment tool to estimate the fate of mobilized sediment by WID.

1.1.1 Water Injection Dredging

Description

Available dredging techniques can be grouped into three categories depending on how sediment is excavated and subsequently transported (PIANC, 2013): hydraulic, mechanical and hydrodynamic dredging. Table 1-1 shows the different techniques in every category.

Table 1-1. General categorization of available dredging techniques (PIANC, 2013)

Conventional dredging		**Hydrodynamic Dredging**
Hydraulic Dredging	**Mechanical Dredging**	
Stationary Suction Dredger	Bucket Ladder Dredger (BLD)	**Water Injection Dredging**
Cutter Suction Dredger (CSD)	Backhoe Dredger (BHD)	Underwater Plough
Trailing Hopper Suction Dredger (THSD)	Grab Dredger (GD)	Agitation Dredging

Hydraulic and mechanical dredging are considered conventional dredging methods. Pipelines, hoppers or barges are used to transport the dredged sediment to the final disposal site. On the other hand, with the hydrodynamic dredging techniques (such as WID), natural processes drive sediment transport. Then, sediment transport is less controlled.

Water Injection Dredging (WID) is one of the available hydrodynamic dredging techniques. In this technique (Figure 1-1), vessel-mounted pumps inject water at relatively high flow velocities (5 to 10 m/s) and low pressure (around 1 bar) into the bed, diluting and fluidizing the material into a suspended sediment-water mixture (Wilson, 2007).

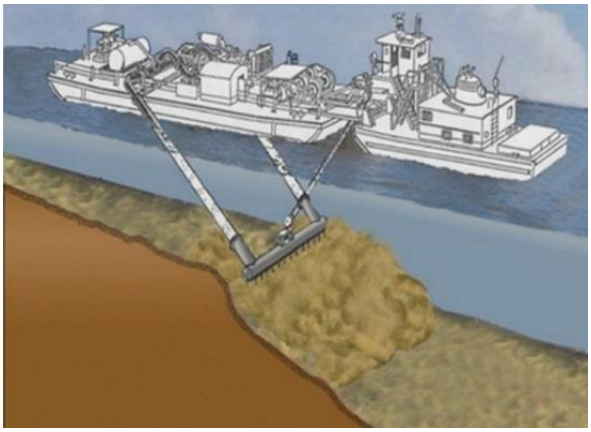

Figure 1-1. Illustration of the Water Injection Dredging process (USACE, 2017)

Once the mixture forms, it flows away as a turbidity current (PIANC, 2013), which is a type of density current. A density current is a wedge of fluid intruding laterally into an ambient body of fluid of a different density (Bonnecaze et al., 1993). In the case of a WID-induced turbidity current, fine sediment produces the density difference to initiate the current and drive its motion. The constituent of the current (fine sediment) can be exchanged with the bed and ambient waters.

Economic and Operational Advantages and Limitations of Water Injection Dredging

From the economic and operational perspectives, WID may present important advantages compared to conventional dredging (PIANC, 2013; IADC, 2013):

- No additional equipment is required to transport the dredged material,
- Higher maneuverability,
- Less hindrance to passing traffic,
- Easier mobilization to other projects (some dredgers can even be transported by road),
- Reduced crew

These advantages provide a feasible low-cost alternative for appropriate locations. However, WID also presents limitations. It has a smaller range of applicability, highly dependent on soil characteristics, hydrodynamic conditions and bathymetry. Due to naturally-driven transport, the final destination of the dredged sediment is difficult to predict (PIANC, 2013).

Environmental Impact of Water Injection Dredging

In addition to economic and operational aspects, environmental impact strongly determines the feasibility of a dredging technique.

One of the main environmental effects of dredging is an increase in the suspended sediment concentration (SSC) in the water column. An increase in SSC increases the turbidity, which is an optical measurement of the cloudiness of the water due to the presence of suspended particles. Turbidity increase may have negative consequences on pelagic and benthic life, due to depression of dissolved oxygen levels, reduction of photosynthesis, interference with respiration and feeding, and impedance to mobility, among other problems (Bray, 2008). Additionally, the deposition of the mobilized sediment changes the composition of bed sediment and may bury benthic fauna. Submerged aquatic vegetation may be sensitive to the deposition of thin fine sediment layers on leaves and stems (Bray, 2008). Hence, the magnitude of the environmental effects of WID depends mainly on the turbidity increase, the sedimentation footprint and the presence of sensitive ecological receptors (organisms to which an ecological risk is imposed).

The assessment of the turbidity increase requires insight into the mobilized sediment mass and the transport of this mass. Transport can be divided into a dynamic phase and a passive phase. For WID, the turbidity current (Figure 1-2) can be interpreted as the dynamic phase. After the passage of the turbidity current, suspended sediment remains available for passive transport. Passive transport is governed by advective and diffusive processes in the ambient waters (Van Eekelen, 2007) and occurs at a larger spatial and temporal scale than the dynamic phase.

In practice, the passive phase is modelled in so-called far-field models, which include the processes of advection, diffusion, and settling (Becker et al., 2015). Far-field models require the input of the suspended sediment that remains available for passive transport at the end of the dynamic phase, which is called turbidity source term (Becker et al., 2015).

In conclusion, just after the passage of the turbidity current, a fraction of the mobilized sediment mass by WID will be deposited on the bed (sedimentation term) and the other will be available for passive transport (turbidity source term). Estimating both fractions is necessary for the assessment of the above-mentioned environmental effects. Additionally, it is important to estimate the transport path of the turbidity current, as most of the time, it is intended to transport the sediment to deeper areas.

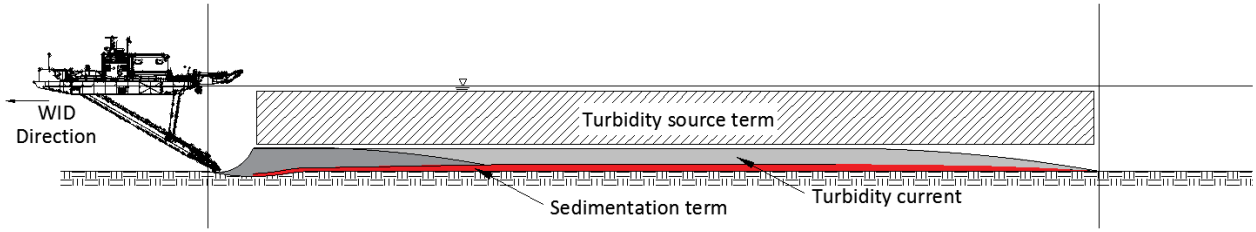

Figure 1-2. Basic sketch of possible states of the dredged sediment near the dredger

1.2 A Rapid Assessment Tool for Water Injection Dredging

1.2.1 Description

Deltares developed with Royal Boskalis Westminster N.V. a numerical tool named “Lagrangian 1DV model” to simulate the transport of mobilized sediment by WID (Deltares, 2019), and its destination, either deposited on the bed (sedimentation footprint) or as part of the turbidity source term.

For operational reasons, the tool was defined to be a rapid assessment tool, as it is necessary at the early stages of WID projects when there is usually a limitation of time and available data. Additionally, a rapid tool is useful to analyze different dredging strategies to optimize the dredging process and solutions to mitigate environmental impact.

The “Lagrangian 1DV model” can calculate the thickness and density of the WID-induced turbidity current at a distance from the dredger, as well as the deposition rate. It provides the required information to estimate the sedimentation term and the turbidity source term.

1.2.2 Generalities about a Lagrangian 1DV Approach

The Lagrangian 1DV model, as its name indicates, follows a Lagrangian 1DV (**1-D**imensional **V**ertical) approach. This approach follows the turbidity current in space as it moves away from the dredger. It is an innovative approach that requires less computational effort than a 3D or a 2DV (**2**-**D**imensions in the **V**ertical plane) approach.

The Eulerian and the Lagrangian frame of references are just two ways of defining the coordinates to analyze a flow field. The Eulerian frame of reference uses control volumes that are fixed in space An analogy is to stand on a bridge and focus for some time on one fixed point or area of a river (Rapp, 2017).

The Lagrangian frame of reference, on the other hand, moves with the flow field at a certain velocity (called Lagrangian velocity). It is able to follow a fluid parcel as it moves in space and time. A similar analogy is to observe a parcel of water next to a boat while traveling on the boat.

In the Lagrangian approach for WID, the moving parcel consists of a one-dimensional (vertical) column of fluid, composed of water and sediment, and vertically delimited by the water surface and the bed. The frame of reference and the fluid column move at a Lagrangian velocity.

Figure 1-3 shows a basic sketch of the Lagrangian and Eulerian frames of references. The Eulerian reference frame (coordinates x and z) remains fixed at the point where the turbidity current starts. The Lagrangian reference frame moves with the fluid column. At time τ_1, the position of the Lagrangian reference frame is ξ_1. At time τ_2, the position of the Lagrangian reference frame is ξ_2.

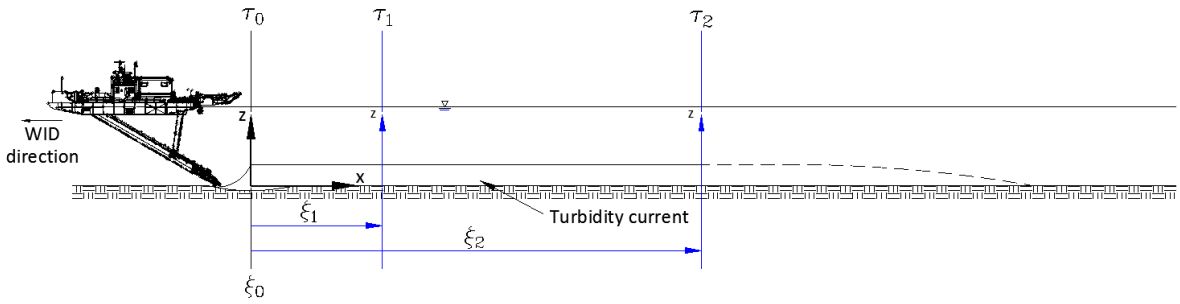

Figure 1-3. Sketch of the Eulerian and Lagrangian reference frames for the WID situation

In the Lagrangian 1DV approach, estimating the distribution of velocity, density and turbulent properties within the column of fluid at each time, requires a 1DV model. For this purpose, the Lagrangian 1DV model is based on the 1DV Point Model (Uittenbogard & Winterwerp, 1997). The 1DV Point Model is a modelling tool that solves the fluid column (water and sediment) integrally with a high vertical resolution. The integrity and continuity of the model in the vertical provide an advantage over two-layer models that limit or empirically parametrize the exchange of sediment between the turbidity current and the ambient waters.

1.3 Problem Description

Three main steps were followed by Deltares (2019) for the conceptual and mathematical modelling of a WID-induced turbidity current:

- Step 1: it was assumed that the process of sediment transport by a WID-induced turbidity current could be conceptualized with a 2DV approach, thus neglecting lateral processes
- Step 2: the 2DV process was further schematized with a Lagrangian 1DV approach.
- Step 3: the 1DV Point Model was selected as a basis to solve velocity and concentration profiles over the vertical.

In order to schematize the 2DV process with a Lagrangian 1DV approach (Step 2), two main points were assumed:

- Uniformity (assumption of the 1DV Point Model) was assumed as stationarity in the Lagrangian frame of reference.
- The Lagrangian velocity was defined as a concentration-weighted velocity (u_c) over the water column, expressed as a ratio between the mass flux and the sediment load (integral of the mass concentration over the water column).

The main reason for this study is that the implications of the previous assumptions to schematize sediment transport with a Lagrangian 1DV approach instead of a 2DV approach have not been analyzed yet. For practical purposes, the implications on the resulting sediment deposition and the increase of suspended sediment concentration must be investigated.

1.4 Research Questions

1.4.1 General Research Question

To what extent is a Lagrangian 1DV approach capable of estimating sediment transport by turbidity currents, and how does this influence the prediction of sedimentation and the increase of the suspended sediment concentration generated by WID-induced turbidity currents?

1.4.2 Specific Research Questions

A. Which physical processes influence the characteristics of a WID-induced turbidity current and the associated sediment suspension in the water column?

B. Which of the processes are included in the Lagrangian 1DV model?

C. Considering the main assumptions of the Lagrangian 1DV approach (Section 1.3), what are the differences between the mathematical descriptions of a Lagrangian 1DV approach and a 2DV approach?

D. Which implications do the main assumptions of the Lagrangian 1DV approach have for sediment transport?

E. Which implications may these assumptions have in sedimentation and in the increase of suspended sediment concentration when the model parameters are in the range of WID application?

1.5 Research Approach

Part 1 (Question A)

A literature review is carried out to describe the WID process and relevant subprocesses, the physical characteristics of a WID-induced turbidity current and the physical processes that determine those characteristics.

Part 2 (Question B and C)

After the theoretical description of WID-induced turbidity currents, the mathematical descriptions of the 2DV approach and the Lagrangian 1DV approach are presented. The assumptions of the Lagrangian 1DV approach are further explained.

Part 3 (Question D)

It is divided into three phases:

- Phase 1: Definition of a method to compare the models
- Phase 2: Setup of a 2DV calculation in Delft3D-FLOW (called Delft3D model, from now on)
- Phase 3: Numerical experiments

In Phase 3, the Lagrangian 1DV model (Lagrangian 1DV approach) is compared to a 2DV computation in Delft3D-FLOW (2DV approach) to analyze the validity of the Lagrangian 1DV approach and estimate the magnitude of the differences between the models, if present. The 2DV computation is assumed to be a closer representation of reality.

Part 4 (Question E)

Possible implications of the differences between a Lagrangian 1DV approach and a 2DV approach are discussed for the case when the parameters are in the range of a WID application.

1.6 Structure of the Report

The report is structured similarly to the research approach. Chapter 2 explains the WID process and WID-induced turbidity currents from a theoretical perspective. Chapter 3 refers to the conceptual and mathematical modelling approach for WID-induced turbidity currents, both for a 2DV approach and, then, for a Lagrangian 1DV approach. Chapter 4 describes the numerical experiments and presents their results.

Finally, Chapter 5 links the results of the previous chapters in a discussion, and Chapter 6 provides conclusions and recommendations.

2 Theoretical framework

This chapter establishes a theoretical framework about how WID mobilizes sediment, and thus, induces a turbidity current. The physical characteristics of the WID-induced turbidity current are described, as well as the physical processes that determine those characteristics.

2.1 The WID process

The WID process was developed in The Netherlands by engineer van Weezenbeek in the early 1980s. In order to prove the effectiveness of the new technology, field demonstrations were executed. In 1985, the first field demonstration was executed by Rijkswaterstaat with the WID dredger 'Woelnix' in the harbor basins of Zijhaven and Buitenhaven in Hansweert, and Veerhaven in Kruiningen (Swart, 2015).

In the early 1990s, the technique was used in the United States. The US Army Corps of Engineers (USACE) started implementing WID contracts in 1992 (Wilson, 2007). Two field demonstrations were done in the Upper Mississippi River during that year.

Nowadays, the WID technique is available all around the world. By 2012, 28 WID dredgers were operative (GEODE, 2015). WID works have been executed in more than 60 different locations, e.g., in United Kingdom, Germany, The Netherlands, Belgium, France, Italy, United States, Brazil, Argentina, Tanzania, New Zealand, China, India, Bangladesh, and Yemen.

This section provides an overview of the WID equipment, the typical conditions the application of WID and the subprocesses related to sediment transport (from soil loosening to the turbidity current).

2.1.1 Dredger characteristics

The dredger consists of a barge with pumps connected to a pipeline that transports water to a wide underwater injection manifold (horizontal pipe with several nozzles of small diameter, also called *jet bar*), which is placed near the bed. Figure 2-1 shows a scheme of the main components of a water injection dredger.

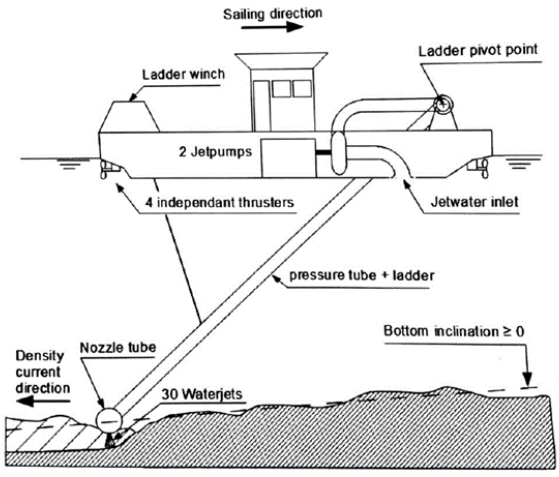

Figure 2-1. Water Injection Dredger components (Van der Schrieck, 2015)

2.1.2 WID application range

The technical feasibility of WID is mainly defined by hydrodynamic conditions, soil characteristics and bathymetry (GEODE, 2015). The delimitation of the range of typical conditions in which it is known

that WID is feasible provides boundaries to the domain of interest when modelling. These conditions are summarized in Table 2-1 and schematized in Figure 2-2.

Table 2-1. Typical range of application of WID (Wilson, 2007; PIANC, 2013; Kranendonk, 2019)

Parameter	Typical range of application
Ambient flow velocity	-2 m/s to 2 m/s
Water depth	3 m to 30 m
Median grain size d_{50}	< 200 μm
Undrained shear strength (cohesive sediment)	< 10 kPa
General bed slope	From flat bed to around 1:100

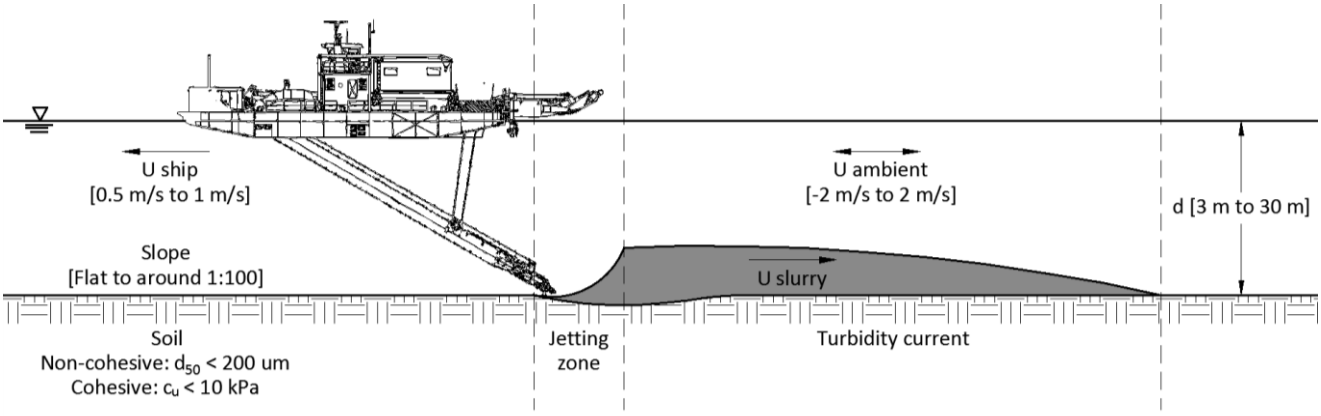

Figure 2-2. Sketch of the application range of WID (U: velocity, and d: depth)

Ambient flow velocities are normally in the range from 0 to 2 m/s (W. Kranendonk, personal communication, 2019). Commonly, the dredger operates in a way that the ambient flow and the turbidity current move in the same direction. However, there may be situations in which it is required to operate in the opposite direction of the ambient flow.

The minimum dredging depth depends on the draught of the WID vessel, which is typically less than 3 m. The maximum dredging depth of the available WID dredgers is around 30 m (PIANC, 2013).

Soil characteristics are very important. WID can be effectively applied for fine sand. The most important soil parameter for non-cohesive material is the grain size. Wilson (2007) concluded that WID is effective when d_{50} is smaller than 200 μm. In the case of cohesive sediment, an important parameter that defines production is the undrained shear strength c_u. Material with c_u up to 10 kPa can be dredged effectively (W. Kranendonk, personal communication, 2019). In maintenance dredging projects, mud may present a c_u below 5 kPa (PIANC, 2013).

WID is mostly applied in channels and harbors with gentle average longitudinal bottom slopes (typical order of magnitude from 1:100 to flat bottom). In special cases, near to banks and quay walls, slopes can attain up to 1:3 (in the order of magnitude of the angle of repose of the material).

2.1.3 WID Sub-processes

The mobilization of sediment starts with the water jets from the jet bar of the dredger at a distance from the bed, called stand-off distance. This distance could be as small as 0.10 m. The water jets trigger the sediment movement.

Kortmann (1994) simplified the sediment mobilization process by dividing it into three subprocesses: injection, transition and density flow (turbidity current). Figure 2-3 shows a schematization of the subprocesses. It is a conceptual definition because, in reality, the limits are hard to distinguish. This report focuses on the last sub-process (turbidity current). However, a qualitative description of the initial sub-processes is important to provide insight about the origin of the turbidity current, which differs, for example, from the origin of a turbidity current in a submarine canyon.

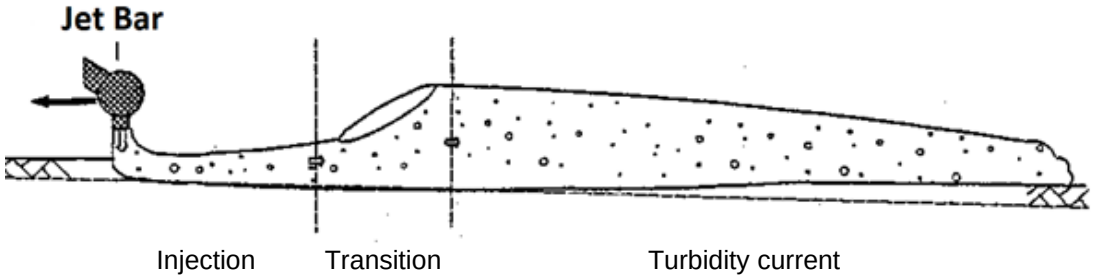

Figure 2-3. Three sub-processes of WID (adapted from Kortmann, 1994)

Injection

In the injection sub-process, a water jet penetrates the soil thereby increasing pressure and the effective shear stress between particles. The injection of a large volume of water fluidizes the soil. The penetration depth of the jet depends on the distance of the nozzles to the soil (stand-off distance), the progress speed of the jet bar, and properties of sediment such as grain size, permeability, density, and cohesion (Verweij, 1997). By multiplying the penetration depth and the progress speed of the jet bar, the amount of mobilized sediment can be estimated.

Siteur (2012) qualitatively described the jetting process in non-cohesive soil (Figure 2-4). First, he observed the jet flow diverges when it leaves the nozzle. Then, the sailing speed of the dredger causes the jet to bend until the velocities of the jet are nearly horizontal. As it bends, the jet loses momentum due to shear stress, and the component of the weight in the direction of the jet movement decreases. Near to the point of maximum penetration depth, the velocities become nearly horizontal and the vertical momentum induced by the jet is not significant anymore. Just downstream of this point, net sedimentation starts and the highly concentrated water-sediment mixture stabilizes.

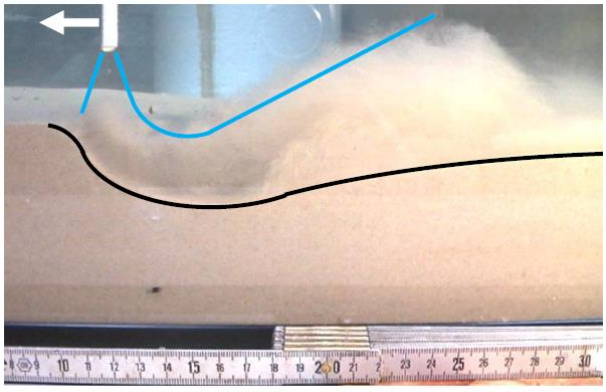

Figure 2-4. Jetting of sand and approximate path of the water-sediment mixture near the jet (Siteur, 2012)

During this process, the jet has a high speed in relation to ambient water. Then, a considerable volume of ambient water is entrained into the water-sediment mixture. The mixing of water dilutes the mixture, which spreads over a higher distance from the bed.

Transition

Information on the transition sub-process is limited. Kortmann (1994) defined the start of the transition sub-process where the velocity of the jet becomes too low to erode the soil.

By mixing with stagnant water, the turbulence of the jet decreases. Kortmann (1994) and Mastbergen (1995) observed a hydraulic jump during this phase. However, it is not known if this is always the case for the parameters in the range of application of WID. No validated mathematical expressions or numerical models were found in the literature to describe what happens specifically in this zone for WID. The evolution of the velocity and concentration profile shapes for this sub-process is unknown.

Density flow (turbidity current)

The third sub-process is the turbidity current. This study focuses on this sub-process. Kortmann (1994) defined the beginning of the current where the sediment-water mixture becomes stable. At this point, the settling velocity of the particles is small compared to the horizontal speed of the turbidity current.

As mentioned before, the transition process is still poorly understood, which makes it difficult to accurately define the upstream boundary conditions for the turbidity current. In practice, different scenarios of upstream boundary conditions must be analyzed to address this uncertainty.

2.2 WID-induced turbidity current

This section starts with a general description of the structure of a turbidity current. Then, the particular characteristics of a WID-induced turbidity current are presented. Finally, the involved processes that influence those characteristics are discussed.

2.2.1 General description of a turbidity current

The driving gravitational force of a density current is generated by density differences between the current and the ambient fluid due to temperature, salinity or other constituents. When this density difference is caused by suspended solids, it is named a particle-driven density current or turbidity current.

The general longitudinal structure of a turbidity current and, in general, of a density current consists of the head and the body (Figure 2-5). According to Middleton (1993), the mass and momentum balances of the head are different from those of the body. In order to advance, the head must displace ambient fluid, which is generally at rest or with low velocity. Accelerating the ambient fluid produces a flow resistance that is larger than friction at the bed or the upper interface. Then, the front of the density current requires more gravitational potential energy and becomes thicker than the body of the current (Middleton, 1993).

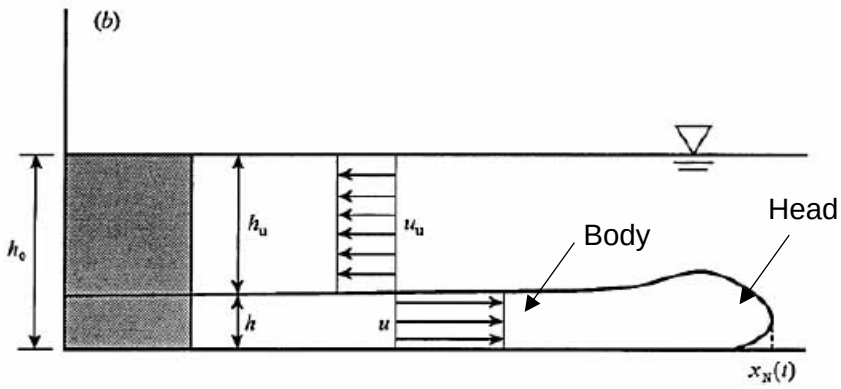

Figure 2-5. Schematic representation of a density current (Bonnecaze et al., 1993)

2.2.2 Vertical structure of a turbidity current

A characteristic feature of turbidity current flow is a significant variation of velocity and concentration over the vertical. The vertical structure of the water column during the passage of a turbidity current can be divided conceptually into two main layers: ambient waters (a_1) and turbidity current (a_2), as shown in Figure 2-6 (based on Sloff, 1994). The turbidity current layer can be split further into two sub-layers: a turbulent mixing layer or interface (a_i) and a lower dense turbulent sub-layer ($a_2 - a_i$).

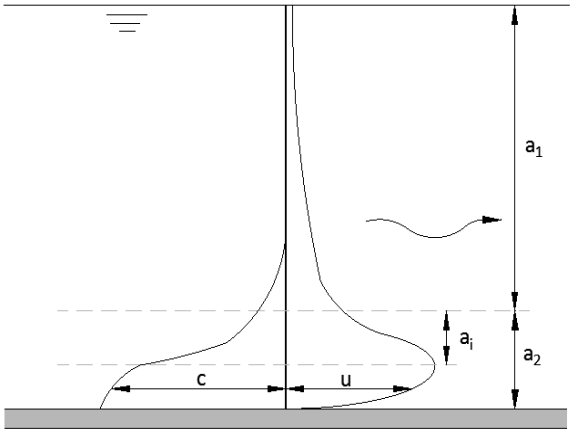

Figure 2-6. Sketch of the vertical structure of the water column: ambient waters (a_1), turbidity current (a_2) and interphase or mixing layer (a_i) (based on Sloff, 1994).

The upper layer (a_1) is characterized by low concentration and low horizontal velocity (compared to the bottom layers). The velocity can be negative depending on the ambient flow velocity and the characteristics of the turbidity current, such as its relative height compared to the depth. This phenomenon is called return flow.

The mixing layer or interface (a_i) presents a negative concentration gradient (the concentration decreases with increasing distance from the bed). The concentration gradient is higher than for the other two sub-layers. It also presents the highest negative velocity gradients. The height of the mixing layer strongly depends on the difference between the velocity of the turbidity current and the ambient flow velocity.

Finally, in the lowest turbulent sub-layer ($a_2 - a_i$), flow is dominated by boundary-generated turbulence (Sloff, 1994), which implies that the velocity profile can be assumed logarithmic.

According to Bonnecaze et al. (1993), vertical velocities and accelerations of turbidity currents are small.

2.2.3 Particular characteristics of a WID-induced turbidity current

WID-induced turbidity currents may differ from natural turbidity currents due to their different origins and the geometrical and environmental conditions through which they travel. Natural currents in submarine canyons, for example, are formed by liquefaction, breaching or avalanching of relatively steep bed slopes (Van Rijn, 2004). They travel at high-velocities and large depths, confined or semi-confined by lateral slopes. WID-induced turbidity currents, on the other hand, travel unconfined or partially confined, at a shallower depth, and milder slopes and are always man-induced. The fact that they travel unconfined or partially confined implies that lateral gradients may play a role in their motion.

Thickness, velocity, and concentration

Concentration, velocity, and (approximate) thickness are typical parameters to characterize a turbidity current. From these parameters, governing scale numbers can be estimated for a general characterization of the behavior of the currents. Van Rijn (2017) reported practical values for turbidity currents generated by WID:

- Current thickness (a_2): between 0.1 m and 1 m,
- Average velocity of the turbidity current: between 0.1 m/s and 1 m/s,
- Average mass concentration: between 50 kg/m^3 and 200 kg/m^3.

Density

The behavior of a turbidity current is strongly determined by the difference between the average density of the current and the density of ambient waters. The density of the mixture ρ_b can be approximated from the following equation:

$$\rho_b = \left(1 - \frac{\rho_w}{\rho_s}\right) \cdot c + \rho_w \tag{2.1}$$

Where c is the mass concentration [kg/m^3], ρ_s the grain density [kg/m^3] and ρ_w the ambient waters density [kg/m^3]. The mixture of freshwater ($\rho_w = 1000$ kg/m^3) and sediment ($\rho_s = 2650$ kg/m^3) with a concentration of 200 kg/m^3, has an approximate density of $\rho_m \approx 1125$ kg/m^3. Hence, the highest WID-induced turbidity current density is approximately 10% to 15% higher than the density of the ambient waters.

Molecular viscosity

An increase in sediment concentration increases the molecular viscosity of a suspension. Molecular viscosity can be estimated with the general expression:

$$\mu = (1 + c_3\, \phi^{c_4}) \cdot \mu_{\mathrm{w}} \tag{2.2}$$

Where μ_{w} is the molecular viscosity of the ambient fluid, c_3 and c_4 are empirical constants determined from experiments and ϕ is the volumetric concentration of particle aggregates. For non-cohesive sediment, viscosity can be estimated with Einstein's formula, with c_3 = 2.5 and c_4 = 1.

Richardson number

According to Winterwerp and Van Kesteren (2004), the governing scale numbers for a mud turbidity current are the Richardson number Ri (stability) and the effective Reynolds number Re^e (flow regime).

The Richardson number Ri is a ratio between the amount of stratification and the amount of turbulence. The amount of stratification is proportional to the vertical density gradient ∂ρ/∂z, and the amount of turbulence is proportional to $|\partial u/\partial z|^2$. Then,

$$Ri = -\frac{g'}{\rho_b} \frac{\frac{\partial \rho_b}{\partial z}}{\left|\frac{\partial u}{\partial z}\right|^2} \tag{2.3}$$

For $Ri > 1/4$, it is known that the damping of turbulence by stratification balances the generation of turbulence and the stratification becomes stable (Pietrzak, 2015). For a turbidity current, an overall Richardson number can be defined for the layer (Van Kessel and Kranenburg, 1996):

$$Ri = \frac{-\frac{g}{\bar{\rho}} \frac{\rho_b - \rho_w}{H} \cos\beta}{\left(\frac{U}{H}\right)^2} = -\frac{g\,(\rho_b - \rho_w)}{\rho_w} \frac{H}{U^2} \cos\theta = -g' \frac{H}{U^2} \cos\theta \tag{2.4}$$

Where: β [°] is the bed slope angle with the horizontal plane, U [m/s] is the layer-averaged velocity parallel to the bed slope, H [m] the layer thickness and g' [m/s^2] is the reduced gravity. Wilson (2007) provided an estimation of the magnitude of the overall Richardson number from (2.4) of the turbidity currents generated by WID in 14 projects in the USA and seven projects in Europe (The Netherlands, Germany, and the UK). The results ranged from 1.16 to 17.32, indicating that WID typically generates stable turbidity currents.

Effective Reynolds number

The flow regime (laminar or turbulent) highly affects bed friction and entrainment of water (Van Kessel & Kranenburg, 1996). Laminar behavior shows a concentration profile with a clear lutocline. Turbulent behavior shows a gradual variation from the bottom upwards, with no clear lutocline (Figure 2-7). Turbulent flow is non-uniform due to the mixing with water from the upper layer, which depends on the Richardson number.

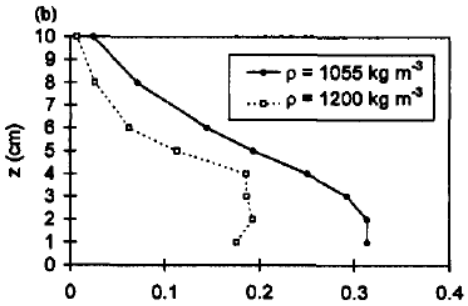

Figure 2-7. Concentration and velocity profiles for laminar (dashed line) and turbulent flow (solid line) (Van Kessel & Kranenburg, 1996).

In order to determine for which conditions the flow can be characterized as laminar or turbulent, Van Kessel and Kranenburg (1996) used the effective Reynolds number Re^e:

$$\frac{1}{Re^e} = \frac{1}{Re^\mu} + \frac{1}{Re^\tau} = \frac{\mu}{4\rho_b UH} + \frac{\tau_y}{8\rho_b U^2} \tag{2.5}$$

With: μ [Pa·s] the dynamic viscosity of and τ_y [N/m^2] the yield stress. Van Kessel and Kranenburg (1996) concluded that the transition between laminar and turbulent flow occurs when $2000 < Re^e < 3000$.

As a comparison, natural turbidity currents at submarine canyons present turbulent and non-Newtonian behavior. WID-induced turbidity currents have lower mean velocities, which means that they may be still turbulent, but closer to the transitional regime. Near the downstream end of the current, a decrease in U is expected. The combination of a slow turbidity current of cohesive sediment with high concentration may produce laminar flow.

2.2.4 Involved Physical Processes

As a turbidity current spreads, sediment particles settle and water is entrained. Then, the main driving force (baroclinic pressure gradient) decays until the current stops or vanishes. Physical processes that influence the change of the density and velocity of the turbidity current are outlined below.

Processes in the water column

Vertical transport processes of water and sediment determine the spatial and temporal variation of the density and velocity of turbidity currents. Density variation along its path and over the vertical is a distinguishing feature of turbidity currents.

(Hindered) Settling

Due to gravity and a higher density than ambient waters, sediment particles fall through the water column. The gravity force on a particle is counteracted by drag forces, turbulence and the effects of the presence of other particles.

When the volumetric concentration of a suspension increases, each particle hinders other particles during settling (hindered settling).

Flocculation

Flocculation is a reversible process that results from simultaneous aggregation and breakup of flocs of cohesive sediment (Winterwerp & Van Kesteren, 2004). Turbulent mixing can induce aggregation but can also induce the breakup of flocs. The conditions for aggregation depend on the turbulence intensity and concentration of the mixture. No experimental data was found specifically related to length and time scales for the formation of flocs in the conditions of a WID-induced turbidity current.

Stratification

Density-driven flows occur for concentrations above approximately 1 kg/m^3 (Van Kessel, 1997). As mentioned above, for Ri > 0.25, stratification dampens turbulence, and the stratification becomes stable. For stratified conditions, the velocity near the bed is different from the depth-averaged velocity (in magnitude and sometimes even in direction).

Mixing

Due to the velocity difference between the turbidity current and the surrounding water, internal waves may arise in the interface (Verweij, 1997). These waves can grow, roll up, and then break with increasing velocity differences. Wave breaking creates a mixing layer.

For homogeneous flow, it is expected that the mixing layer keeps growing and fully mixes the flow. In stratified flow, as in a turbidity current, stratification counteracts the mixing process (Pietrzak, 2015). A particle transported to the upper layer tends to go down due to its higher density, reversing the eddy effect. The same holds for lighter particles transported to the lower layer. This process is named turbulence damping (Pietrzak, 2015). Then, due to turbulence damping, for stable conditions the mixing layer keeps a limited thickness. The thickness of the mixing layer δ for a gravity current can be approximated as (Thorpe, 1971):

$$\delta = 0.3 \frac{(\Delta u)^2}{g'} \tag{2.6}$$

Where Δu is the relative velocity between layers. Mixing is more intense when turbidity currents are less stable (less turbulence damping).

Mixing of water and sediment at the interface is commonly known as water entrainment. Parker et al. (1987) parametrized entrainment as a function of the overall Richardson number. A higher Richardson number (more stable stratification) is related to less water entrainment.

Segregation

Segregation or sorting occurs because larger particles tend to settle faster than smaller particles, leading to a vertical gradient in particle size. Segregation results in a steeper vertical concentration gradient (Hanssen, 2016), compared with the case of uniform particle size. Heavier particles will remain close to the bed and lighter particles can be mixed over the water column. In the case of stratified flow, segregation increases the stability of stratification.

Deposition

The deposition is the gross flux of sediment into the bed. For cohesive sediment, it can be estimated with the Partheniades-Krone formulation (Partheniades, 1965) described in Appendix C. It depends on the settling velocity, the near-bed concentration and the ratio between the bed shear stress and a critical bed shear stress for deposition $\tau_{cr,d}$. Typical values of $\tau_{cr,d}$ for cohesive sediment are in the order of 0.05 to 0.1 Pa (Winterwerp & Van Kesteren, 2004).

Erosion

Sediment particles or flocs are eroded when the bed shear stress is higher than a critical shear stress for erosion τ_e. The critical shear stress for erosion depends on the deposition and consolidation history of the material (Van Rijn L. , 1994).

Morphological (bed level) changes

Accretion occurs when the net deposition rate is positive (Deposition > Erosion). Bed level changes can vary longitudinally. Parker et al. (1987) reported the generation of bedforms during the passage of a turbidity current of non-cohesive material. Bedforms increase bed roughness, which affects the velocity and concentration profiles.

Large scale processes

Two processes of a larger scale than the processes in the water column may produce sediment transport in a different direction than the main one of the turbidity current (main direction interpreted as the direction in which most of the mobilized sediment moves): lateral spreading and return flow. Depending on the hydrodynamic conditions and bathymetry, these processes may influence the distribution of the mobilized sediment.

Lateral spreading

It is known that unconfined turbidity currents traveling on a longitudinally sloped plane spread laterally. However, experimental data on lateral spreading specifically for turbidity currents is limited, especially in the range of concentrations and bed slopes of WID.

According to Choi and Garcia (2001), mostly saline gravity currents have been used in the laboratory as substitutes for turbidity currents. Alavian (1986) found that the magnitude of the spreading of a gravity current depends on the bed slope and initial buoyancy flux. He proposed relations to estimate the variation of the width of the turbidity current with time. Moosavi-Hekmati et al. (2018) studied the lateral spreading of initially supercritical turbidity currents of low concentration and proposed relations to estimate the width of the current and the position of the front as a function of time. These relations were found for different ranges of concentration and bed slopes from the typical values for WID-induced turbidity currents.

Return flow

The passage of a large turbidity current may generate return flow in the ambient waters (Figure 2-8). The magnitude of this flow depends on the ratio of the thickness of the turbidity current (named h_1 in Figure 2-8) to water depth H (Ungarish, 2009).

Longo et al. (2018) studied the return flow due to a gravity current for small depths. They confirmed by experiments that a larger gravity current thickness (for the same depth) causes a larger return flow in the ambient water. From CFD simulations, they concluded that the return flow velocity was in the same order of magnitude of the gravity current velocity for a ratio $h_1/H \approx 1/4$. For $h_1/H \approx 1/10$, which is closer to the expected values in WID applications, the return flow velocities decreased considerably to values around one order of magnitude below the gravity current velocities.

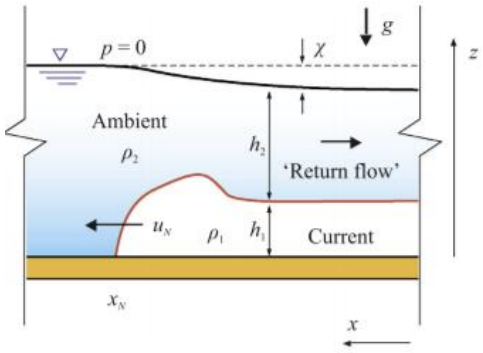

Figure 2-8. Return flow and water level depression (Longo et al., 2018)

For WID, the turbidity current thickness is in the order of magnitude of 1 m. Then, for depths below 5 m, the effect of the return flow may be significant. Return flow transports sediment in a direction opposite to the ambient current. The magnitude of the sediment transport by return flow depends on its velocity and the sediment characteristics (especially the grain size).

3 Modelling a WID-induced turbidity current

For the development of the rapid assessment tool, it was first assumed by Deltares (2019) that a WID-induced turbidity current can be represented with a 2DV approach, which means that lateral gradients and processes are neglected (Deltares, 2019). However, the computational effort and time required to model the process with a 2DV approach are excessive for a rapid assessment tool. Hence, the 2DV approach was transformed into a Lagrangian 1DV approach.

This section explains the 2DV approach. Then, the transformation from a 2DV approach into a Lagrangian 1DV approach is described, and the mathematical expressions of this transformation are explained.

3.1 Eulerian 2DV approach

3.1.1 Eulerian Frame of Reference

The Eulerian frame of reference is fixed in space. In the case of a 2DV flow field (two dimensions in the vertical plane), the coordinates of a fixed point are defined as the horizontal and vertical distances to the origin, respectively x and z. There is no variation of the physical quantities in the direction perpendicular to this plane (y). Time is identified as t. For this section, $z = -d$ at the bed and $z = \zeta$ at the water surface ($H = \zeta + d$).

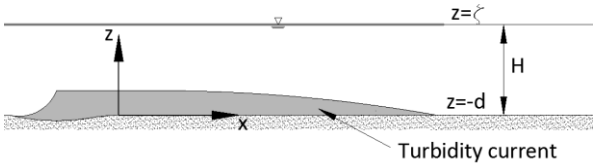

Figure 3-1. Sketch of the Eulerian frame of reference

3.1.2 Key assumptions

The derivation of the 2DV formulation included the next considerations and assumptions:

- The fluid is incompressible and Newtonian
- The Boussinesq approximation is valid
- Flow is turbulent
- Vertical accelerations are small and, then, the pressure is hydrostatic

More detail about these assumptions is given in Appendix A.

3.1.3 Governing equations

Mass conservation equation

Starting from the 3D fluid mass conservation equation for an infinitesimal control volume in its general form (Navier-Stokes), the terms in the y-direction (perpendicular to the x-z plane) are not considered (2DV) and the fluid is assumed to be incompressible. Then, the fluid mass conservation equation is written as:

$$\frac{\partial u}{\partial x} + \frac{\partial w}{\partial z} = 0 \tag{3.1}$$

Where: u is the horizontal fluid velocity and w is the vertical fluid velocity.

Momentum equation

The momentum equation for the 2DV approach was derived from the Navier-Stokes momentum equation (Appendix A). The equation can be written as:

$$\frac{\partial u}{\partial t} + u\frac{\partial u}{\partial x} + w\frac{\partial u}{\partial z} = -g\frac{\partial \zeta}{\partial x} - \frac{g}{\rho_w}\int_{z'}^{\xi}\frac{\partial \rho_b}{\partial x}\,dz + \frac{\partial}{\partial z}\left[(\upsilon + \upsilon_T)\frac{\partial u}{\partial z}\right] \tag{3.2}$$

Where ρ_b [kg/m^3] is the density of the water-sediment mixture, ρ_w [kg/m^3] is the density of water, ζ [m] is the water level, and υ_T [m/s^2] is the eddy viscosity.

Suspended sediment transport equation

The suspended sediment transport is represented by the 2DV advection-diffusion equation:

$$\frac{\partial c}{\partial t} + u\frac{\partial c}{\partial x} + w\frac{\partial c}{\partial z} = \frac{\partial (w_s c)}{\partial z} + \frac{\partial}{\partial x}\left(\Gamma_x \frac{\partial c}{\partial x}\right) + \frac{\partial}{\partial z}\left(\Gamma_T \frac{\partial c}{\partial z}\right) \tag{3.3}$$

Where w_s [m/s] is the effective settling velocity (a function of the concentration), Γ_x [m^2/s] is the horizontal eddy diffusivity and Γ_T [m^2/s] is the vertical eddy diffusivity. The vertical diffusion term $\frac{\partial}{\partial z}\left(\Gamma_T \frac{\partial c}{\partial z}\right)$ is assumed to be much larger than the horizontal diffusion term $\frac{\partial}{\partial x}\left(\Gamma_T \frac{\partial c}{\partial x}\right)$. Then, the horizontal diffusion term is often neglected (Dorrell & Hogg, 2012). The suspended sediment transport equation for a 2DV approach can then be expressed as:

$$\frac{\partial c}{\partial t} + u\frac{\partial c}{\partial x} + w\frac{\partial c}{\partial z} = \frac{\partial (w_s c)}{\partial z} + \frac{\partial}{\partial z}\left(\Gamma_T \frac{\partial c}{\partial z}\right) \tag{3.4}$$

3.2 Transformation to a Lagrangian 1DV approach

For the rapid assessment tool, the 2DV approach was schematized as a Lagrangian 1DV approach (Deltares, 2019). Due to its Lagrangian nature, the model advances in the turbidity current direction. The model is not applicable to subcritical turbidity currents, in which downstream boundary conditions control the flow.

The transformation to the Lagrangian 1DV approach was proposed by Winterwerp (personal communication, August 9, 2019). The Lagrangian frame of reference moves with the flow field at a certain velocity (called Lagrangian velocity). It is able to follow a fluid parcel as it moves in space and time. The position of the moving frame of reference is named ξ (horizontal coordinate) and z remains as the vertical coordinate. Time is named as τ (Figure 1-3).

The transformation of Eulerian coordinates (x, t) to the Lagrangian coordinates (ξ, τ) is defined as:

$$\frac{\partial}{\partial t} = \frac{\partial \tau}{\partial t}\frac{\partial}{\partial \tau} + \frac{\partial \xi}{\partial t}\frac{\partial}{\partial \xi}$$
$$\frac{\partial}{\partial x} = \frac{\partial \tau}{\partial x}\frac{\partial}{\partial \tau} + \frac{\partial \xi}{\partial x}\frac{\partial}{\partial \xi} \tag{3.5}$$

Time is the same in the Lagrangian and Eulerian frames of reference $(\tau = t)$. The position of the Lagrangian frame of reference can be calculated considering the initial horizontal coordinate in the Eulerian frame of reference, time and the Lagrangian velocity:

$$\xi = x_0 + u_c t \tag{3.6}$$

Where u_c is the Lagrangian velocity. Substituting with (3.6) in (3.5) and considering that $\tau = t$, the transformation reads:

$$\frac{\partial}{\partial t} = \frac{\partial}{\partial \tau} + u_c \frac{\partial}{\partial \xi}$$
$$\frac{\partial}{\partial x} = \frac{\partial}{\partial \xi} \tag{3.7}$$

3.3 The Lagrangian 1DV model

3.3.1 Key assumptions

The Lagrangian 1DV model follows a Lagrangian 1DV approach. Two particular assumptions give the final particular shape to the Lagrangian 1DV model:

Assumption 1

The assumption of uniformity of the 1DV Point Model (Appendix B) is assumed as stationarity in the Lagrangian frame of reference ($\partial/\partial\tau = 0$), then according to Equation (3.7):

$$\frac{\partial}{\partial t} = u_c \frac{\partial}{\partial \xi}$$
$$\frac{\partial}{\partial x} = \frac{\partial}{\partial \xi} \tag{3.8}$$

This means that as the fluid column travels at a velocity u_c, the change of any physical quantity in time equals the change of the quantity in space (in the direction in which the fluid column moves).

Assumption 2

The Lagrangian velocity is defined as a concentration-weighted velocity over the water column, expressed as (Deltares, 2019):

$$u_c = \frac{\int_{-d}^{\zeta} uc \, dz}{\int_{-d}^{\zeta} c \, dz} \tag{3.9}$$

3.3.2 Governing equations

Considering (3.8), the momentum and sediment transport equation can be written as:

$$u_c \frac{\partial u}{\partial \xi} = -g \frac{\partial \zeta}{\partial \xi} - \frac{g}{\rho_w} \int_z^{\xi} \frac{\partial \rho_b}{\partial \xi} \, dz \frac{\partial}{\partial z} \left[(\upsilon + \upsilon_T) \frac{\partial u}{\partial z} \right] \tag{3.10}$$

$$u_c \frac{\partial c}{\partial \xi} + w \frac{\partial c}{\partial z} = \frac{\partial (w_s c)}{\partial z} + \frac{\partial}{\partial z} \left(\Gamma_T \frac{\partial c}{\partial z} \right) \tag{3.11}$$

The final governing equations were derived by Winterwerp (personal communication, August 9, 2019). The derivation is shown in Appendix C. The resulting momentum equation of the Lagrangian 1DV model is:

$$u_c \frac{\partial u}{\partial \xi} + \frac{U_{ref} - \bar{u}}{T_{rel}} + \frac{\tau_b - \tau_s}{\rho_b H} - \left[\frac{\alpha g \tan\beta}{\rho_b} c + \frac{\alpha g}{\rho_b u_c}\left\{w_s c + \Gamma_T \frac{\partial c}{\partial z}\right\}\right] = \frac{\partial}{\partial z}\left\{(\nu + \nu_T)\frac{\partial u}{\partial z}\right\} \quad (3.12)$$

In which: U_{ref} [m/s] is the prescribed depth-mean flow velocity, $\bar{u}$ [m/s] is the actual depth-mean velocity, T_{rel} [s] is the relaxation time ($T_{rel} = 2\Delta t$), Δt [s] is the time step, τ_s and τ_b [Pa] are the surface and bed shear stress, the relation $\alpha = (\rho_b - \rho_w)/c$ and β [°] is the bed slope angle.

The suspended sediment transport equation is as follows:

$$u_c \frac{\partial u}{\partial \xi} - \left[u_c \tan\beta \frac{\partial c}{\partial z}\right] - \frac{\partial w_s c}{\partial z} = \frac{\partial}{\partial z}\left\{\Gamma_T \frac{\partial c}{\partial z}\right\} \quad (3.13)$$

It is important to remark here that the Lagrangian velocity is present in both the momentum and sediment transport equation, which means that both water and sediment are transported at a velocity u_c. The value of u_c varies from one fluid column to the next one (it is only constant if velocity and concentrations are uniform).

3.4 Physical processes from the theoretical framework

From the identified physical processes described in Chapter 2, settling, erosion, deposition, turbulent mixing and stratification are considered in the Lagrangian 1DV model. Flocculation, morphological changes, and lateral spreading were not considered in the Lagrangian 1DV approach, in line with the approach and the development of a rapid assessment tool.

The Lagrangian 1DV approach is not able to represent sediment transport by return flow. However, return flow is only significant in closed basins or for large turbidity currents.

Both approaches assume non-Newtonian fluid and turbulent flow conditions.

4 Numerical experiments

In this chapter, the Lagrangian 1DV model (Lagrangian 1DV approach) is compared to a 2DV computation in Delft3D-FLOW (2DV approach) to determine the validity of the Lagrangian 1DV approach and estimate the magnitude of the differences, if present.

For this purpose, four sets of experiments were carried out (Figure 4-1):

1) Set 1: Analysis of vertical processes in uniform flow conditions

2) Set 2: Analysis of non-uniform flow in a channel

3) Set 3: Based on Run 13 of Parker et al. (1987)

4) Set 4: Based on Run 2 of van Kessel and Kranenburg (1996)

Experiments Set 1 intended to understand and to compare the results for concentration and velocity of the Delft3D-FLOW model (called Delft3D model, from now on) and the Lagrangian 1DV model when including the available vertical sediment transport processes in uniform flow conditions in a channel. Uniformity in the Eulerian frame of reference is one of the assumptions of the 1DV Point Model. The initial depth-averaged concentration was very low (1 kg/m^3).

The objective of Experiments Set 2 was to identify differences between the results of the models for velocity, concentration, mass flux, sediment load and concentration-weighted velocity for the non-uniform flow stage in a channel and determine their cause and behaviour. Differences between the models were expected as the uniformity assumption was not satisfied. The concentration-weighted velocity for the Delft3D model was defined here as for the Lagrangian 1DV model, as the ratio between the mass flux at a certain station and the sediment load in the water column at the same station. The initial depth-averaged concentration was increased to 10 kg/m^3 to analyze the effect of the density difference. The bed slope was the same as In Experiments Set 1. The baroclinic pressure gradient was still small compared to the expected order of magnitude of a WID-induced turbidity current.

In Experiments Set 3 and Set 4, the numerical models were based on the laboratory experiments of Parker et al. (1987) and van Kessel and Kranenburg (1996), respectively. Turbidity currents were generated in these experiments. The first objective was to compare the results of the models with the measured data for velocity and concentration. The second objective was to identify and to explain differences between the results of the models for velocity, concentration, mass flux, sediment load and concentration-weighted velocity. In Experiments Set 3, based on Parker et al. (1987), the bed slope was considerably higher than in the previous sets of experiments (0.05). In Experiments Set 4, both the bed slope (0.0235) and the initial depth-averaged concentration (166 kg/m^3) increased significantly compared to Experiments Set 1 and Set 2. Then, the baroclinic pressure gradient was significantly higher than in Experiments Set 1 and Set 2 and closer to the order of magnitude of the baroclinic pressure gradient for the typical parameters of a WID-induced turbidity current.

4.1 Experiments plan

4.1.1 Structure

The numerical experiments plan is shown in Figure 4-1. The studied vertical sediment transport processes were settling (S), turbulent mixing (T), deposition (D) and erosion (E).

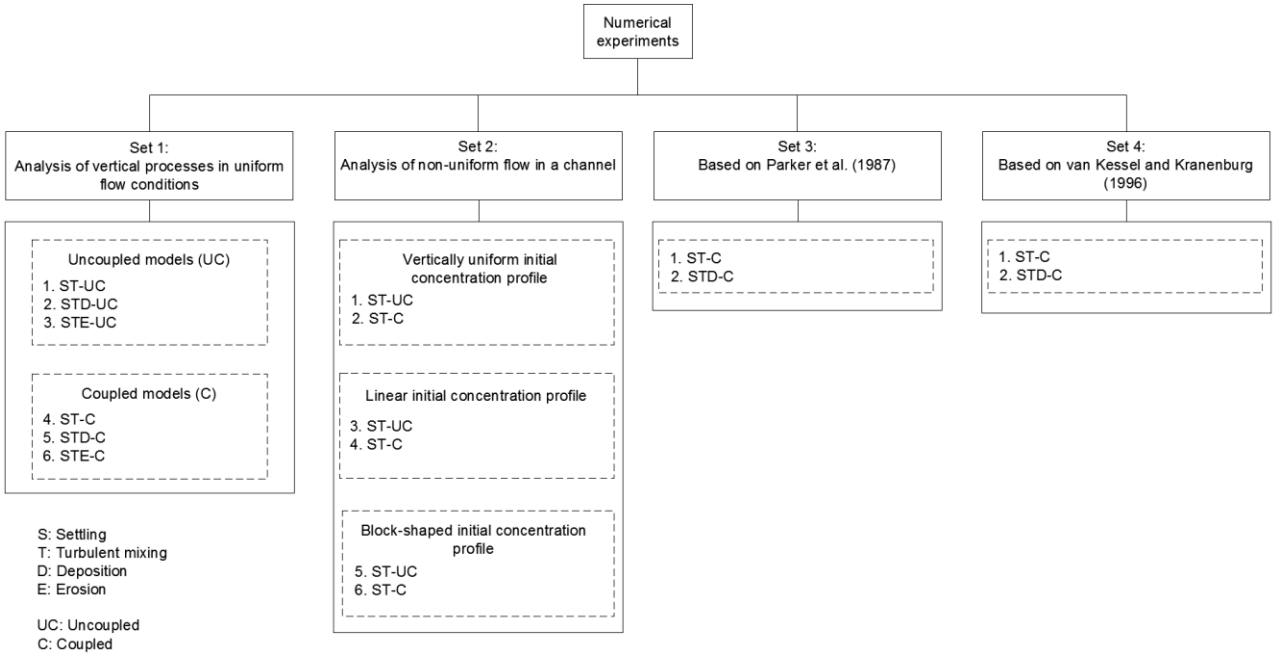

Figure 4-1. Numerical experiments plan.

4.1.2 Methodology

The methodology of the first set of experiments was based on the controlled addition of the above-mentioned physical processes. This set of experiments studied the vertical processes in uniform flow conditions in a channel with a very small bed slope.

Erosion and deposition were studied with the Partheniades-Krone formulations (Partheniades, 1965). The formulations for the erosion of non-cohesive sediment differ between the Lagrangian 1DV model and Delft3D. To be able to identify the differences produced by the assumptions of the Lagrangian 1DV approach, it was necessary to model the physical processes of settling, turbulent mixing, erosion, and deposition with the same formulations in the Lagrangian 1DV model and Delft3D model. Then, the erosion of non-cohesive sediment was left out of the scope of this study.

A baroclinic pressure gradient occurs when there are density differences in the fluid, caused in this case by the effect of sediment on the fluid density. When this happens, the sediment transport equation and the momentum equation are coupled by the baroclinic pressure gradient. This was indicated with a “C” for coupled mode. When the effect of sediment on fluid density is not considered in the model (the sediment density ρ_s is defined as equal to the reference density of water ρ_w), there is no influence of the solution of the sediment transport equation on the momentum equation. This was indicated as “UC” for uncoupled mode.

The first part of Set 1 was done with uncoupled (UC) models and the second part with coupled (C) models. Experiment ST-UC was the first experiment with uncoupled models. It included the processes of settling and turbulent mixing. In Experiment STD-UC, the deposition process was considered. Finally, in Experiment Experiment STE-UC, the erosion process was added (no deposition).

After the previous three experiments, the models were run in their coupled mode to verify that coupling the models did not produce any significant difference between the results. This could only happen for a very small baroclinic pressure gradient. Aligned with this purpose, a low concentration of 1 kg/m^3 was used (density difference below 0.1% of ρ_w).

Set 2 analyzed non-uniform flow in a channel with a very small bed slope. This set was divided into three parts according to the shape of the concentration profile at the upstream boundary of the channel. The experiments were done for a depth-averaged concentration of 10 kg/m^3 at the upstream boundary.

Three different shapes were defined to investigate the effect of non-uniformity. The selected initial profiles are available in the Lagrangian 1DV model: vertically uniform, linear and block-shaped profile up to half of the depth (they will be illustrated in the sections corresponding to each experiment). For each part, the models were run in coupled and uncoupled modes. The models of this set did not consider erosion or deposition to facilitate the identification and understanding of the origin of the differences between the Lagrangian 1DV approach and the Eulerian 2DV approach.

Set 3 consisted of two numerical experiments based on the laboratory experiments of Parker et al. (1987) in a flume with a significant bed slope. Parker et al. (1987) studied turbidity currents over an erodible bed (non-uniform flow). The numerical models' setup was based on Run 13, with a depth-averaged concentration of 10.9 kg/m^3 at the upstream boundary. First, the models considered only settling and turbulent mixing (no deposition) in order to determine and understand the differences in the concentration-weighted velocity and sediment transport. Then, deposition was added to get insight into the difference in the deposition rate between the models and possible implications on sedimentation. In this case, the baroclinic pressure gradient was more important than in the previous sets, affecting significantly the velocity profile along the turbidity current. The results of the models with deposition for velocity and concentration were compared to the measurements.

Set 4 consisted of two numerical experiments based on the laboratory experiments of van Kessel and Kranenburg (1987) in a flume with a significant bed slope. They studied highly concentrated gravity currents over a non-erodible bed (non-uniform flow). The numerical models' setup was based on Run 2, with a depth-averaged concentration of 166 kg/m^3 at the upstream boundary. First, the models considered only settling and turbulent mixing (no deposition) in order to determine and understand the differences in the concentration-weighted velocity and sediment transport. Then, deposition was added. The results for the model with deposition were compared to measurements.

4.1.3 Approach for the comparison

Before the start of the experiments, it was required to define the flow conditions in which the results of both models can be compared.

The Lagrangian 1DV model was conceptualized by Deltares (2019) to represent a single release of water and sediment (a single fluid column). The solution of the Lagrangian 1DV model at every position can be represented in the 2DV Eulerian reference frame. Using the transformation rules, summarized in (3.7), the governing equations of the Lagrangian 1DV model [(3.10), (3.11)] can be represented in the Eulerian reference frame as:

$$u_c \frac{\partial u}{\partial x} - g\frac{\partial \zeta}{\partial x} - \frac{g}{\rho_w}\int_z^{\xi} \frac{\partial \rho_b}{\partial x}\, dz = \frac{\partial}{\partial z}\left[(\upsilon + \upsilon_T)\frac{\partial u}{\partial z}\right] \tag{4.1}$$

$$u_c \frac{\partial c}{\partial x} + w\frac{\partial c}{\partial z} = \frac{\partial (w_s c)}{\partial z} + \frac{\partial}{\partial z}\left(\Gamma_T \frac{\partial c}{\partial z}\right) \tag{4.2}$$

Represented in the Eulerian reference frame, u_c is a function of x.

To perform the comparison between the models, the representation of the Lagrangian 1DV model's solution in the Eulerian reference frame was compared to the solution of the Delft3D model (continuous release of sediment from a static source). Then, the governing equations of this 2DV approach [(3.2), (3.3)] become:

$$u \frac{\partial u}{\partial x} - g\frac{\partial \zeta}{\partial x} - \frac{g}{\rho_w}\int_{z'}^{\xi} \frac{\partial \rho_b}{\partial x}\, dz = \frac{\partial}{\partial z}\left[(\upsilon + \upsilon_T)\frac{\partial u}{\partial z}\right] \tag{4.3}$$

$$u \frac{\partial c}{\partial x} + w\frac{\partial c}{\partial z} = \frac{\partial (w_s c)}{\partial z} + \frac{\partial}{\partial z}\left(\Gamma_T \frac{\partial c}{\partial z}\right) \tag{4.4}$$

The Eulerian 2DV approach of the Delft3D model is assumed in this analysis as a more accurate representation of reality, as it does not assume flow uniformity at any point.

4.2 Experiments Set 1: Analysis of uniform flow in a channel

The Delft3D model setup consisted of a 1000 m long channel with a very mild bed slope. At the upstream boundary, a logarithmic velocity profile was defined with a depth-averaged velocity of $\bar{u}$ =1 m/s. A vertically uniform sediment concentration profile of 1 kg/m^3 was also defined at that boundary. At the downstream boundary, the water level was fixed to produce a depth H of 1 m.

The single-particle settling velocity w_{s0} of the inflowing sediment was defined as 1 mm/s, which is an intermediate value between the practical minimum settling velocity of 0.1 mm/s and 10 mm/s (order of magnitude of settling velocity of fine sand).

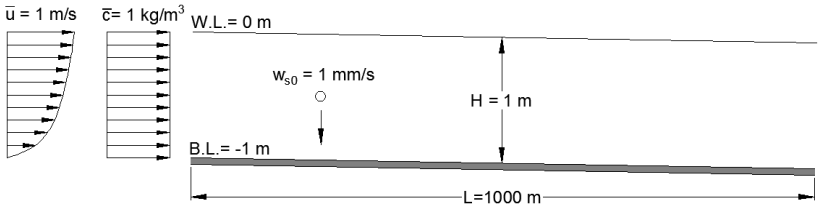

Figure 4-2. Characteristics of the channel and upstream boundary conditions.

The bed slope was calculated to produce uniform flow with a theoretical equilibrium depth of 1 m. A roughness length z_0 of 1 x 10^{-4} m was selected for the calculation. For a value of the Von Karman constant of $\kappa = 0.41$, the obtained bed slope to obtain the equilibrium depth of 1 m was 2.4 x 10^{-4} m/m. The simulation time was long enough to obtain stationary flow (the time was variable for each run).

When running the Delft3D model for the calculated parameters, a backwater curve was generated, producing a water depth of 1.02 m at the upstream boundary. The deviation of the water depth of a 3D model in Delft3D-FLOW from the theoretical solution for uniform flow in a simple channel is further discussed in the Validation Document of Delft3D-FLOW (Deltares, 2008). To obtain a uniform depth of 1 m, the roughness length was then reduced to z_0= 6.5 x 10^{-5} m.

The input parameters of the Lagrangian 1DV model matched the setup of the Delft3D model. The initial conditions were the same as the upstream boundary conditions of the Delft3D model. It was not necessary to define a length. The depth is constant in the Lagrangian 1DV model by definition. Evidently, a downstream boundary condition was not required. The summary of the models' set-up for Experiments Set 1 is shown in Table 4-1.

Table 4-1. Models' input parameters for Set 1: Analysis of steady uniform flow in a channel.

Parameter	Lagrangian 1DV model	Delft3D model
Time step [s]	0.3	0.3
Number of vertical layers	20	20
Bed slope [-]	2.4x10^{-4}	2.4x10^{-4}
Water depth H [m]	1	1
Domain length L [m]	-	1000
Roughness length z_0 [m]	6.5 x 10^{-5}	6.5 x 10^{-5}
Vertical eddy viscosity ν_T [m^2/s]	From k-ϵ model	From k-ϵ model
Vertical eddy diffusivity Γ_T [m^2/s]	From k-ϵ model	From k-ϵ model
Background eddy viscosity ν_{BCK} [m^2/s]	0	0
Background eddy diffusivity Γ_{BCK} [m^2/s]	0	0
Downstream boundary conditions	-	$H = 1\ m$
Initial conditions (Lagrangian 1DV model) Upstream boundary conditions (Delft3D model)	$\bar{u}$ = 1 m/s (log profile) $\bar{c}$ = 1 g/l (vertically uniform)	$\bar{u}$ = 1 m/s (log profile) $\bar{c}$ = 1 g/l (vertically uniform)

4.2.1 Experiment ST-UC (settling, turbulent mixing - uncoupled models)

This experiment included the processes of settling and turbulent mixing (no erosion or deposition). The uniform flow stage in the channel is preceded by a non-uniform flow stage. For this set of experiments, the results were analyzed where the flow was already uniform. Non-uniform flow is analyzed in Experiments Set 2.

As commented above, the first step was to calculate the analytical solution for the velocity and concentration profiles for uniform flow. As an uncoupled (UC) model, the velocity does not depend on the concentration. The velocity profile can be then expressed as:

$$u(z) = \frac{u_*}{\kappa} ln\left(\frac{z}{z_0}\right) \tag{4.5}$$

Where u_* [m/s] is the friction velocity and z [m] is defined here as the vertical distance from the bed. For the parameters of this experiment:

$$u(z) = 0.122 \cdot ln(6.5\ x\ 10^5 z)$$

With no erosion or deposition, the concentration profile achieves equilibrium. Assuming a parabolic distribution of eddy diffusivity (the same shape as in the k-ϵ model), the development of a Rouse profile was expected:

$$c(z) = c_a \left(\frac{H-z}{z}\frac{a}{1-a}\right)^{\frac{\sigma_T w_s}{\kappa u_*}} \tag{4.6}$$

In this case ($H = 1\,m;\ w_s = 0.001\,m/s;\ \kappa = 0.41;\ u_* = 0.05\,m/s$) and with a Prandtl-Schmidt number σ_T of 0.7 (default value in both models), the expected concentration profile was:

$$c(z) = c_a \left(\frac{1-z}{z}\frac{a}{1-a}\right)^{0.0342}$$

Knowing that the depth-averaged concentration was $\bar{c}$ = 1 kg/m^3, a relation between the reference height a and the concentration at that height from the bed (c_a) was obtained. For a value of $a = 0.025$ m (center of the lowest layer in both models), c_a = 1.132 kg/m^3 in order to keep $\bar{c}$ = 1 kg/m^3. Figure 4-3 shows the analytical and modelled velocity and concentration profiles at x=500 m.

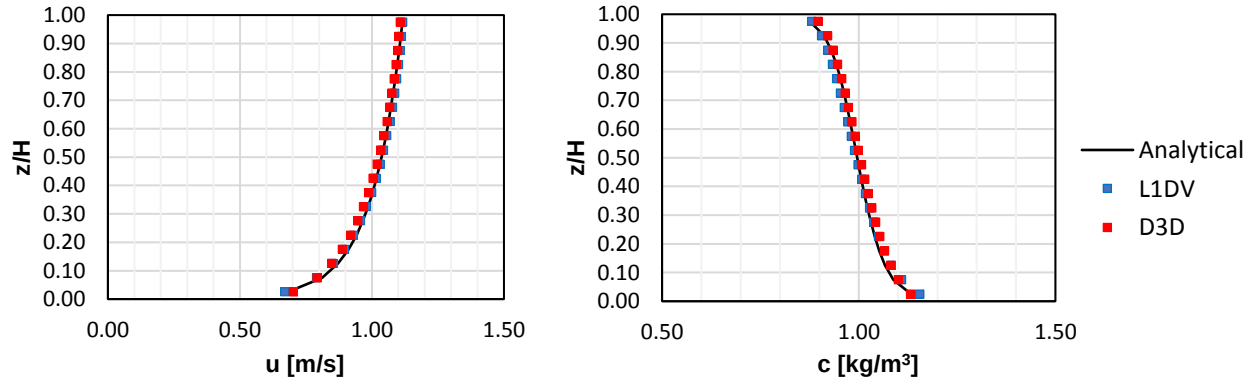

Figure 4-3. Velocity and concentration profiles for the Lagrangian 1DV model (L1DV) and the Delft3D model (D3D) at x=500 m for Experiment ST-UC

The velocity and concentration profiles of the models presented a good agreement with the analytical solution and between them. The concentration distribution for the first 100 m in both models (Figure 4-4) showed that the concentration was not uniform for the first ~ 70 m ($\partial c/\partial x \neq 0$). The concentration profile required a length to adapt from non-uniform to uniform flow. This was expected because the

initial concentration profile did not correspond to the equilibrium Rouse profile. A deeper analysis of the non-uniform stage is presented in Experiments Set 2.

(a) L1DV

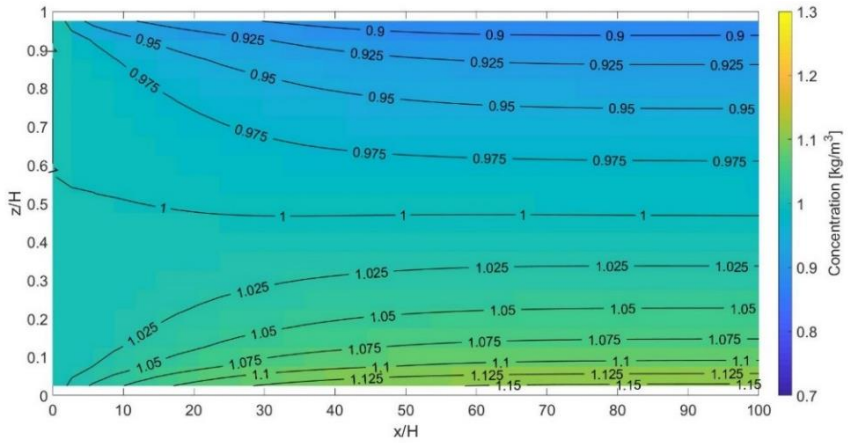

(b) D3D

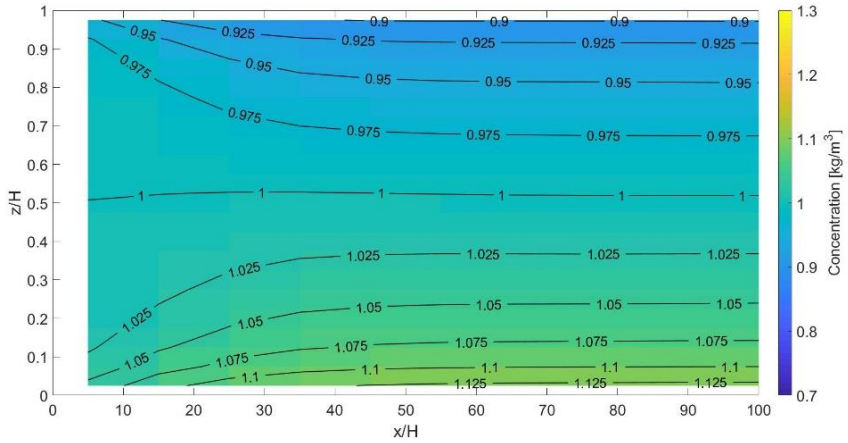

Figure 4-4. Concentration distribution of the initial 100 m of (a) the Lagrangian 1DV model and (b) the Delft3D model for Experiment ST-UC.

4.2.2 Experiment STD-UC (settling, turbulent mixing, deposition - uncoupled models)

This experiment is a variation of Experiment ST-UC, but now including full deposition, with the Partheniades-Krone formulation (Partheniades, 1965) in both models (this formulation is described in Appendix C). The hydrodynamics were the same as in Experiment ST-UC. A very high value of $\tau_{cr,d}$ $\left(\tau_{cr,d} = 1000\ Pa\right)$ was defined to ensure full deposition. Then, the deposition rate D was not sensitive to the bed shear stress $(D = w_s c_b)$. The deposition rate varies along the channel because the near-bed concentration c_b also varies.

For uniform steady flow, the depth H and the depth-averaged velocity $\bar{u}$ are constant along the channel. Then, the change of the depth-averaged sediment mass flux q_s is reflected in a change of the depth-averaged concentration:

$$\frac{dq_s}{dx} = \bar{u}\,H\frac{d\bar{c}}{dx} = -w_s c_b \rightarrow \frac{d\bar{c}}{dx} = \frac{-w_s c_b}{\bar{u}H} \tag{4.7}$$

Assuming that c_b equals the concentration at the reference height c_a and that the vertical concentration profile instantaneously tends to the Rouse profile (approximation as the profile is not strictly in equilibrium), for 20 layers $(a = 0.025\ H)$:

$$\frac{d}{dx}\left[\frac{c_a}{H}\int_0^H \left(\frac{H-z}{z}\frac{0.025H}{d-0.025H}\right)^{\frac{\sigma_T w_s}{\kappa u_*}} dz\right] = \frac{-w_s}{\bar{u}H}\, c_a$$

An approximate discrete calculation was done assuming that the initial c_b was equal to the near-bed concentration of the equilibrium profile in Experiment ST-UC (c_b = 1.13 kg/m^3). The estimated result for c_b at x=1000 m was 0.366 kg/m^3.

Figure 4-5 shows the concentration profiles at x=1000 m for both models. The concentration near the bed was close to the estimated value for both models. The Lagrangian 1DV model showed a slightly higher deposition rate (below 1% difference). The estimated near-bed concentration for the Lagrangian 1DV model was 0.367 kg/m^3, while for the Delft3D model a value of 0.369 kg/m^3 was obtained (difference below 1% between the models).

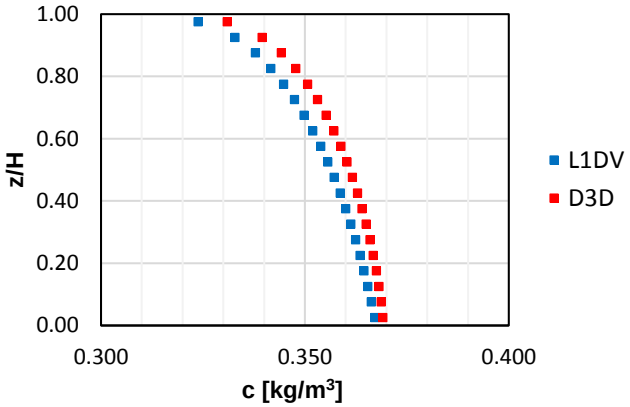

Figure 4-5. Concentration profiles for the Lagrangian 1DV model (L1DV) and Delft3D model (D3D) at x=1000 m for Experiment STD-UC

4.2.3 Experiment STE-UC (settling, turbulent mixing, erosion - uncoupled models)

The hydrodynamics were the same as in Experiment ST-UC. A value of 1 Pa was defined as critical shear stress for erosion $\tau_{cr,e}$. A value of 0.0001 was used for the erosion parameter. Deposition was turned off by establishing a critical shear stress for deposition of $\tau_{cr,d} = 0\ Pa$. The Partheniades-Krone formulation (Partheniades, 1965) was used in both models.

In a case with erosion and no deposition, the depth-averaged mass flux varies along x at an erosion rate E. In uniform steady flow, the depth H and the depth-averaged velocity $\bar{u}$ are constant along the channel. Then, the change of the depth-averaged sediment mass flux q_s along the channel is reflected in a change of the depth-averaged concentration:

$$\frac{dq_s}{dx} = \bar{u}\,H\frac{d\bar{c}}{dx} = E \rightarrow \frac{d\bar{c}}{dx} = \frac{E}{\bar{u}H}$$
$$\rightarrow \bar{c}(x) = \bar{c}_0 + \frac{E}{\bar{u}H}\cdot x \qquad (4.8)$$

For a theoretical value for the bed shear stress τ_b of 2.25 Pa, the estimated erosion rate E was 1.25 x 10^{-4} kg/(m^2/s). Then, a depth-averaged concentration $\bar{c}$ of 1.125 kg/m^3 was expected at x = 1000 m, from (4.4).

Figure 4-6 shows the obtained results from the models. The depth-averaged concentration at x=1000 m was 1.11 kg/m^3 for the Lagrangian 1DV model and 1.14 kg/m^3 for the Delft3D model. These values were close to the theoretical value of 1.125 kg/m^3.

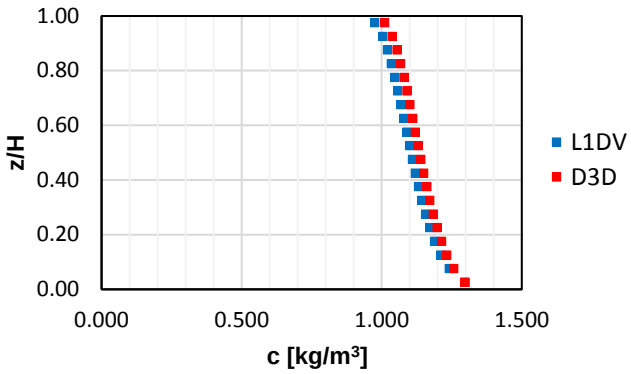

Figure 4-6. Concentration profile for the Lagrangian 1DV model (L1DV) and Delft3D model (D3D) at x=1000 m for Experiment STE-UC

The small difference in the results is consistent in magnitude with the results for the velocity profile for uniform flow, from Experiment ST-UC. The velocity of the lowest layer in the Delft3D model was 2% higher than the theoretical value. The bed shear stress, calculated with this velocity, was then 4% higher than the theoretical one resulting in an erosion rate of 1.1 x 10^{-4} kg/m^2/s. The velocity of the lowest layer in the Lagrangian 1DV model was 2% lower than the theoretical value. The bed shear stress, calculated with this velocity, was then 4% lower than the theoretical one resulting in an erosion rate of 1.1 x 10^{-4} kg/m^2/s.

Differences in the bed shear stress and the velocity of the lowest layer are influenced by differences in the bed friction formulation between the models. Both models estimate velocity as:

$$\frac{u}{u_*} = \frac{1}{\kappa} ln\left(\alpha + \frac{z}{z_0}\right)$$

The Lagrangian 1DV model uses a value of $\alpha = 9$, as in Kranenburg (2013). Delft3D-FLOW uses a value of $\alpha = 1$.

It is important to remark here that, for this set of experiments, the deposition and erosion rates were in the same order of magnitude. However, in WID applications, the near-bed concentrations are one or two orders of magnitude higher than 1 g/l. Deposition rates increase in a linear proportion with the near-bed concentration, so they become one or two orders of magnitude larger than the erosion rates. Hence, the next sections of the study do not focus on the erosion process.

4.2.4 Experiment ST-C (settling, turbulent mixing – coupled models)

This experiment included the same processes as Experiment ST-UC (settling and turbulent mixing). Now, the effect of sediment on the fluid density was considered, for a low concentration of 1 kg/m^3. The velocity and concentration profiles of both models at the uniform stage (x = 500 m) are presented in Figure 4-7.

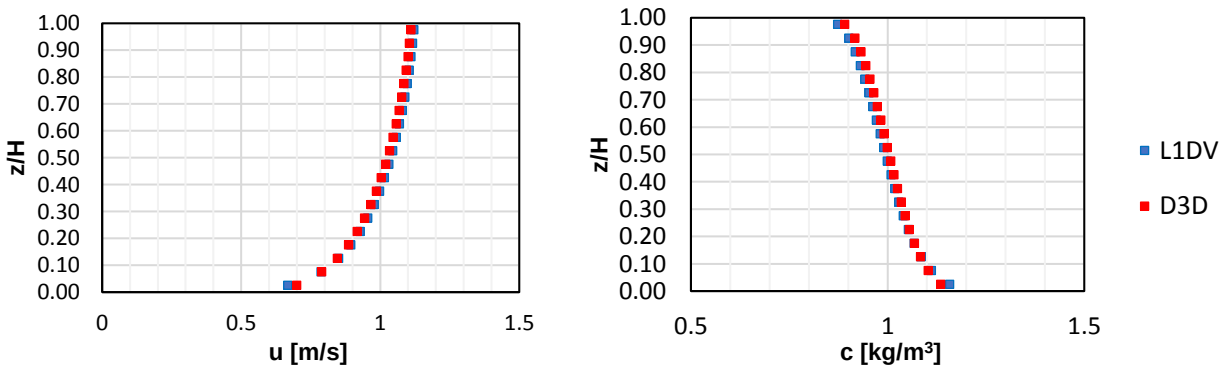

Figure 4-7. Velocity and concentration profiles for the Lagrangian 1DV model (L1DV) and the Delft3D model (D3D) at x=500 m for Experiment ST-C

The results were very close to the Experiment ST-UC results, which was expected due to the small density differences. Differences in velocities were below 0.7% at every level, while differences in concentration were below 0.6%. The near-bed velocity decreased by 0.4% in both models, compared to the uncoupled case.

4.2.5 Experiment STD-C (settling, turbulent mixing, deposition – coupled models)

This experiment was a variation of Experiment STD-UC, but considering the effect of sediment on fluid density (coupled models).

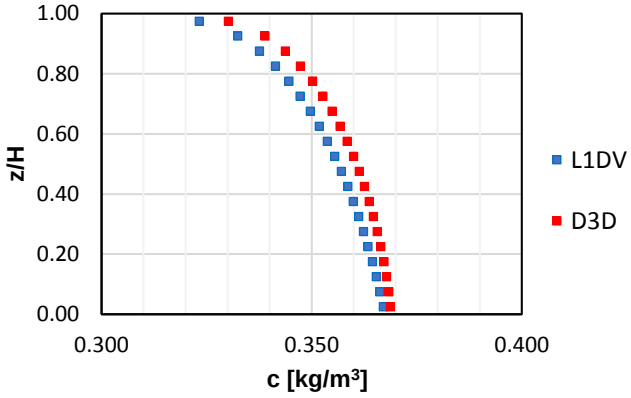

Figure 4-8. Concentration profiles for the Lagrangian 1DV model (L1DV) and the Delft3D model (D3D) at x=1000 m for Experiment STD-C

The difference between the Lagrangian 1DV model and the Delft3D in the near-bed concentration was below 0.5%. Compared to the uncoupled model, the depth-averaged concentration of the Lagrangian 1DV model decreased by 0.5% at x=1000 m. A decrease of 0.5% in the depth-averaged concentration was also observed for the Delft3D model compared to the uncoupled model at x = 1000 m. This means that considering the effect of sediment on fluid density (for a very low concentration) produced a similar and very small effect on the deposition rate for both models.

4.2.6 Experiment STE-C (settling, turbulent mixing, erosion – coupled models)

No important differences in the concentration profiles were identified with respect to the uncoupled version of the models (Experiment STE-UC). The depth-averaged concentration at x=1000 m decreased 0.1% in the Lagrangian 1DV model and 0.1% in the Delft3D model. Less erosion in both models is consistent with the decrease of the near-bed velocity that was identified in Experiment ST-UC.

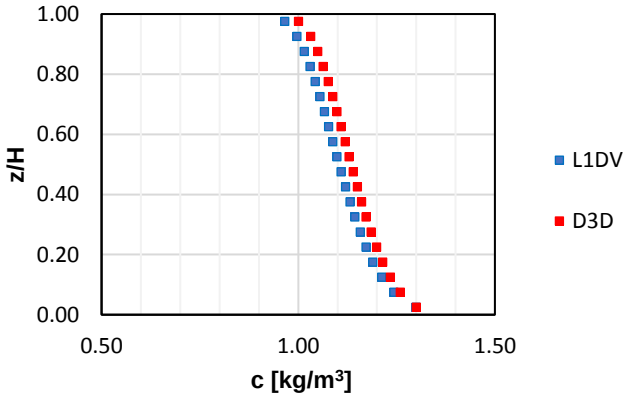

Figure 4-9. Concentration profiles for the Lagrangian 1DV model (L1DV) and the Delft3D model (D3D) at x=1000 m for Experiment STE-C

4.2.7 Summary

General conclusions can be obtained from the set of experiments for steady uniform flow in a channel:

a. The Lagrangian 1DV model and the Delft3D model performed in good agreement with the analytical solution for the uncoupled models.

b. The formulations and parameters for settling, turbulence, turbulent mixing, and deposition produced almost the same results in both models.

c. There was a small difference in the bed shear stress between the models that was reflected in differences in the erosion rates. The bed shear stress and the erosion rate were slightly higher for the Delft3D model, for the same bed slope, z_0, $\bar{u}$ and H.

d. The concentration of the models was low as well as the corresponding density differences ($\partial\rho/\partial z \approx 0$). Hence, the influence of the baroclinic pressure gradient in the models was not reflected in significant differences between the coupled models. The baroclinic pressure gradient was then increased for Experiments Set 2.

e. The non-uniform stage of the first ~70 m did not produce any significant difference between the results of the models. Part of the minimal differences observed between the coupled models may be a result of this non-uniform reach.

f. In general, there was no significant difference between the velocity and concentration profiles obtained with the 2DV approach and the Lagrangian 1DV approach. This was expected because the setup of the Delft3D model fulfilled the uniform flow assumption (in the Eulerian reference frame) of the Lagrangian 1DV model.

4.3 Experiments Set 2: Non-uniform flow in a channel

The objective of this set of experiments was to compare the solution for velocity and concentration of the Lagrangian 1DV model and the Delft3D model in Eulerian non-uniform conditions and to identify and understand the origin of the differences between the Lagrangian 1DV approach and the Eulerian 2DV approach.

The geometrical setup of the Delft3D model was the same as in Set 1 (bed slope of 2.4 x 10^{-4} and length of the studied domain of 1000 m). The downstream boundary conditions in the Delft3D model were also the same. Table 4-2 summarizes the main parameters of the models.

Table 4-2. Models' parameters for Set 2 (Non-uniform flow in a channel).

Parameter	Lagrangian 1DV model	Delft3D model
Time step [s]	0.3	0.3
Vertical layers	20	20
Bed slope [-]	2.4x10^{-4}	2.4x10^{-4}
Water depth H [m]	1	1
Domain length L [m]	1000	1000
Roughness length z_0 [m]	6.5 x 10^{-5} for uncoupled models Increased for coupled models	6.5 x 10^{-5} for uncoupled models Increased for coupled models
Vertical eddy viscosity ν_T [m^2/s]	From k-ϵ model	From k-ϵ model
Vertical eddy diffusivity Γ_T [m^2/s]	From k-ϵ model	From k-ϵ model
Background eddy viscosity ν_{BCK} [m^2/s]	1 x 10^{-4}	1 x 10^{-4}
Background eddy diffusivity Γ_{BCK} [m^2/s]	1 x 10^{-4}	1 x 10^{-4}
Downstream boundary conditions	-	$H = 1\ m$
Upstream boundary conditions	Described for each case	Described for each case

The initial depth-averaged concentration $\bar{c}$ was increased to 10 kg/m^3 to be able to observe the effect of sediment in the non-uniformity of flow and the differences that it causes between the models.

The bed roughness length (z_0=6.5 x 10^{-5} m) was the same for the uncoupled models. For the coupled models, z_0 had to be increased to maintain a water depth of 1 m in the Delft3D model, because the increase of concentration reduces the velocity gradient near the bed and, consequently, reduces the bed friction. A reduction of bed friction produces a decrease in the water level, compared to the uncoupled version of the models.

Three velocity profile shapes for the slurry are available in the Lagrangian 1DV model (Deltares, 2019):

- Logarithmic: this velocity profile corresponds to turbulent boundary layer flow with a free surface on its upper boundary (Deltares, 2019).
- Double-log: it occurs for turbulent flow between an upper and lower boundary (no free surface)
- Hybrid: as indicated by Deltares (2019), it is similar to the velocity profiles found by Parker et al. (1987) and Mastbergen and van den Berg (2003) for turbidity currents. It is a combination of a logarithmic profile at the lower part of the turbidity current and a mixing layer at the upper part, which is described by a hyperbolic tangent function. The height of the mixing layer can be adjusted in the model.

The options for the initial velocity profile are sketched in Figure 4-10. The distance above the bed z is normalized against the initial slurry height h_{fl}.

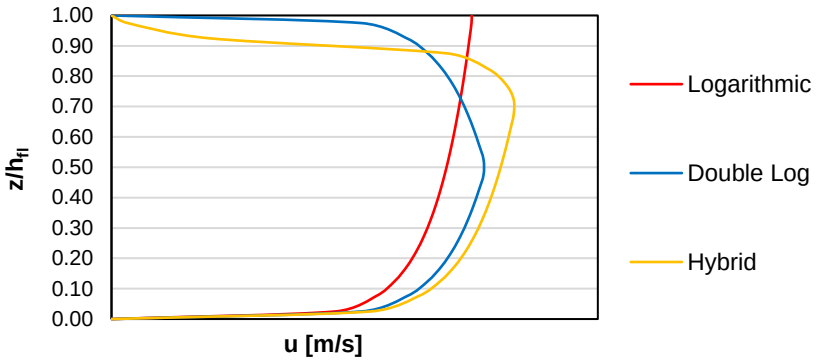

Figure 4-10. Sketch of the available initial velocity profile shapes for the Lagrangian 1DV model

For this set of experiments, the logarithmic profile was selected, which is closer to the velocity profile for uniform flow.

Non-uniformity was generated by the initial concentration profile. The release of sediment with an initial concentration profile different from the equilibrium profile generates (Eulerian) non-uniformity. The experiments were divided into three parts depending on the shape of the initial concentration profile that was selected in the Lagrangian 1DV model (upstream boundary concentration profile in the Delft3D model). Three shapes were tested (these profiles can be chosen in the Lagrangian 1DV model):

- Vertically uniform: constant concentration over the water column
- Linear profile
- Block-shaped profile: constant concentration from the bed up to a certain level (half the depth for these experiments)

Figure 4-11 shows the mentioned profiles. The initial profiles had the same depth-averaged concentration $\bar{c}$ of 10 kg/m^3 and, consequently, the same sediment load m ($= \int c\, dz$) of 10 kg/m^2. The method to define the initial profile in the Delft3D model is described for every experiment. The results

for every profile were obtained first for uncoupled models (UC) and, later, for coupled models (C). In total, six experiments were completed.

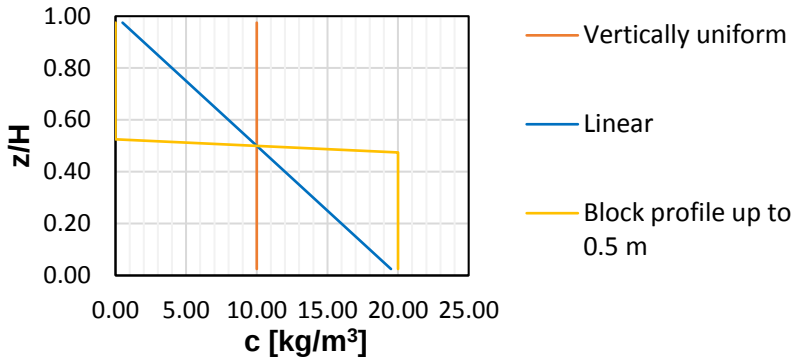

Figure 4-11. Available initial concentration profile shapes for the Lagrangian 1DV model

4.3.1 Experiment ST-UC (vertically uniform initial profile)

Description

The initial profiles were firstly defined in the Lagrangian 1DV model (according to the available functions) and, then, translated to the upstream boundary of the Delft3D model. A vertically uniform initial concentration profile was defined in the input file of the Lagrangian 1DV model, with an average concentration of c_{fl}= 10 kg/m^3, where c_{fl} is the average concentration of the slurry over the slurry height h_{fl}. In this case, the slurry height was equal to the water depth ($H = h_{fl}$ =1 m), then $c_{fl} = \bar{c}$. The depth-averaged velocity $\bar{u}$ was defined as 1 m/s. A logarithmic profile was selected for the initial slurry velocity. The same value was used for the average slurry velocity (u_{fl}= 1 m/s).

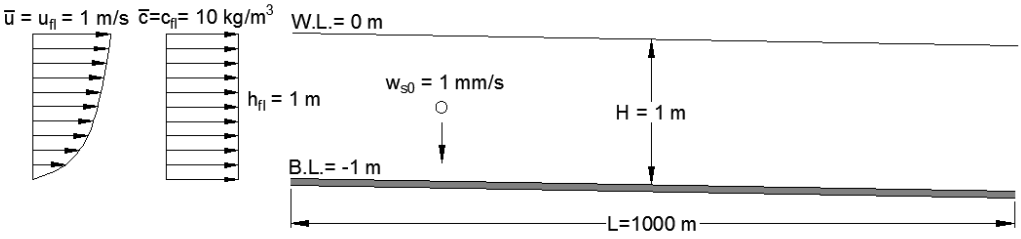

Figure 4-12. Sketch of the Experiment ST-UC (vertically uniform initial concentration profile)

When the Lagrangian 1DV model builds the initial velocity and concentration profiles at t=0 (x=0 in Eulerian coordinates), it conserves the mass and keeps the same mass flux of the initially defined average slurry velocity u_{fl}, average slurry concentration c_{fl} and slurry height h_{fl} (Deltares, 2019). For this purpose, $\bar{u}$ is adjusted at x=0 (or t=0) with the following equation:

$$\overline{u} = \frac{u_{fl}c_{fl} + \overline{\Delta u \Delta c}}{c_{fl}} \tag{4.9}$$

Where Δu is the deviation of $u(z)$ around the depth-averaged velocity $\overline{u}$ and Δc is the deviation of $c(z)$ around the depth-averaged concentration. In the case of this experiment, Δc is zero at every level (the concentration is vertically uniform). Hence, the term $\overline{\Delta u \Delta c}$ is also zero and $\overline{u} = u_{fl}$ =1 m/s. Then, for this particular case, the initial depth-averaged velocity $\overline{u}$ remained as defined in the input file.

Results

Concentration

The concentration distribution in 2DV is shown in Figure 4-13, for the first 100 m from the source.

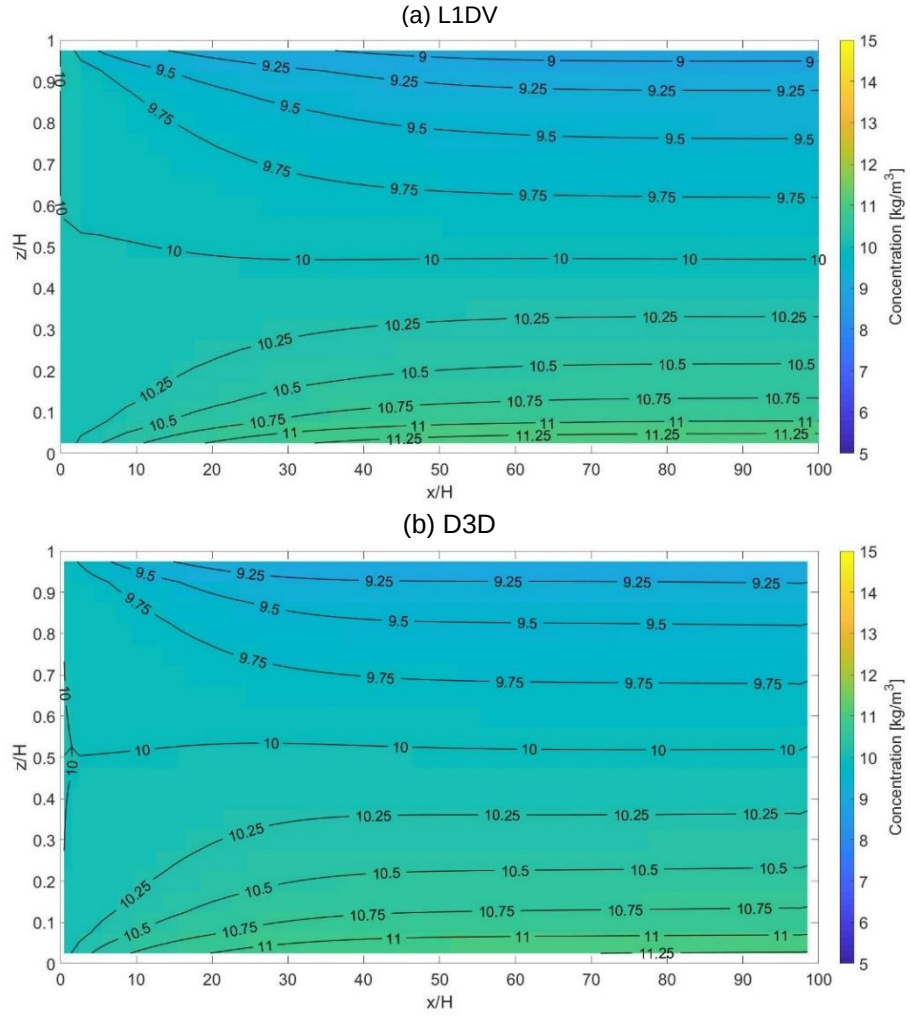

Figure 4-13. Concentration distribution for Experiment ST-UC (vertically uniform initial concentration profile)

The detailed concentration distribution shows that the adaptation length from non-uniform to uniform flow was approximately 60 m for both models. The horizontal concentration gradient $\partial c/dx$ was slightly larger for the Delft3D model than for the Lagrangian 1DV model. To analyze the small differences, the concentration profiles were plotted at 5.5 m, 55.5 m and 105.5 m (Figure 4-14).

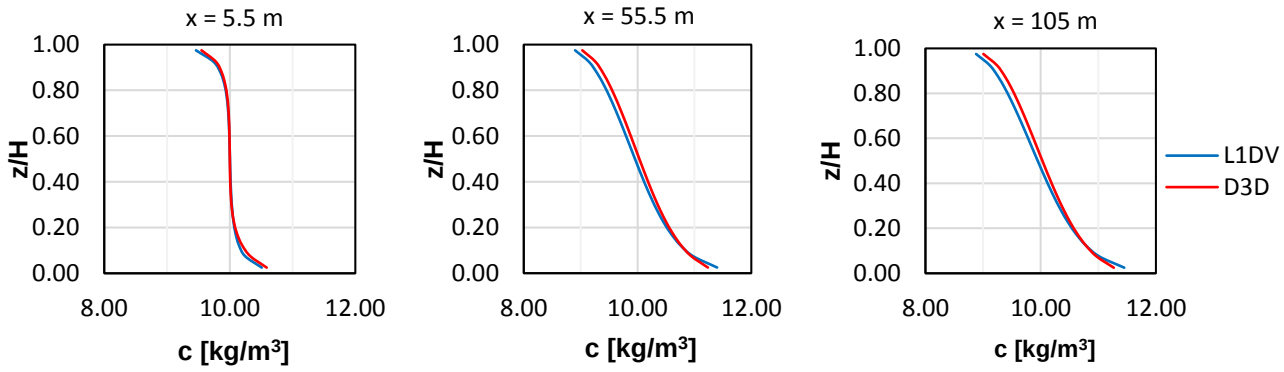

Figure 4-14. Concentration profiles at x=5.5 m, x= 55.5 m and x = 105 m for Experiment ST-UC (vertically uniform initial concentration profile)

The profiles show a small increase of the sediment load m of the Delft3D model from x=5.5 m to x=55.5 m. The sediment load increased by 0.6% and then remained constant. On the other hand, the Lagrangian 1DV model showed a constant sediment load along the channel (this is by definition when there is no erosion or deposition). The increase of sediment load in the Delft3D model along the channel is aligned with the observed higher $\partial c/\partial x$.

The concentration profile at x = 105 m showed a steeper profile for the Delft3D model than for the Lagrangian 1DV model. The concentration for the Delft3D model was higher in the upper part of the water column and lower near the bed.

A possible explanation for the steeper concentration profile is that the friction velocity u_* was slightly higher for the Delft3D model than for the Lagrangian 1DV model for the same roughness length, depth, bed slope, and depth-averaged velocity, as it was mentioned in the previous set of experiments. A higher u_* increases turbulent mixing and, consequently, generates a steeper concentration profile. Figure 4-15 shows the eddy diffusivity profiles at x = 105 m. Consistently with the previous comments, the eddy diffusivity was slightly higher for the Delft3D model. Another sign of higher turbulent mixing was that the adaptation length to uniform flow for the Delft3D model seemed to be slightly shorter in Figure 4-13 (larger $\partial c/\partial x$ in the Delft3D model).

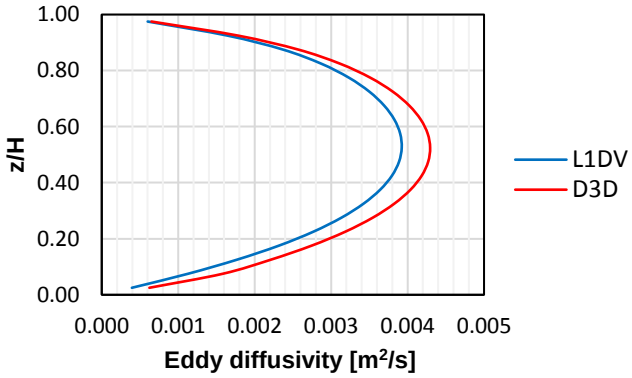

Figure 4-15. Eddy diffusivity at x=105 m for Experiment ST-UC (vertically uniform initial profile)

Velocity

Figure 4-16 shows the velocity profiles at the same stations.

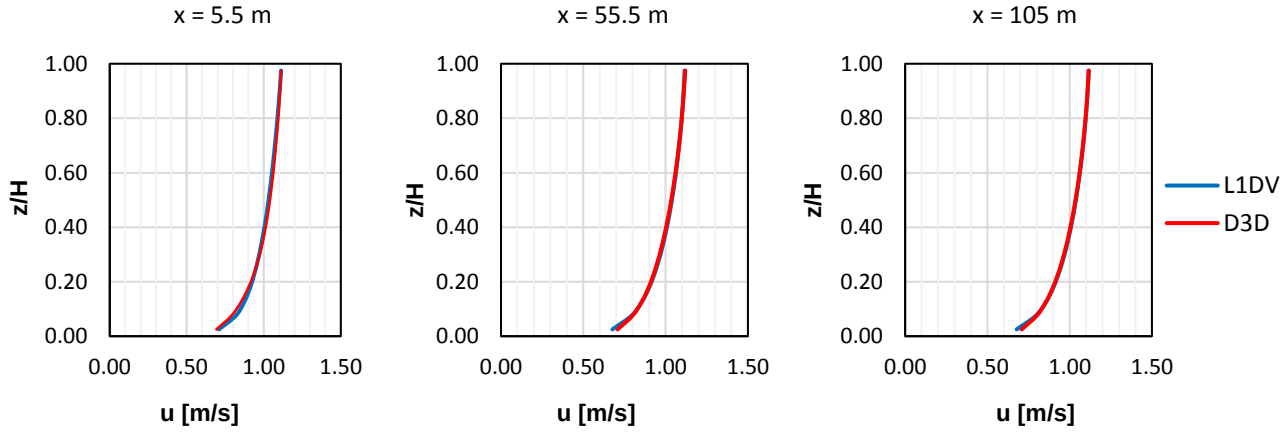

Figure 4-16. Velocity profiles at x=5.5 m, x= 55.5 m and x = 105 m for Experiment ST-UC (vertically uniform initial concentration profile)

The differences in velocity were negligible between the models.

Variation of u_c along the channel

Figure 4-17 shows the variation of u_c along the first 100 m from the sediment source. Here, x refers to the distance from the stationary sediment source.

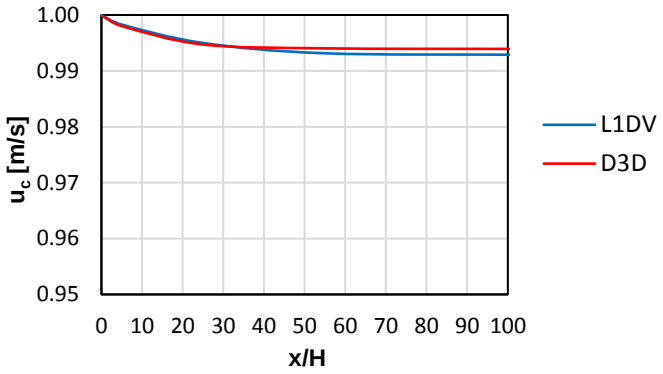

Figure 4-17. Variation of u_c with the distance from the source for Experiment ST-UC (uniform initial concentration profile)

The velocity u_c was 1 m/s in both models at the upstream boundary. In the Lagrangian 1DV model, this is because the initial u_c equals u_{fl} in order to keep the same mass flux from the user-prescribed values. In the Delft3D model, for a vertically uniform initial concentration profile, the initial u_c corresponds to:

$$u_c = \frac{\int_0^H u\, c\, dz}{\int_0^H c\, dz} = \frac{\bar{c}\int_0^H u\, dz}{\bar{c}\int_0^H dz} = \bar{u} = 1\ m/s$$

No significant differences in the value of u_c were observed between the models within 100 m from the source. At a distance of around 60 m, the value of u_c became fairly constant. At that distance, u_c was 0.993 m/s for the Lagrangian 1DV model and 0.994 m/s for the Delft3D model.

The obtained u_c for uniform flow was in agreement with the calculation of u_c for the combination of a logarithmic velocity profile and a Rouse profile:

$$u_c = \frac{\int_{z_0}^H u\, c\, dz}{\int_{z_0}^H c\, dz} = \frac{\frac{u_*}{\kappa}\int_{z_0}^H ln\left(\frac{z}{z_0}\right)\cdot\left(\frac{H-z}{z}\right)^{\beta} dz}{\int_{z_0}^H \left(\frac{H-z}{z}\right)^{\beta} dz}$$

Where:

$$\beta = \frac{\sigma_T w_s}{\kappa u_*}$$

The terms of the Rouse profile related to the reference concentration c_a are constant in the numerator and denominator, so they were canceled. The evaluation of u_c with the specific values for this experiment gave $u_c = 0.994\ m/s$.

A (0.1%) higher u_c for the Delft3D model is consistent with the fact that the concentration profile at the uniform stage presented higher concentrations for the Delft3D model at the upper part of the water column, where velocities are higher.

Mass flux

For stationary flow conditions with no erosion or deposition, the mass flux is constant for the Delft3D model along the channel ($q_s = q_{s0}$=10 kg/s/m). The Lagrangian 1DV model, on the other hand, has a constant sediment load, but the mass flux can vary along the channel (observed in the Eulerian reference frame).

The variation of the mass flux ($q_s = m \cdot u_c$) in the Lagrangian 1DV model is linearly proportional of u_c, because the sediment load m is constant. The mass flux varied in the Lagrangian 1DV model from an initial value of q_{s0}=10 kg/s/m to 9.93 kg/s/m ($= 0.993 q_{s0}$) at the uniform flow stage.

For this experiment, the Lagrangian 1DV model showed a 0.7% lower mass flux than the Delft3D model.

4.3.2 Experiment ST-C (vertically uniform initial profile)

Description

This model is the coupled version of the previous one. The same initial concentration profile as in the previous experiment was used (vertically uniform initial concentration profile with a depth-averaged concentration of $\bar{c}$= 10 kg/m^3). The depth-averaged velocity $\bar{u}$ (1 m/s), the average slurry velocity (u_{fl}= 1 m/s) and the height of the slurry (h_{fl}=1 m) were also the same as in the previous experiment. A logarithmic profile was selected again for the initial slurry velocity, as shown in Figure 4-18.

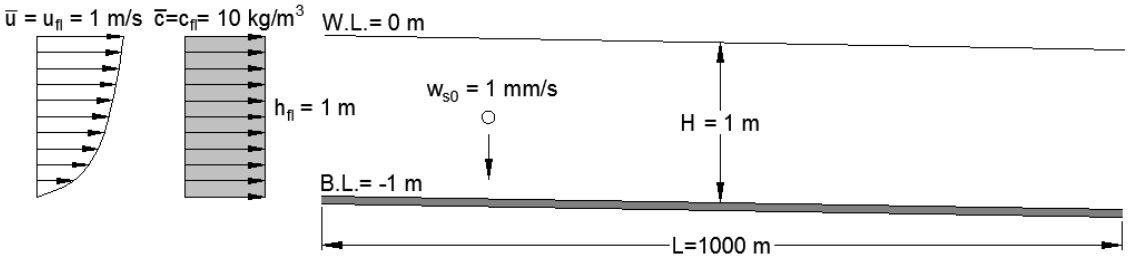

Figure 4-18. Sketch of the Experiment ST-C (vertically uniform initial concentration profile)

The same profiles of the Lagrangian 1DV model were defined at the upstream boundary of the Delft3D model, To obtain a water depth of 1 m in the Delft3D model it was necessary to increase z_0 to 8.5 x 10^{-5} m. The same value was then defined for the Lagrangian 1DV model.

The initial depth-averaged velocity at x=0 (or t=0 in the Lagrangian 1Dv model) remained as it was defined in the input file. As in the previous experiment, the adjustment of $\bar{u}$ to conserve mass and keep the same mass flux was not required (no variation of the concentration Δc around the depth-averaged value $\bar{c}$).

Results

Concentration

The concentration distribution in the 2DV field is shown in Figure 4-19, for the first 100 m from the source. The adaptation length from non-uniform to uniform flow was approximately 150 m for the Lagrangian 1DV model and 130 m for the Delft3D model. These were longer distances than the adaptation lengths for the uncoupled model (~60 m).

Above the 10 kg/m^3 contour, the concentration decreased along x (negative $\partial c/\partial x$) for both models. Below that contour, the concentration increased (positive $\partial c/\partial x$). The settling flux was larger than the turbulent diffusive flux until flow became uniform.

The concentration profiles were plotted at 5.5 m, 55.5 m and 105 m (Figure 4-19) to observe the evolution of the concentration along the channel in the non-uniform stage.

(a) L1DV

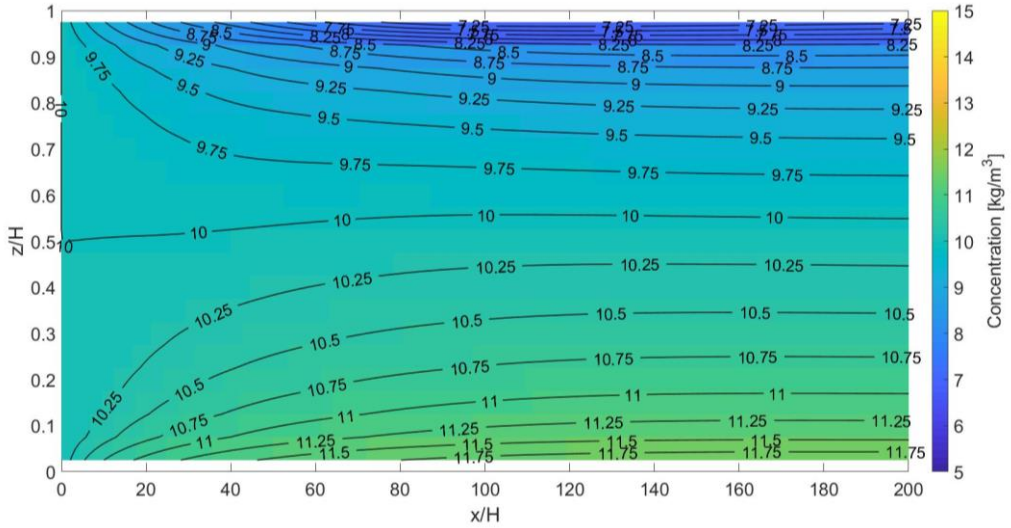

(b) D3D

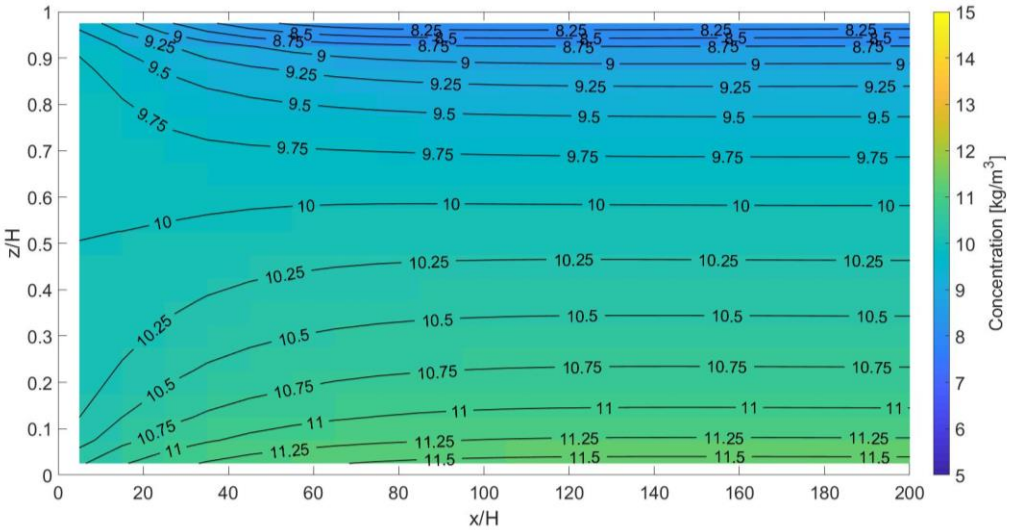

Figure 4-19. Concentration distribution for Experiment ST-C (vertically uniform initial concentration profile)

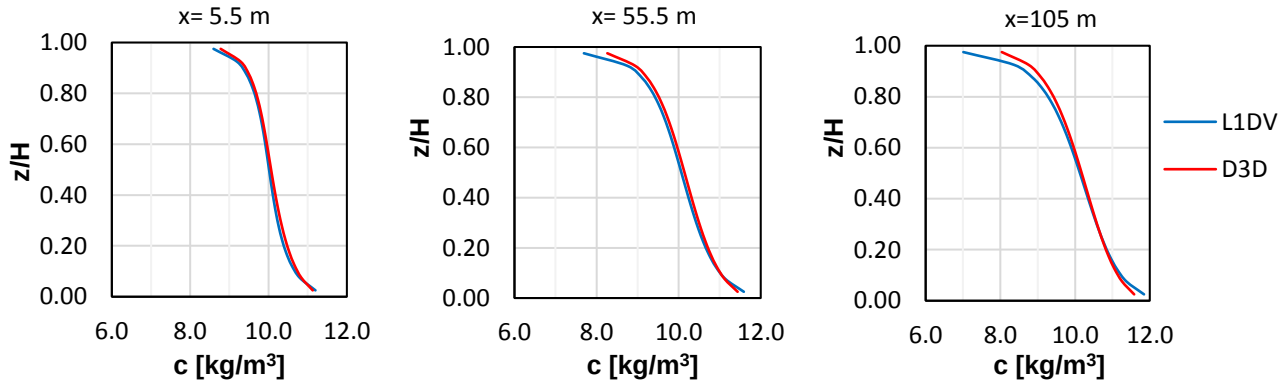

Figure 4-20. Concentration profiles at x=5.5 m, x= 55.5 m and x = 105 m for Experiment ST-C (vertically uniform initial concentration profile)

The horizontal concentration gradient $\partial c/dx$ was slightly larger for the Lagrangian 1DV model. It was more negative for the upper part of the water column and higher (positive) for the lower part. Then, the profiles show a higher concentration in the Delft3D model at the upper part of the water column and a lower concentration near to the bed.

A small increase of the sediment load m of the Delft3D model was observed from x=0 m to x=105 m. The sediment load increased by 1% and then remained constant. On the other hand, the Lagrangian 1DV model showed a constant sediment load along the channel (this is by definition when there is no erosion or deposition).

To eliminate the effect of the sediment load increase along the channel in the Delft3D model of Figure 4-21, the concentration from both models was multiplied by the ratio of the initial sediment load to the sediment load at the specific station m_0/m $(c' = c \cdot m_0/m)$.

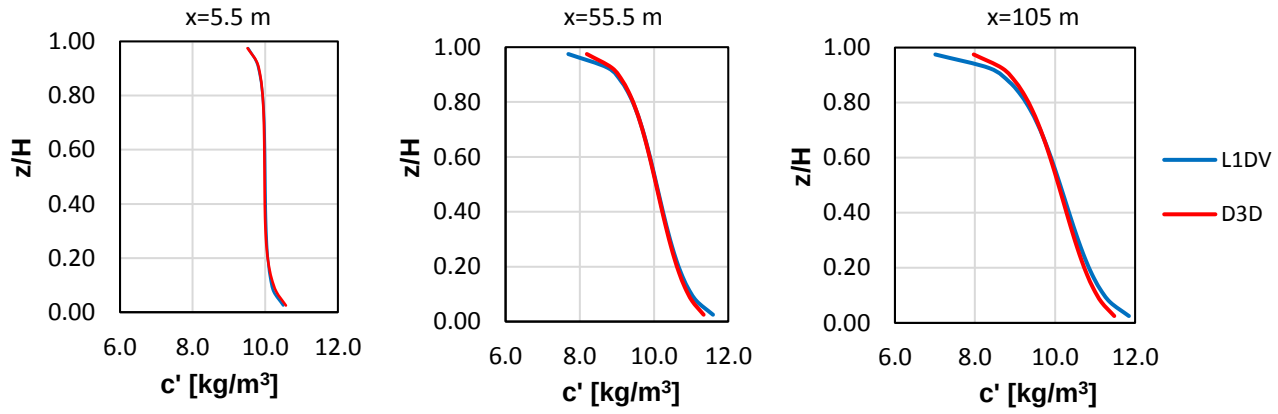

Figure 4-21. Profiles of normalized concentration at x=5.5 m, x= 55 m and x = 105 m for Experiment ST-C (vertically uniform initial concentration profile)

The differences in concentration between the models showed the same trend: higher horizontal concentration gradient (more negative) for the Lagrangian 1DV model at the upper part of the water column, and higher $\partial c/\partial x$ (positive) at the lower part.

Velocity

Figure 4-22 shows the velocity profiles at the same stations.

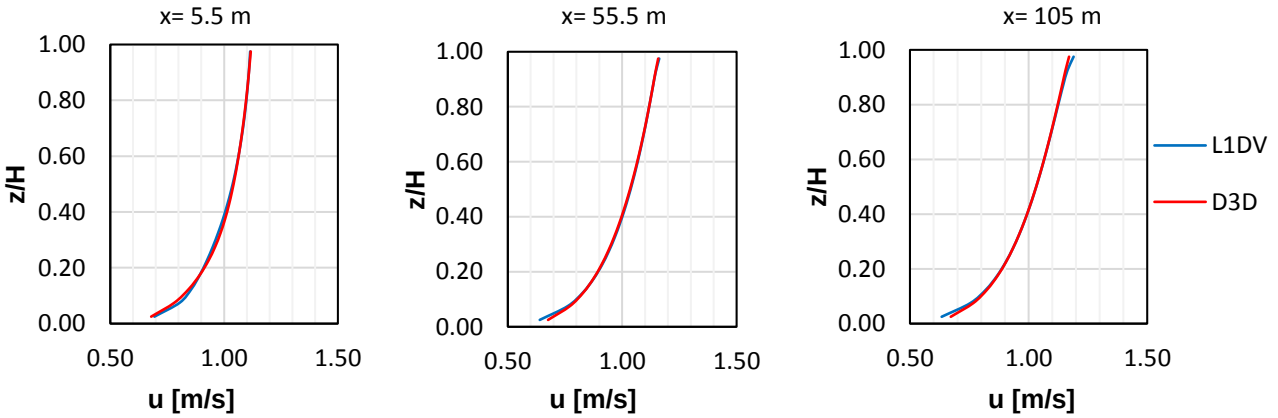

Figure 4-22. Velocity profiles at x=5.5 m, x= 55.5 m and x = 105 m for Experiment ST-C (vertically uniform initial concentration profile)

Along the channel, the profile deviated slightly from the initial logarithmic function. The velocity increased in the upper part of the water column and decreased near the bed. The near-bed velocity decreased more for the Lagrangian 1DV model. This is consistent with a larger positive $\partial c/\partial x$, which produces a larger deceleration of the flow in that region.

Variation of u_c along then channel

Figure 4-23 shows the variation of u_c along the channel for both models.

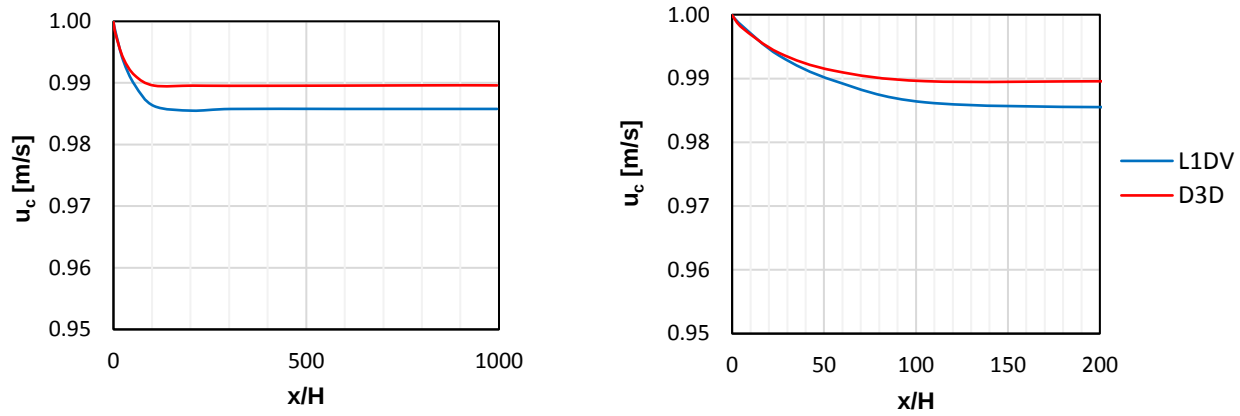

Figure 4-23. Variation of u_c with the distance from the source for Experiment ST-C (uniform initial concentration profile) from x = 0 m to x = 995 m (left) and from x = 0 m to x = 200 m (right).

For the same reasons as in the previous experiment, both models started with an u_c value of 1 m/s. In the Lagrangian 1DV model, u_c became fairly constant at $x \approx$150 m, staying at a u_c value of 0.986 m/s). This value remained constant downstream (corresponding to uniform flow). For the Delft3D model, the velocity decreased for the first ~130 m to a value of 0.990 m/s and stayed constant downstream from that station.

It is observed that u_c was lower for the Lagrangian 1DV model along the channel. This is consistent with the observed concentration profiles, which showed higher concentrations for the Delft3D model at the upper part of the water column, where velocities are higher.

Additionally, the difference in u_c between the coupled models increased compared to the difference in u_c between the uncoupled ones.

Mass flux

The mass flux varied in the Lagrangian 1DV model from an initial value of q_{s0}=10 kg/s/m to 9.86 kg/s/m ($= 0.986 q_{s0}$) at x=150 m. Meanwhile, the mass flux was constant along the channel for the Delft3D model ($q_s = q_{s0}$=10 kg/s/m). For this experiment, the mass flux was lower for the Lagrangian 1DV model.

<u>Interpretation of the results for u_c</u>

The c' profiles indicated that $\partial c/\partial x$ was larger (more negative) at the upper part of the water column for the Lagrangian 1DV model. To interpret this result, the sediment transport equations for this set of experiments [(4.2) and (4.4)] were analyzed. In the case of this set of experiments, the bed slope was very small. Therefore, the vertical velocity w was also very small. Then, $\partial c/\partial x$ became a function of the vertical gradient of the net vertical sediment flux J_c (sum of the settling flux and the turbulent diffusive flux):

$$u_c \frac{\partial c}{\partial x} = \frac{\partial J_c}{\partial z} = \frac{\partial (w_s c)}{\partial z} + \frac{\partial}{\partial z}\left(\Gamma_T \frac{\partial c}{\partial z}\right) \qquad \text{Lagrangian 1DV model}$$

$$u \frac{\partial c}{\partial x} = \frac{\partial J_c}{\partial z} = \frac{\partial (w_s c)}{\partial z} + \frac{\partial}{\partial z}\left(\Gamma_T \frac{\partial c}{\partial z}\right) \qquad \text{Delft3D model}$$

The settling velocity w_s is modelled with the same formulation in both models. The eddy diffusivity is calculated in both models with the $k-\epsilon$ model. Finally, $\partial c/\partial z$ is approximately the same for similar

concentration profile shapes. Then, the value of $\partial J_c/\partial z$ should be similar for both models, at least near the sediment source. To confirm this, the net vertical sediment flux J_c was plotted at x=5.5 m.

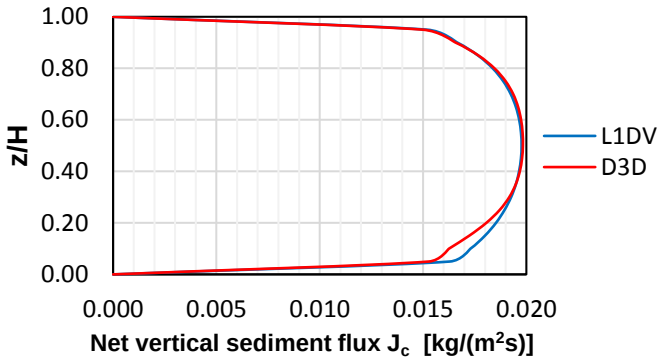

Figure 4-24. Net vertical sediment flux (positive downwards) at x=5.5 m for Experiment ST-C.

The net vertical sediment flux was similar for both models at x = 5.5 m. In both cases, the settling flux governed the net vertical sediment flux (except for a small part near the bed, probably related to initial turbulence conditions). Then, according to Figure 4-24, $\partial J_c/\partial z$ was approximately the same for both models. Then, the following relation was established according to the sediment transport equations of both models:

$$u_c\left(\frac{\partial c}{\partial x}\right)_{L1DV} \approx u\left(\frac{\partial c}{\partial x}\right)_{D3D} \rightarrow \frac{\left[\frac{\partial c}{\partial x}\right]_{L1DV}}{\left[\frac{\partial c}{\partial x}\right]_{D3D}} \approx \frac{u}{u_c} \tag{4.10}$$

At the upper part of the water column (above z/H=0.40 according to Figure 4-22), $u > u_c$ for a logarithmic profile. Then, $\partial c/\partial x_{L1DV}$ should be larger in magnitude (in this case, more negative) than $\partial c/\partial x_{D3D}$. This was observed in Figure 4-20. A larger (more negative) $\partial c/\partial x$ at the upper part of the water column, where settling flux dominated, means that more sediment was transported to the lower part of the water column in the Lagrangian 1DV model than in the Delft3D model. In this case, the lower part of the water column presented lower velocities. Then, the concentration-weighted velocity u_c became lower for the Lagrangian 1DV model than for the Delft3D model, as it was observed in Figure 4-23.

It was analyzed if this reasoning held at a longer distance away from the source. At x=55.5 m, the vertical net sediment flux was not exactly the same for both models along the channel (Figure 4-25), but the results indicate that it was similar enough to keep the explained behavior. The horizontal concentration gradient was larger (more negative) at the upper part of the water column from x=55.5 m to x=105 m. The net vertical sediment flux was still dominated by settling, as shown in Figure 4-25.

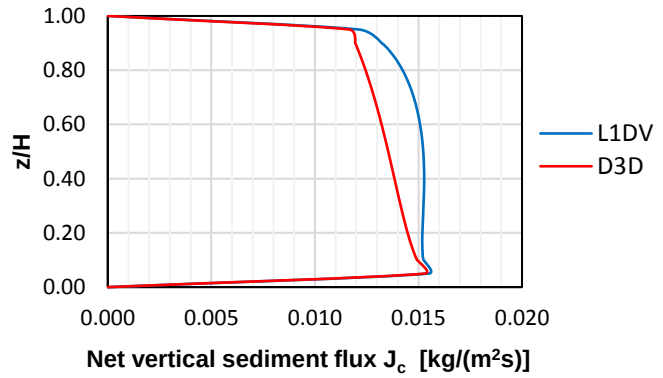

Figure 4-25. Net vertical sediment flux (positive downwards) at x=55.5 m for Experiment ST-C

It is important to remark that the previous interpretation is valid when the baroclinic term in the momentum equation is small so that the differences in the baroclinic pressure gradient (due to differences in $\partial c/\partial x$) do not produce important differences in the velocity profiles between the models. In this case, for a concentration in the order of 10 kg/m^3 and a very small bed slope, the baroclinic term was small and it did not produce a significant difference between the models in the velocity profiles, as shown in Figure 4-22. Then, the differences in u_c could be explained by analyzing only the concentration gradients and leaving the velocity gradients out of the analysis.

4.3.3 Experiment ST-UC (linear concentration profile)

Description

A linear initial concentration profile was prescribed in the Lagrangian 1DV model, with an average slurry concentration of c_{fl}= 10 kg/m^3 (Figure 4-26). A logarithmic profile was selected for the initial velocity. The same values as in the previous experiments were defined for the depth-averaged velocity, the average slurry velocity u_{fl}, and the height of the slurry h_{fl}. Again, the slurry height was equal to the water depth ($H = h_{fl}$ =1 m), then $c_{fl} = \bar{c}$.

A roughness length z_0 of 6.5 x 10^{-5} m was defined to produce a water depth of 1 m in the Delft3D model (this value was used for all the uncoupled models).

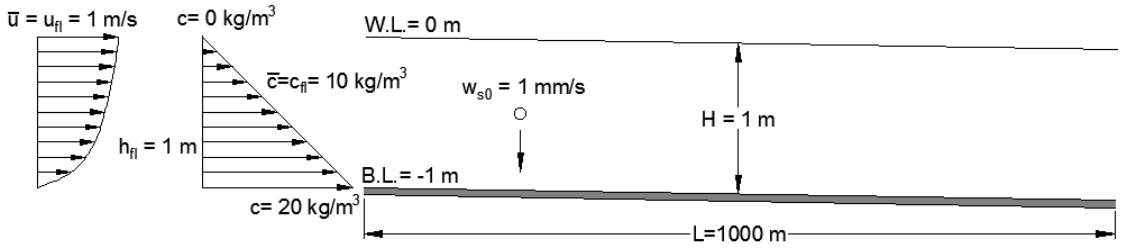

Figure 4-26. Sketch of the Experiment ST-UC (linear initial concentration profile).

In the Lagrangian 1DV model, the depth-averaged velocity $\bar{u}$ was adjusted at x=0 (or t=0) with Equation (4.9). In this case, the deviation Δc of $c(z)$ around the depth-averaged concentration $\bar{c}$ was important. Hence, the Lagrangian 1DV model initially generated a surplus of $\bar{u}$ ($\bar{u} = 1.06$ m/s instead of 1 m/s at x = 0 m, after correction).

At x = 0.10 m, $\bar{u}$ was already back to the user-defined value of $\bar{u} = 1$ m/s. Then, the velocity and concentration profiles of the Lagrangian 1DV model at x = 0.10 m were considered the upstream boundary profiles for the Delft3D model. Running the Delft3D model with the same setup but $\bar{u} = 1.06$ m/s would have produced a backwater curve and a water depth larger than 1 m.

Results

Concentration

The concentration distribution in the 2DV field is shown in Figure 4-27, for the first 300 m from the source.

The adaptation length from non-uniform to uniform flow was approximately 130 m for both models. This length is approximately two times longer than the adaptation length for the vertically uniform initial profile (uncoupled). A linear profile starts with a higher concentration gradient, then, it requires a longer distance to adapt.

The horizontal concentration gradient $\partial c/dx$ was larger for the Delft3D model than for the Lagrangian 1DV model. Part of the explanation for this observation is that from x=0 to x=105 m, the sediment load decreased significantly (5%) along the channel for the Delft3D model.

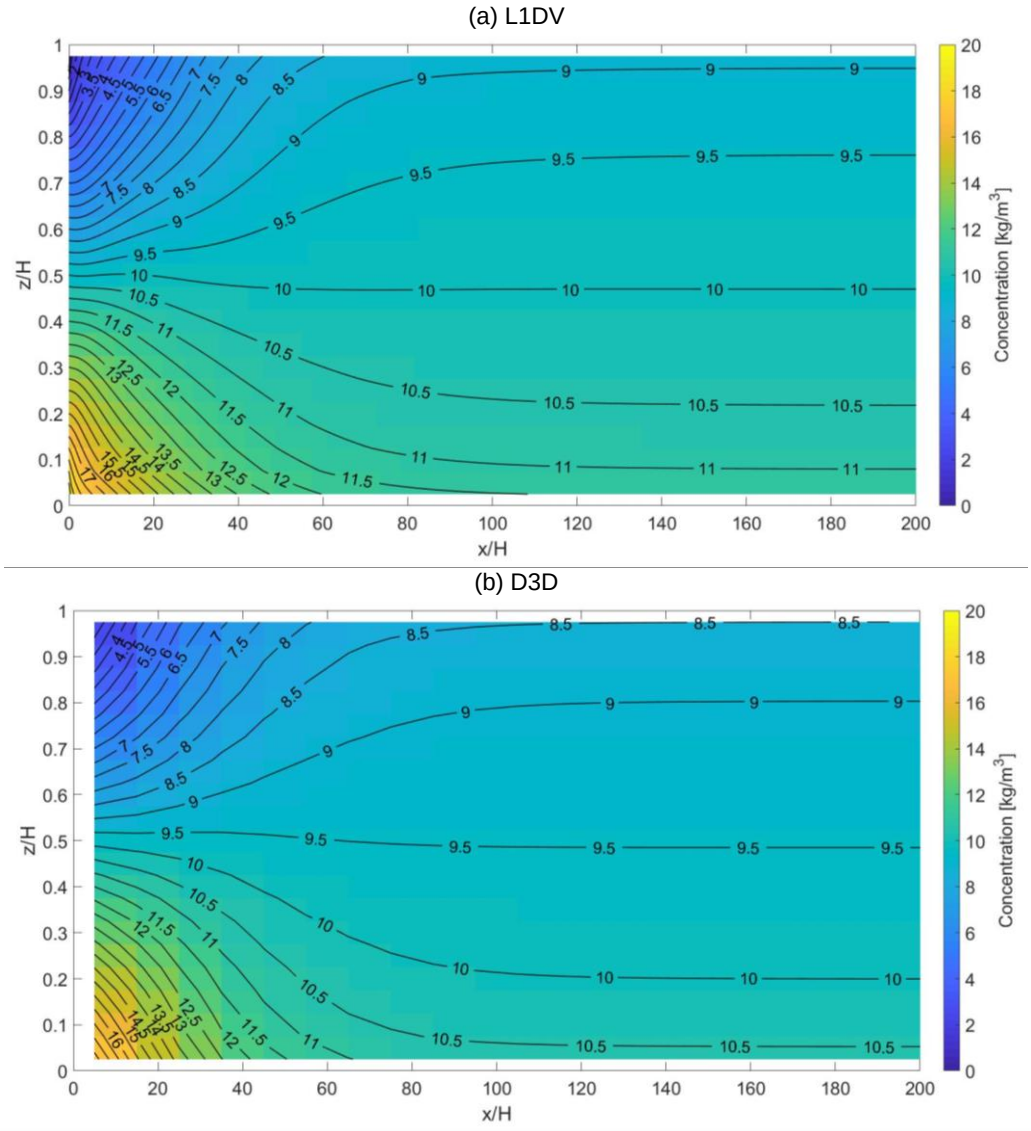

Figure 4-27. Concentration distribution for Experiment ST-UC (linear initial concentration profile).

To analyze in detail the differences, the concentration profiles were plotted at x=5.5 m, 55.5 m, and 105 m (close to uniform, according to Figure 4-27). The profiles show the decrease of the sediment load m of the Delft3D model from x=5.5 m to x=105 m, which is aligned with the larger $\partial c/\partial x$ observed in the Delft3D model.

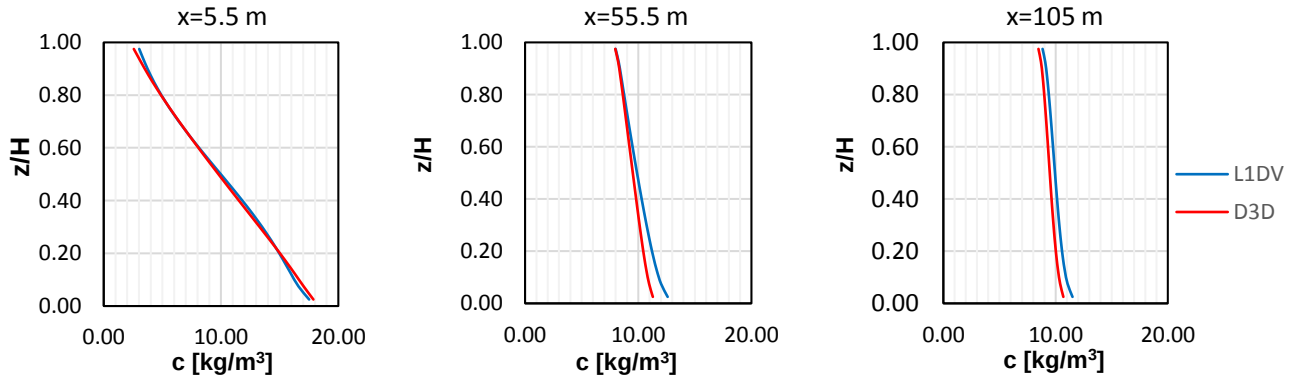

Figure 4-28. Concentration profiles at x=5.5 m, x= 55.5 m, x = 105 m for Experiment ST-UC (linear concentration profile).

Velocity

The difference in velocity between the models was negligible, as it was expected for an uncoupled model. The velocity profiles are the same shown in Figure 4-16, for Experiment ST-UC with a vertically uniform initial concentration profile, because the velocity profile is not affected by sediment concentration in uncoupled models.

Variation of u_c along then channel

Figure 4-29 shows the variation of u_c along the channel for the Lagrangian 1DV and the Delft3D model.

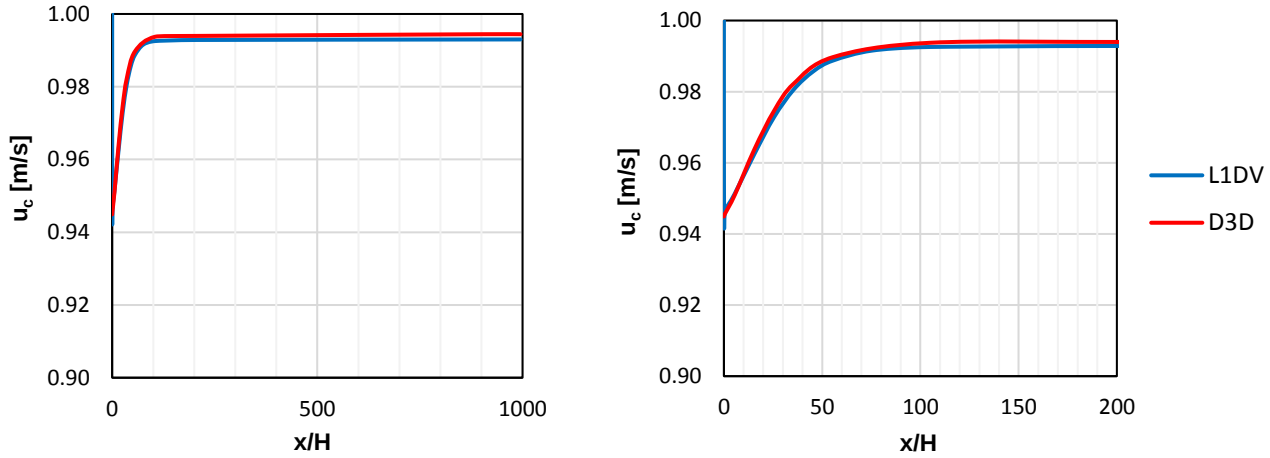

Figure 4-29. Variation of u_c with the distance from the source for Experiment ST-C (linear initial concentration profile) from x = 0 m to x = 995 m (left) and from x = 0 m to x = 200 m (right)

The initial linear concentration profile can be expressed as:

$$c = 2\, c_{fl} \left(1 - \frac{z}{H}\right)$$

Where c_{fl} is the average concentration of the slurry layer. Then, u_c can be expressed as ($z_0 \ll H$):

$$u_c = \frac{\int_{z_0}^{H} ln\left(\frac{z}{z_0}\right)\left(1 - \frac{z}{H}\right) dz}{\int_{z_0}^{H} \left(1 - \frac{z}{H}\right) dz} = \frac{u_*}{2\kappa}\left(2 \cdot ln\left(\frac{H}{z_0}\right) - 3\right)$$

Evaluating for the analyzed case, u_c = 0.94 m/s was obtained. When the flow becomes uniform, u_c approximates to the value of 0.994 m/s, corresponding to the combination of a Rouse profile and a logarithmic velocity profile (same value as the uncoupled model with a vertically uniform initial concentration profile).

It can be observed that the Lagrangian 1DV model started with u_c= 1 m/s ($u_c = u_{fl}$ by definition in the Lagrangian 1DV model). However, as explained above, u_c rapidly adjusted to a lower value of 0.94 m/s, matching the theoretical value for u_c for a combination of a logarithmic velocity profile and a linear concentration profile.

No significant difference was observed between in the variation of u_c along the channel for these models. There was an increase in u_c (acceleration of the mass) for the first ~130 m in both cases, which corresponds to the non-uniform stage of the flow.

As expected, both models converged to a uniform flow condition with the same values of u_c that were observed in Experiment ST-UC with a vertically uniform initial concentration profile (0.993 m/s for the Lagrangian 1DV model and 0.994 m/s for the Delft3D model).

Mass flux

The results for the velocity, concentration and mass flux profiles at the uniform stage (x=205 m) are shown in Figure 4-30.

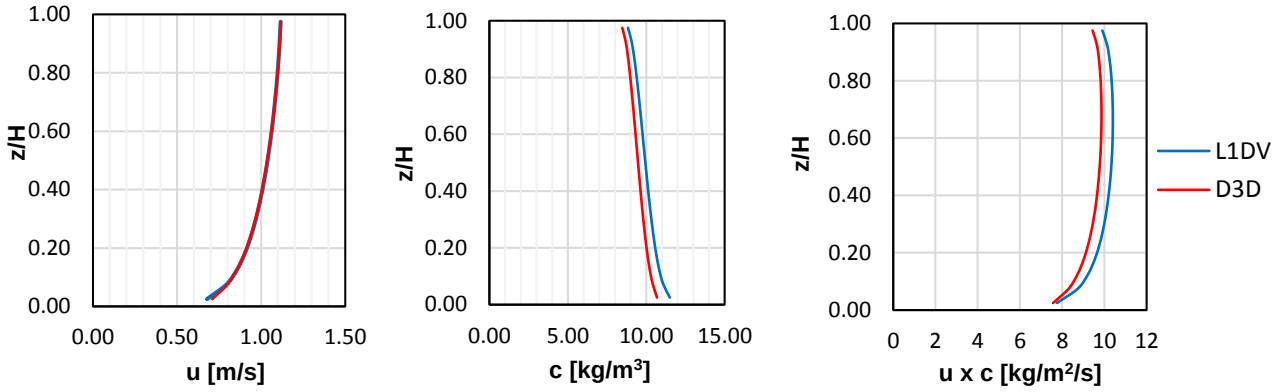

Figure 4-30. Velocity, concentration, and mass flux profiles at x=900 m for Experiment ST-UC (linear initial concentration profile).

The concentration profiles showed that the sediment load decreased along the channel for the Delft3D model. This produced a higher mass flux in the Lagrangian 1DV model. However, as the sediment load decreased, u_c was still higher for the Delft3D model.

The mass flux decreased in the Lagrangian 1DV model from an initial value of q_{s0}=10 kg/s/m to 9.4 kg/s/m ($= 0.94q_{s0}$) at x=0.10 m and later increased to 9.93 kg/s/m. Meanwhile, in the Delft3D model, the mass flux was a constant q_{s0}=10 kg/s/m. The Lagrangian 1DV model underestimated the mass flux along the channel, for this experiment.

4.3.4 Experiment ST-C (linear concentration profile)

Description

This experiment was done with coupled models. The same initial concentration profile as in the previous experiment was used for the Lagrangian 1DV model (linear initial concentration profile with an average slurry concentration of c_{fl}= 10 kg/m^3). The initial depth-averaged velocity $\bar{u}$, the average slurry velocity (u_{fl}= 1 m/s) and the height of the slurry (h_{fl}=1 m) were also the same as in the previous experiment. A logarithmic profile was selected again for the initial slurry velocity. Finally, to obtain a water depth of 1 m in the Delft3D model, it was necessary to increase z_0 to 0.0001 m. The increase of roughness was applied in both models.

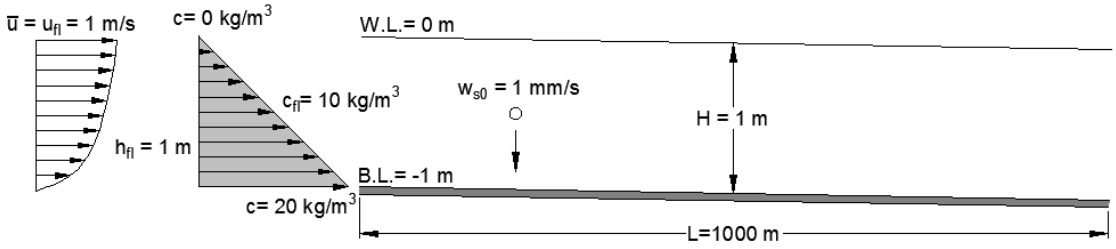

Figure 4-31. Sketch of the Experiment ST-C (linear initial concentration profile).

The same procedure of the previous experiment was applied to define the upstream boundary velocity and concentration profiles in the Delft3D model. The profiles at the upstream boundary of the Delft3D model were the same as the profiles at x=0.10 m for the Lagrangian 1DV model.

Results

Concentration

Figure 4-32 shows the concentration distribution for both models for the first 400 m from the source.

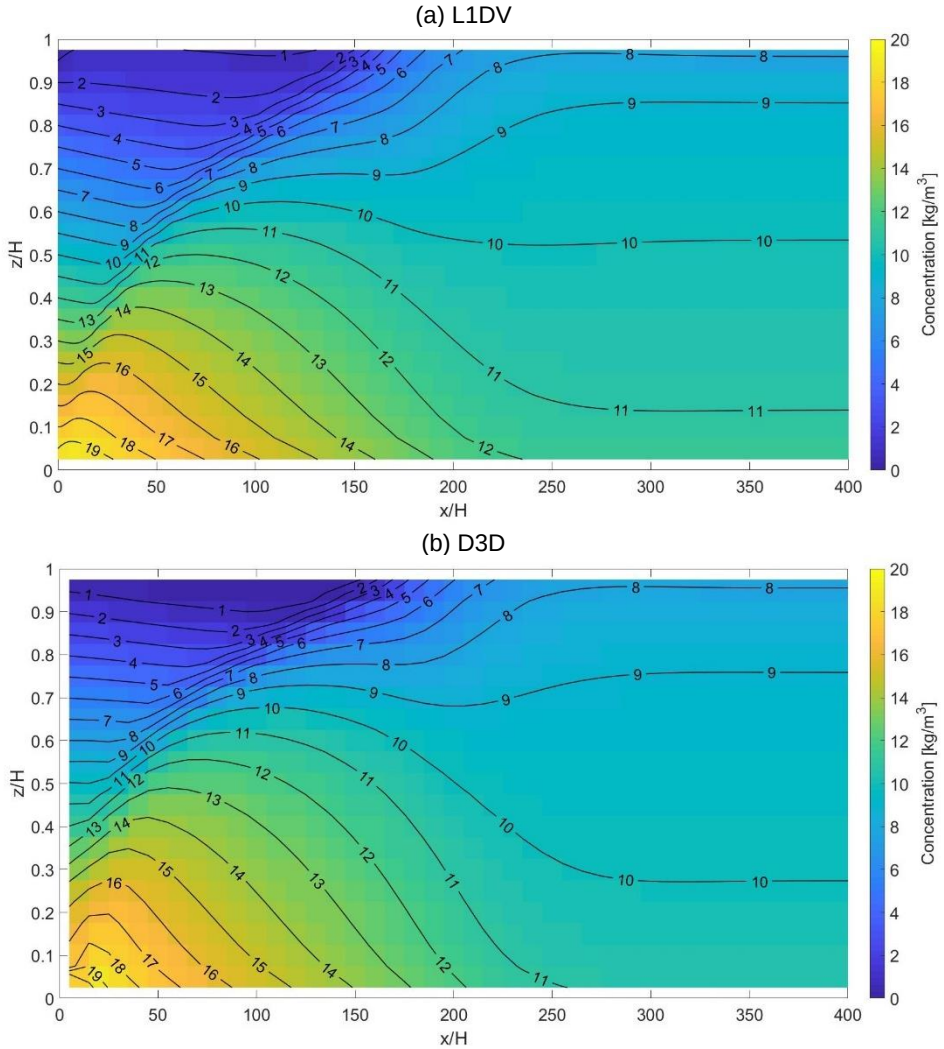

Figure 4-32. Concentration distribution for Experiment ST-C (linear initial concentration profile)

The adaptation length to uniform flow for the models was approximately 300 m in both models. This is approximately two times the adaptation length for the vertically uniform initial concentration profile (coupled).

Based on the level of the 10 kg/m^3 contour, in the region from the source to x ≈ 100 m, settling flux seemed to be higher than the turbulent diffusive flux. The contour reached a higher level, indicating that concentration increased at lower levels. Downstream, the contour went down again, indicating that the turbulent diffusive flux dominated.

The sediment load increased 4% in the Delft3D model from x=0 to x=50 m and then decreased to 9.5 kg/m^2 (5% decrease from the initial value).

The concentration profiles (Figure 4-33) are shown at x=55.5 m, x=105 m, and x=305 m (fairly uniform). At x=55.5 m, the concentration for the Lagrangian 1DV model was higher below z/H=0.40. The difference decreased at x=105 m. Downstream from x=305 m, the profiles did not show any significant difference between them and they were fairly uniform.

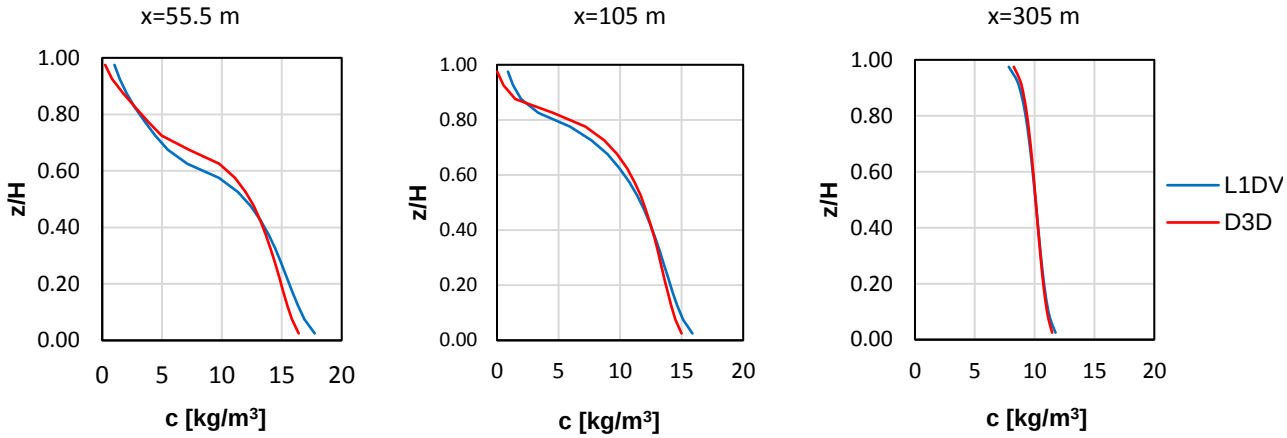

Figure 4-33. Concentration profiles at x=55 m, x= 105 m, and x = 305 m for Experiment ST-C (linear initial concentration profile).

Variation of u_c along then channel

Figure 4-34 shows the variation of u_c along the channel for both models.

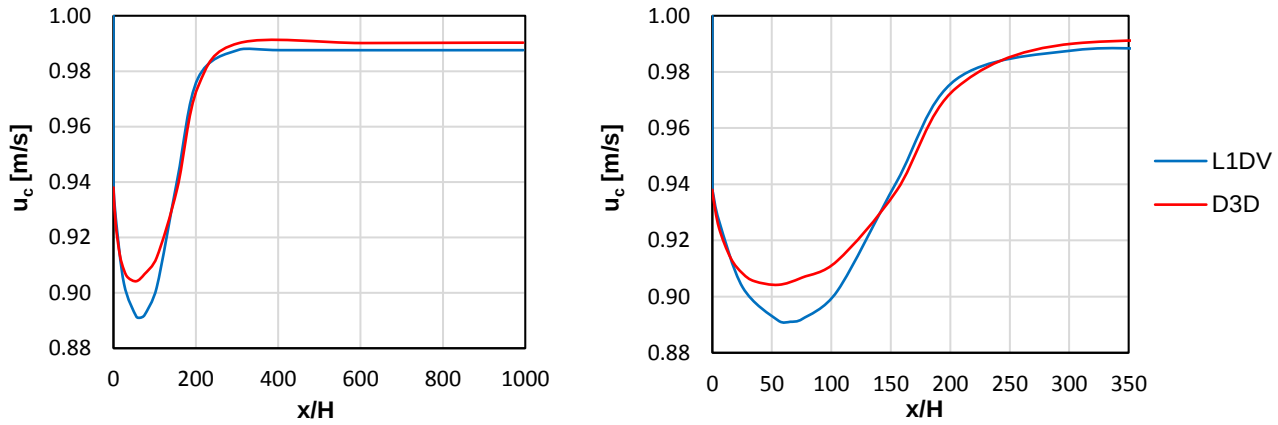

Figure 4-34. Variation of u_c with the distance from the source for Experiment ST-C (linear initial concentration profile) from x = 0 m to x = 1000 m (left) and from x = 0 m to x = 300 m (right).

As in the uncoupled version, the Lagrangian 1DV model presented a u_c value of 0.94 m/s at x=0.10 m. The Delft3D model started with the same value.

It was observed that the magnitude of u_c decreased for both models, compared to the previous experiment (uncoupled). It was observed that when the models were coupled, the concentrations were lower at the upper part of the water column where velocities are higher, producing a lower u_c.

The Lagrangian 1DV model showed a decrease in u_c for the first ~65 m. The minimum value of u_c was 0.891 m/s. After that point, the sediment mass accelerated. The velocity increased up to a value of 0.988 m/s. Finally, u_c reached a fairly constant value at x ≈ 300 m. The velocity u_c of 0.988 m/s for uniform flow was also obtained in the Experiment ST-C for a vertically uniform initial concentration profile. When the input parameters are the same and there is no erosion or deposition, the velocity and concentration profiles when the flow is uniform are independent of the shape of the initial profile.

The Delft3D model showed similar behavior. A decrease in u_c occurred for the first ~55 m. The minimum value of u_c was 0.904 m/s (1.5% higher than the minimum value for the Lagrangian 1DV model). Finally, u_c reached a fairly constant value of 0.990 m/s at x ≈ 300 m. The value of 0.990 m/s was also the result for u_c at the uniform flow stage of Experiment ST-C for a vertically uniform initial concentration profile.

Mass flux

The mass flux varied in the Lagrangian 1DV model from an initial value of q_{s0}=9.4 kg/s/m to 8.9 kg/m/s as u_c decreased. Then, it increased to 9.9 kg/s/m at x≈300 m and remained constant. Meanwhile, the Delft3D model conserved the initial mass flux of q_{s0}=9.4 kg/s/m. At the uniform flow stage, the mass flux was higher for the Lagrangian 1DV model. The mass flux in the Lagrangian 1DV model was lower from x=0 to x=150 m.

Interpretation of the results for u_c

Following a similar reasoning to analyze the origin of the difference as in Experiment ST-C for a vertically uniform initial profile, the concentration and the net vertical sediment flux profiles were analyzed at x=5.5 m.

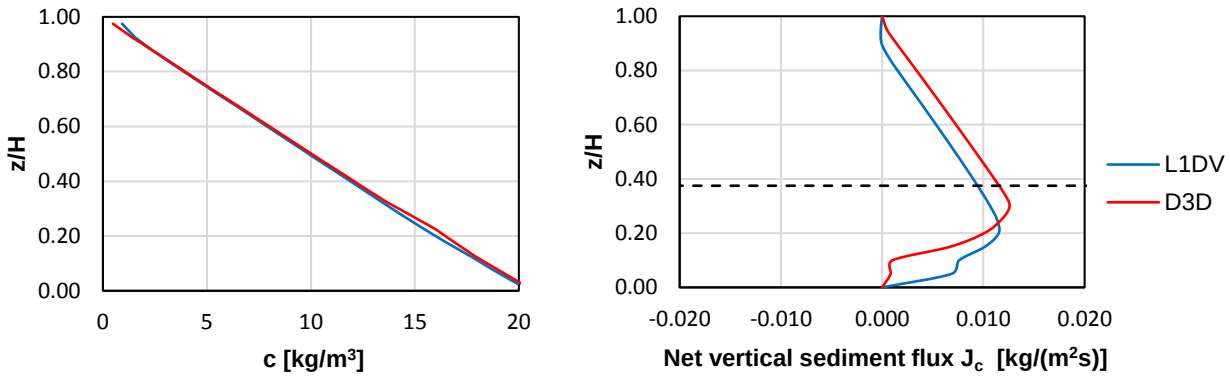

Figure 4-35. Concentration and net vertical sediment flux (positive downwards) profiles at x=5.5 m

The net vertical flux profiles presented a similar shape. The dashed line indicates the level at which $u = u_c$. According to the approximation of relation of (4.10), above the dashed line, $\partial c/\partial x_{L1DV}$ should be larger than $\partial c/\partial x_{D3D}$. As settling governed in the region above the dashed line (net vertical flux goes downwards), this means that, for a certain horizontal distance, more sediment was transported to the region below the dashed line in the Lagrangian 1DV model than in the Delft3D model. The result can be observed in the concentration profile at x = 25.5 m (Figure 4-36).

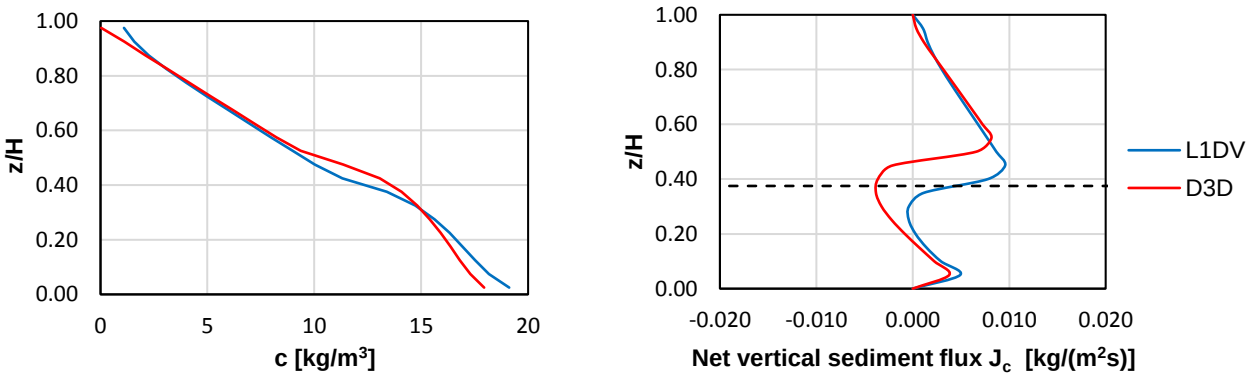

Figure 4-36. Concentration (left) and net vertical sediment flux (positive downwards) profiles at x=25.5 m

Compared to the profile at x=5.5 m, the concentration increased more in the Lagrangian 1DV model at the region below the black dashed line, where velocities were lower. This led to a lower u_c for the Lagrangian 1DV model.

At x=25.5 m, the vertical sediment flux had a positive value above the black dashed line for both models. Then, the net sediment transport was directed downwards. The same behavior was expected: a larger horizontal concentration gradient (more negative) for the Lagrangian 1DV model above the dashed, resulting in more sediment transported downwards for a certain horizontal

distance, from the region of higher velocities to the region of lower velocities. Consequently, a lower u_c in the Lagrangian 1DV model was expected.

The concentration profile at x=55.5 m confirmed this expectation (Figure 4-37).

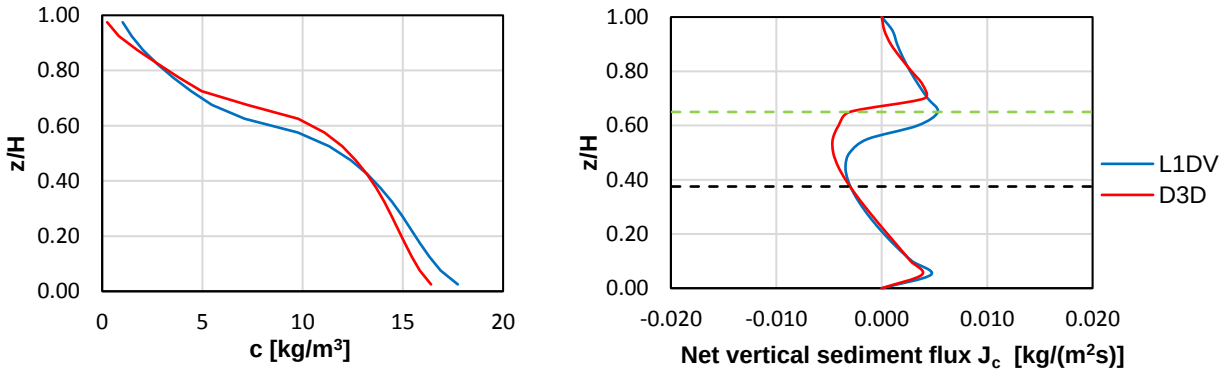

Figure 4-37. Concentration (left) and net vertical sediment flux (positive downwards) profiles at x=55.5 m

At x=55.5 m, above the black dashed line there were now two regions divided by a green dashed line. Above the green dashed line, settling dominated. The height of the region where settling dominated decreased compared to the previously analyzed stations. From this region, more sediment was transported downwards in the Lagrangian 1DV model than in the Delft3D model. Below the green dashed line and above the black one, turbulent diffusion dominated. With a larger negative $\partial c/\partial x_{L1DV}$, this means that, from this region, more sediment was transported upwards in the Lagrangian 1DV model.

With a similar amount of sediment being transported above and below the green dashed line, the sediment above the black dashed line seemed to be close to an equilibrium. This explains why, approximately at this station, the difference in u_c between the models stopped increasing.

Finally, at x=155 m (Figure 4-38), the difference in u_c between the models was very small, which is consistent with a governing turbulent diffusive flux in the region above the black dashed line (sediment is kept in that region in both models).

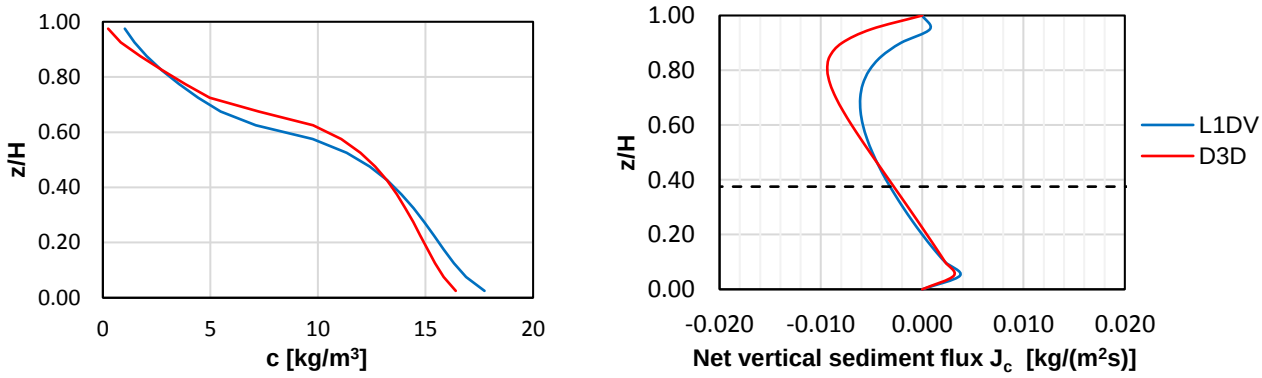

Figure 4-38. Concentration (left) and net vertical sediment flux (positive downwards) profiles at x=155 m.

4.3.5 Experiment ST-UC (block-shaped concentration profile)

Description

A block initial concentration profile was prescribed in the Lagrangian 1DV model, with a vertically uniform concentration of c_{fl} =20 kg/m^3 at the lower half of the water column (h_{fl} =0.5 m) as seen in Figure 4-39. This value was selected in order to have the same sediment load over the water column

of the previous experiments (10 kg/m^2). This was the first experiment in which c_{fl} differed from the initial depth-averaged concentration $\bar{c}$ (10 kg/m^3).

The average slurry velocity u_{fl} was defined as 1 m/s as in the previous experiments. A logarithmic profile was defined for the initial slurry velocity.

Finally, a roughness length z_0 of 6.5 x 10^{-5} m was defined to produce a water depth of 1 m in the Delft3D model (same as the previous uncoupled models).

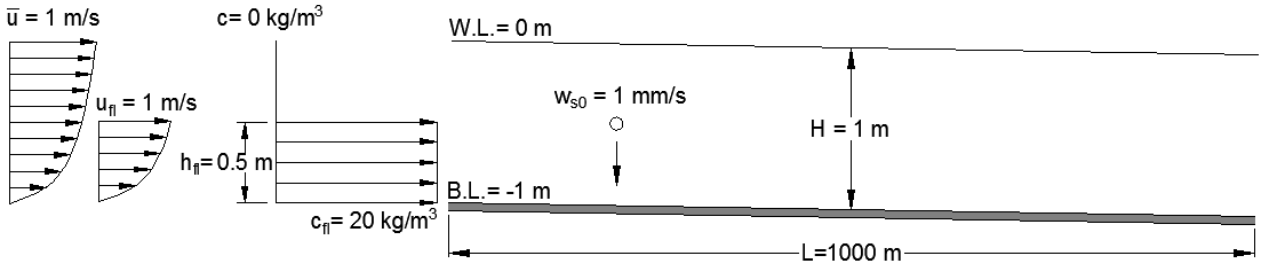

Figure 4-39. Sketch of the Experiment ST-UC (block initial concentration profile).

In the Lagrangian 1DV model, the depth-averaged velocity $\bar{u}$ was adjusted at x=0 (or t=0) with Equation (4.9). For this case, the correction of the velocity profile to conserve mass and mass flux did not generate an increase of $\bar{u}$. However, due to a different definition for the slurry velocity, the corrected velocity profile differed significantly from the one of the previous experiments (Figure 4-40).

Following the same procedure of the experiments with a linear initial velocity profile, the velocity and concentration profiles at the upstream boundary of the Delft3D model were defined to match the initial profiles of the Lagrangian 1DV model at x=0.10 m.

The initial velocity and concentration profiles of the models are shown in Figure 4-40. An important consequence of the definition of the velocity profiles of ambient flow and slurry, in this case, is that the highest velocities are now located at z/H=0.4.

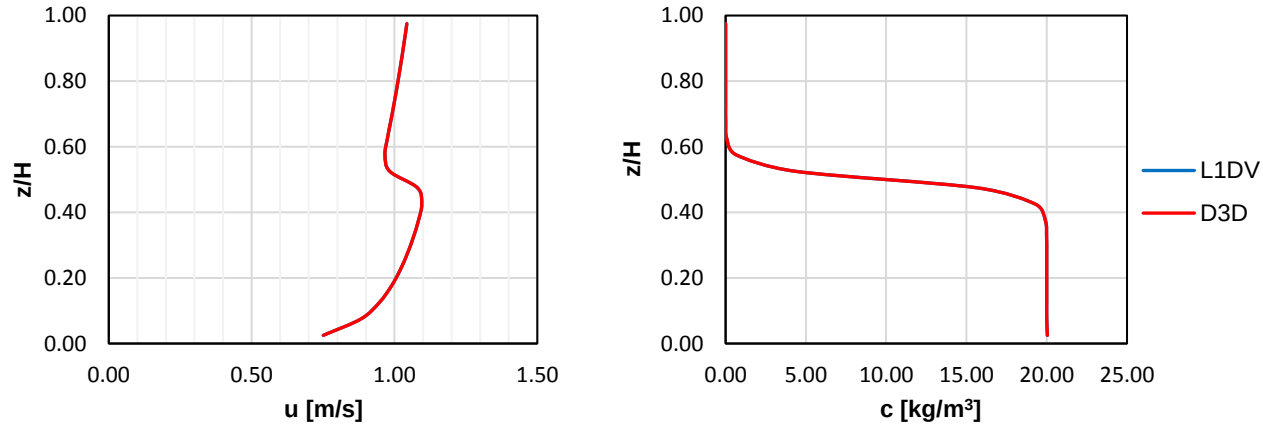

Figure 4-40. Initial velocity and concentration profiles for Experiment ST-UC (block initial concentration profile)

Results

Concentration

The concentration distribution in the 2DV field is shown in Figure 4-41, for the first 100 m from the source.

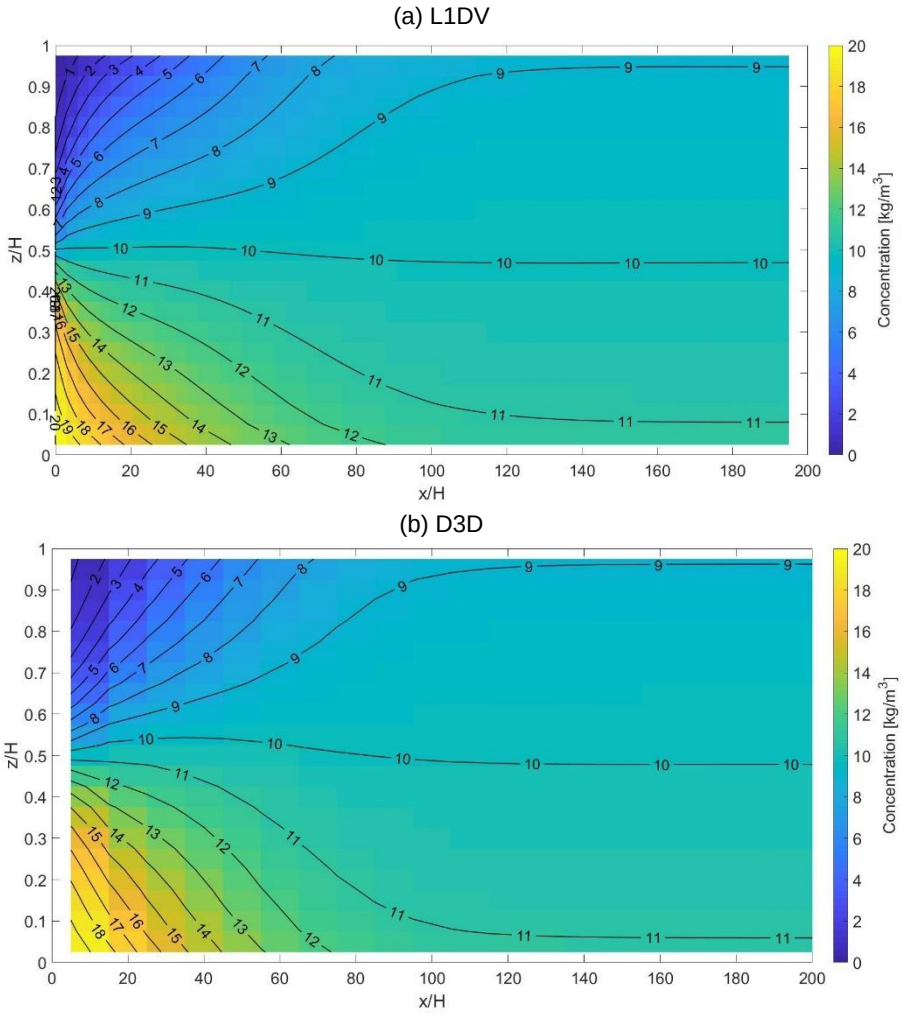

Figure 4-41. Concentration distribution for Experiment ST-C (block-shaped initial concentration profile)

The concentration distribution showed a similar length of adaptation to uniform flow of approximately 160 m. The Lagrangian 1DV model showed a more negative $\partial c/\partial x_{L1DV}$ at the lower half of the water column within the first ~20 m from the source. In that reach of the channel, the Delft3D model experimented an increase in the sediment load of 3%, which in part explains a lower $\partial c/\partial x_{D3D}$. Downstream from that x=20 m, $\partial c/\partial x_{L1DV}$ became less negative than $\partial c/\partial x_{D3D}$. According to Figure 4-41, the upper half of the water column did not present a significant difference in the horizontal concentration gradient. The concentration profiles are shown at x=5.5 m, x=55.5 m, and x=205 m (fairly uniform).

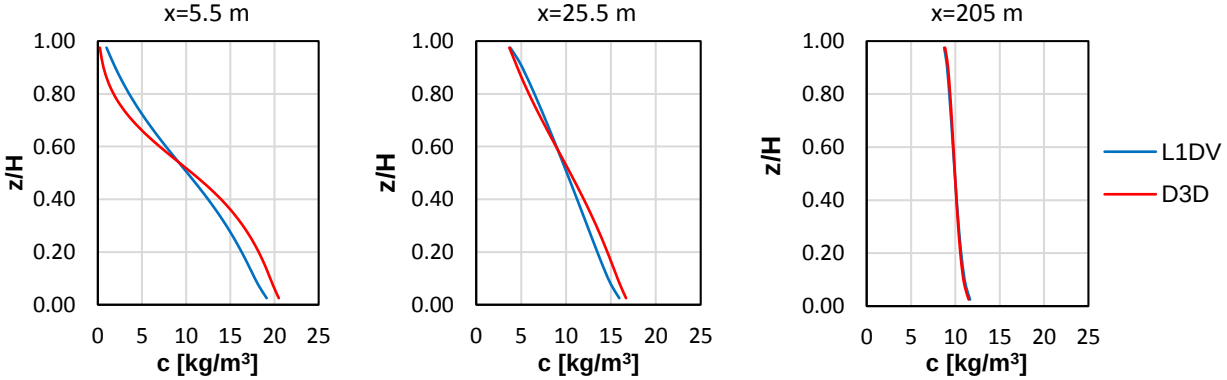

Figure 4-42. Concentration profiles at x=5.5 m, x= 25.5 m, x = 205 m for Experiment ST-UC (linear initial concentration profile).

The profiles are consistent with the previous observations. At x=5.5 m, the Lagrangian 1DV model showed higher turbulent mixing and lower concentration at the lower part of the water column as a result of a more negative $\partial c/\partial x_{L1DV}$ at that region, within the first meters from the source. A higher turbulent mixing may be explained by differences between the models in the initial (or upstream boundary) turbulent kinetic energy profiles.

At x=205 m, the equilibrium profile was obtained, for a sediment load of 10 kg/m^2 in both models.

Velocity

Figure 4-43 shows that the shape of the velocity profile near to the source was in transition from the corrected profile to a logarithmic profile.

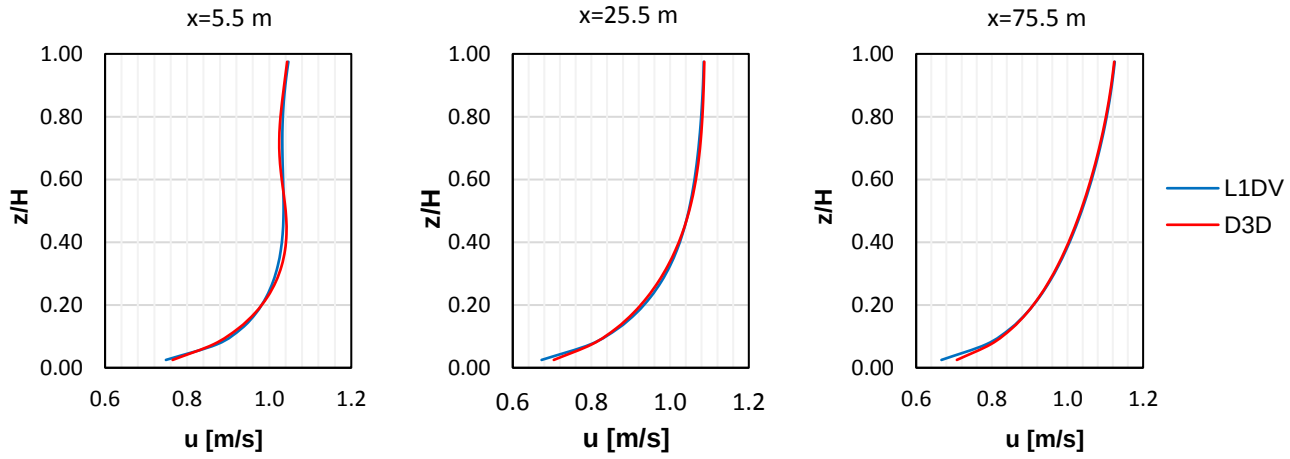

Figure 4-43. Velocity profiles at x=5.5 m, x=25.5 m and x=75.5 m for Experiment ST-C (block-shaped initial concentration profile)

The transition extended approximately 75 m. The observed differences in velocity between the models were not significant (the transition was similar in both models).

Variation of u_c along then channel

Figure 4-44 shows the variation of u_c along the channel for the Lagrangian 1DV and the Delft3D model.

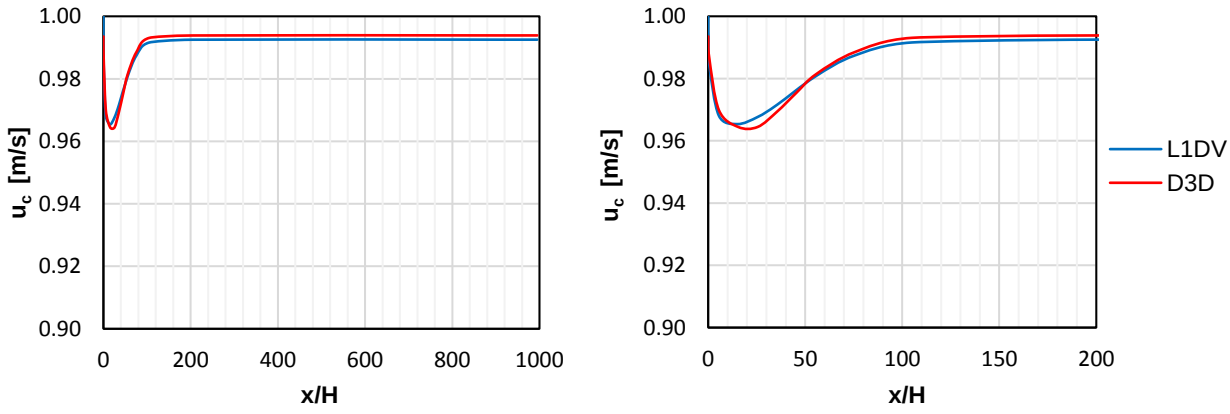

Figure 4-44. Variation of u_c with the distance from the source for Experiment ST-C (block initial concentration profile) from x = 0 m to x = 995 m (left) and from x = 0 m to x = 200 m (right).

It can be observed that the Lagrangian 1DV model started with u_c= 1 m/s (by definition in the Lagrangian 1DV model to keep the same mass flux as defined by the user). The Delft3D model also started with u_c= 1 m/s because the same initial profiles of the Lagrangian 1DV model were defined at its upstream boundary.

The difference in the magnitude of u_c along the channel for both models was not significant. There was a decrease in u_c for the first 15 m in the Lagrangian 1DV model and for the first 20 m in the Delft3D model. The minimum value of u_c in the Delft3D model (0.964 m/s at x=20 m) was slightly shifted to the right, compared to the Lagrangian 1DV model's minimum (0.965 m/s at x=15 m). This could be an effect of a difference in the initial turbulent kinetic energy profile between the models.

Downstream from the stations of minimum u_c, the models transitioned to uniform flow. The sediment mass accelerated and converged to a constant u_c of 0.994 m/s in the Delft3D model and 0.993 m/s in the Lagrangian 1DV model. These were the same velocities for the uniform flow stage of the previous experiments for uncoupled models.

Mass flux

The mass flux decreased in the Lagrangian 1DV model from an initial value of q_{s0}=10 kg/s/m to 9.65 kg/s/m ($= 0.965 q_{s0}$) at x=15 m. Then, it increased up to a value of 9.93 kg/s/m at x=100 m and remained constant. Meanwhile, the Delft3D model mass flux was constant at q_{s0}=10 kg/s/m. The mass flux in the Lagrangian 1DV model was lower than in the Delft3D model for this experiment.

4.3.6 Experiment ST-C (block-shaped initial concentration profile)

Description

This experiment was done with coupled models. The same initial concentration profile as in the previous experiment was defined for the Lagrangian 1DV model (block-shaped initial concentration profile with an average slurry concentration of c_{fl}= 20 kg/m^3). The initial depth-averaged velocity $\bar{u}$, the average slurry velocity and the height of the slurry were also the same as in the previous experiment. A logarithmic profile was selected again for the initial slurry velocity in the Lagrangian 1DV model. Figure 4-45 shows a sketch that describes the experiment.

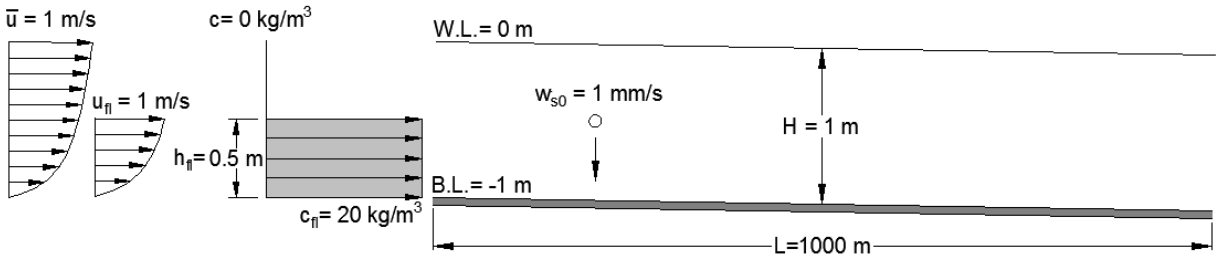

Figure 4-45. Sketch of the Experiment ST-C (block initial concentration profile).

The profiles at the upstream boundary of the Delft3D model were the same as the profiles at x=0.10 m for the Lagrangian 1DV model. The initial profiles are presented in Figure 4-46, as defined in the Delft3D model input. To obtain a water depth of 1 m in the Delft3D model, it was necessary to increase z_0 to 1.1 x 10^{-5} m. The increase of roughness was applied in both models.

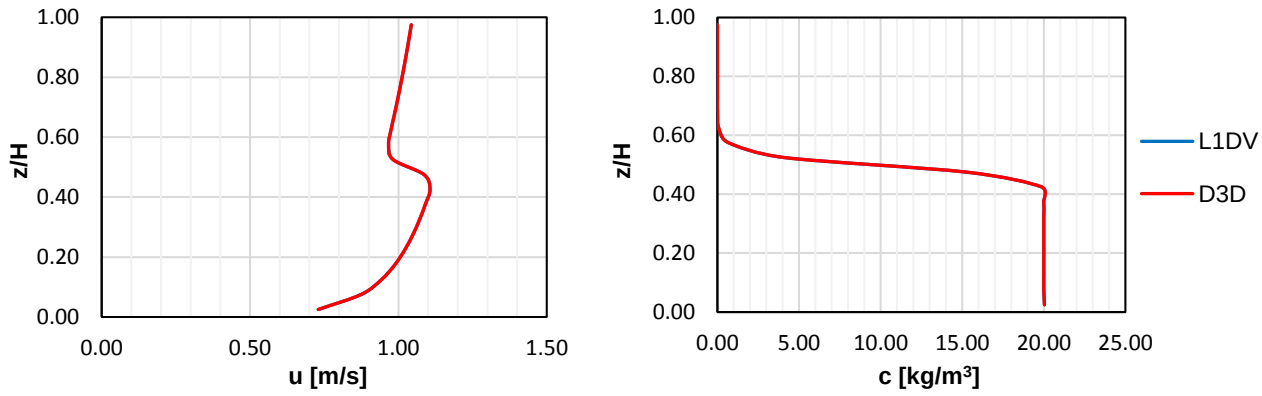

Figure 4-46. Initial velocity and concentration profiles for Experiment ST-C (block initial concentration profile)

Results

Concentration

Figure 4-47 shows the concentration distribution for both models for the first 400 m from the source.

(a) L1DV

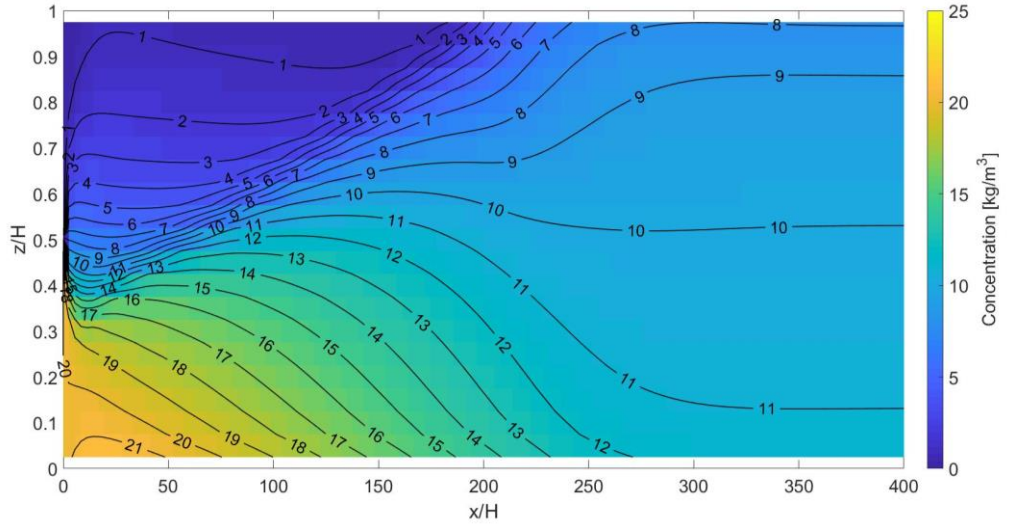

(b) D3D

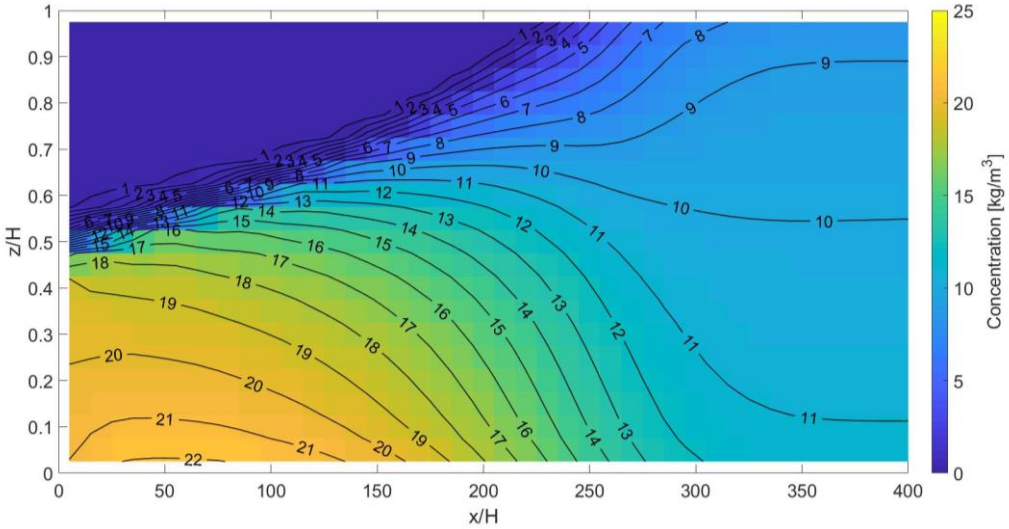

Figure 4-47. Concentration distribution for Experiment ST-C (linear initial concentration profile)

The concentration distribution shows a clear interfacial mixing layer, with a larger vertical concentration gradient for the Delft3D model. The Lagrangian 1DV model showed more initial turbulent mixing, which produced larger concentrations above the mixing layer. This suggests a very large impact on the increase of suspended sediment concentration. The concentration increases near the source at the upper part of the water column. Looking at the contours, the suspended sediment by initial mixing remains suspended at the upper part of the water column for a long distance (especially in this case in which the ambient flow velocity is high).

The Lagrangian 1DV model also presented larger (more negative) concentration gradients from x=0 to x=100 m at the lower half of the water column.

The sediment load increased 18% in the Delft3D model, from 10 kg/m^2 at x=0 to 11.8 kg/m^2 at x=105 m. This partly explains the observed difference in the concentration gradients within that reach. Then, the sediment load decreases back again to 10 kg/m^2 at the uniform flow stage (approximately at x=375 m).

The adaptation length to uniform flow was longer for the Delft3D model (~375 m) than for the Lagrangian 1DV model (~350 m). The concentration profiles are shown at x=5.5 m, x=105 m, and x=375 m (fairly uniform).

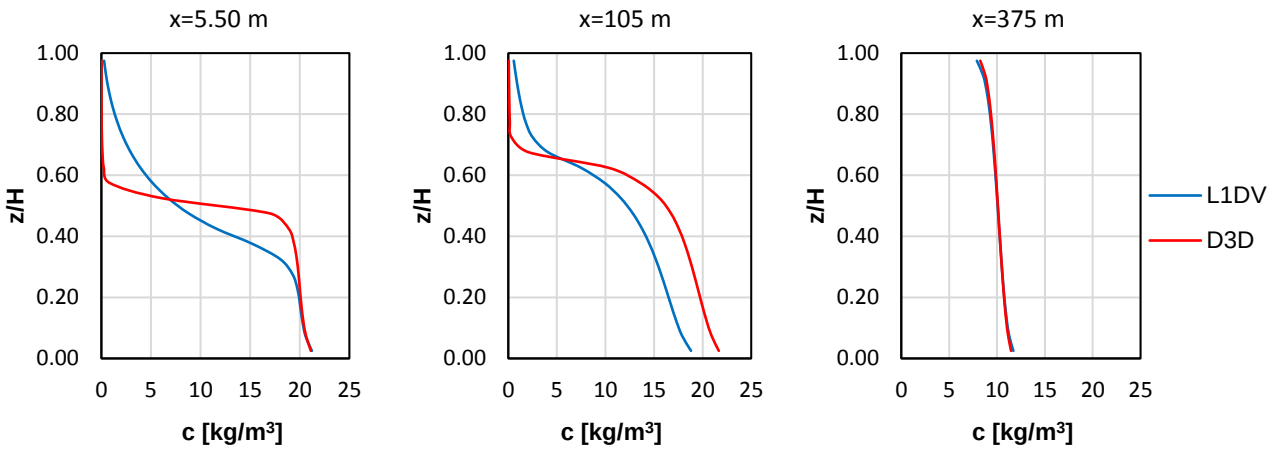

Figure 4-48. Concentration profiles at x=55 m, x= 105 m, and x = 375 m for Experiment ST-C (block-shaped initial concentration profile)

The concentration profile of the Lagrangian 1DV model at x=5.5 m showed more turbulent mixing, as commented before. The difference in sediment load between the models was not appreciable at that station.

From x=0 m to x=5.5 m, a higher $\partial c/\partial x$ was observed in the Lagrangian 1DV model. The gradient was more positive in the upper part of the water column and more negative at the lower part, between z/H=0.25 and z/H=0.50. The profile at x=105 m showed considerably more sediment load (18%) in the Delft3D model. Finally, the profile at x=375 m showed the profiles at the uniform flow stage. No significant difference was observed at that station.

Variation of u_c along then channel

Figure 4-49 shows the variation of u_c along the channel for both models.

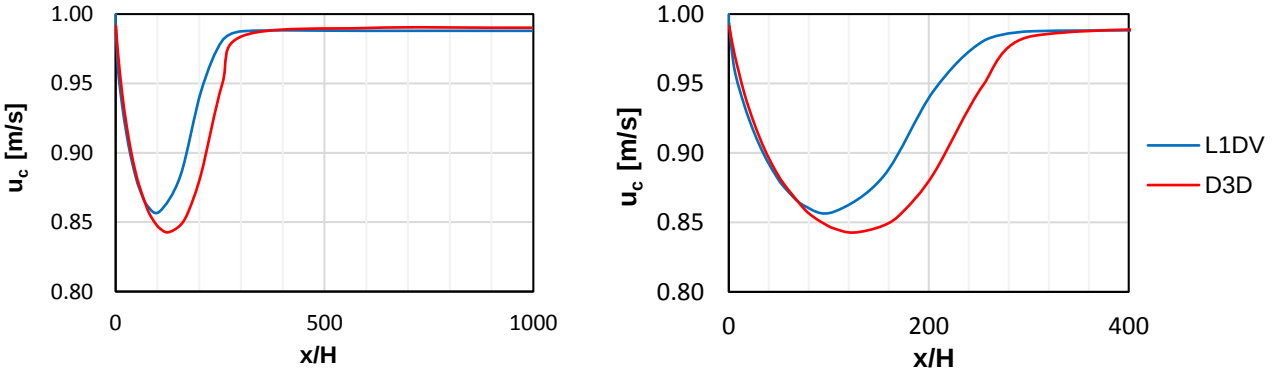

Figure 4-49. Variation of u_c with the distance from the source for Experiment ST-C (block initial concentration profile) from x = 0 m to x = 995 m (left) and from x = 0 m to x = 200 m (right)

The Lagrangian 1DV model showed a decrease in u_c for the first 95 m. The minimum value of u_c was 0.855 m/s. Downstream from that point, the sediment mass accelerated for approximately 250 m. The velocity increased to a value of 0.988 m/s. The velocity u_c of 0.988 m/s for uniform flow was also obtained in the coupled Lagrangian 1DV models for vertically uniform and linear initial concentration profile. This was expected because the velocity and concentration profile shapes for uniform flow are independent of the initial profiles when the input parameters are the same.

The Delft3D model showed similar behavior in terms of du_c/dx. The value of u_c at the non-uniform stage was lower for the Delft3D model. The deceleration stage occurred for a longer distance (approximately 120 m). The minimum value of u_c was 0.843 m/s (1.5% lower than the minimum value for the Lagrangian 1DV model). Downstream from that point, the velocity increased along a distance of approximately 250 m. The velocity u_c increased to a value of 0.990 m/s. This value for uniform flow was also obtained in the Delft3D model for the previous experiments with coupled models.

In general, at the first 80 m from the source, u_c was approximately the same for both models. From x=80 m to x = 350 m, the Delft3D model showed a lower u_c. Along this reach, there was a significant difference between the models. Downstream from x = 350 m, u_c was higher in the Delft3D model by a very small difference.

Mass flux

The mass flux varied in the Lagrangian 1DV model from an initial value of q_{s0}=10 kg/s/m to 8.6 kg/s/m during the deceleration phase. Then, it increased to a constant 9.88 kg/s/m. Meanwhile, in the Delft3D model, the initial mass flux remained constant along the channel (q_s=9.94 kg/s/m).

The Lagrangian 1DV model presented a lower mass flux along the channel (even when u_c was higher for the Lagrangian 1DV model).

Interpretation of the results for u_c

As in the previous analysis, the concentration and the net vertical sediment flux profiles were analyzed at x=5.5 m (Figure 4-50). In this case, the velocity profile differs from the logarithmic function, due to the initial conditions.

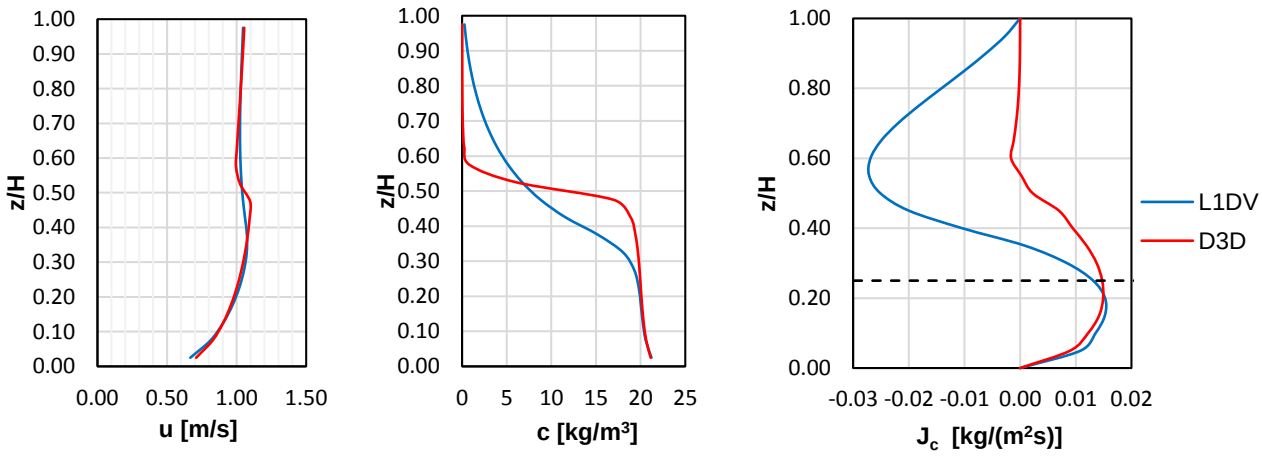

Figure 4-50. Velocity, concentration and net vertical sediment flux (positive downwards) profiles at x=5.5 m

The dashed line indicates the level at which $u = u_c$. In this case, differently from the previous coupled experiments, the shape and magnitude of the net vertical flux profile differed significantly between both models. The Lagrangian 1DV model presented a net turbulent diffusive flux above z=0.30 m, while the Delft3D model showed a net turbulent diffusive flux only above z/H=0.60, and a net settling flux below that level.

One of the reasons why the turbulent diffusive flux was larger in the Delft3D model is that there was a significant difference between the models in the initial eddy diffusivity and its development near to the source. The eddy diffusivity is shown at x=0.5 m and x= 5.5 m in Figure 4-51.

Above z=0.40 m, the diffusivity was significantly larger for the Lagrangian 1DV model (above the slurry), while Delft3D showed a higher diffusivity at the slurry layer. The differences in the eddy diffusivity and the net vertical sediment flux near to the source are a limitation for the method of analysis applied in the previous cases.

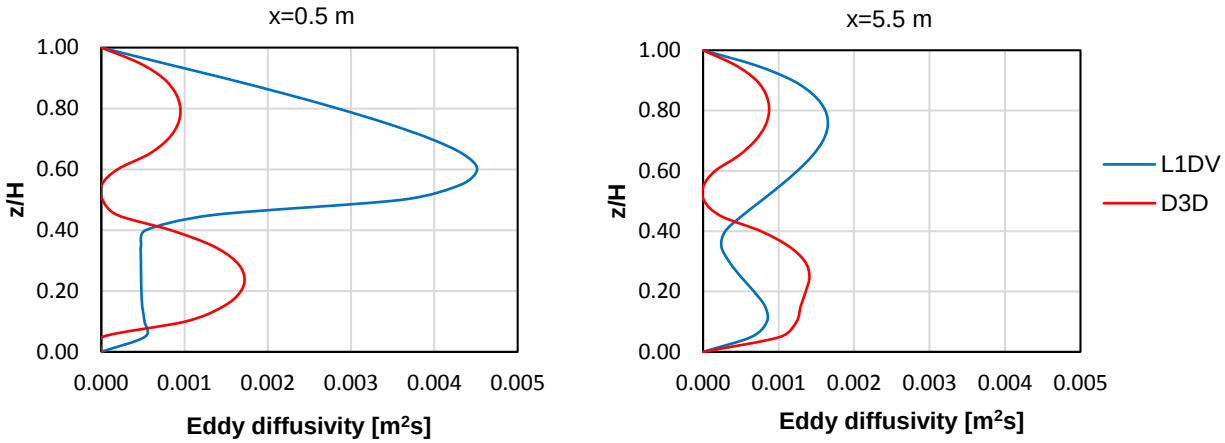

Figure 4-51. Eddy diffusivity profile at x=0.5 m and x=5.5 m

Regardless of the observed differences in the net vertical sediment flux, the difference in u_c between the models was not significant from x=0 to x=75 m. The reason could be the following:

- In the region above the dashed line where settling dominates, $|\partial J_c/\partial z_{L1DV}| > |\partial J_c/\partial z_{D3D}|$.
- Then, $u_c|\partial c/\partial x_{L1DV}| > u|\partial c/\partial x_{D3D}|$
- In this region $u > u_c$, which means that the inequality is only valid if $|\partial c/\partial x_{L1DV}| > |\partial c/\partial x_{D3D}|$

On one hand, $\partial c/\partial x_{L1DV}$ just above the black dashed line was larger for the Lagrangian 1DV model (more negative). On the other hand, the downwards flux just above the black dashed line was larger for the Delft3D model. This situation could produce an equilibrium in which a similar amount of mass was sent to the region below the dashed line, causing a similar change in u_c.

The net vertical sediment flux was analyzed also at x=75 m, close to the point where the difference in u_c between the models started to increase. Even though the eddy diffusivity was similar for both models at that point, the concentration profiles and the net vertical sediment flux profiles were significantly different. The magnitude of the net vertical sediment flux differed significantly between the models, probably as an effect of the initial conditions.

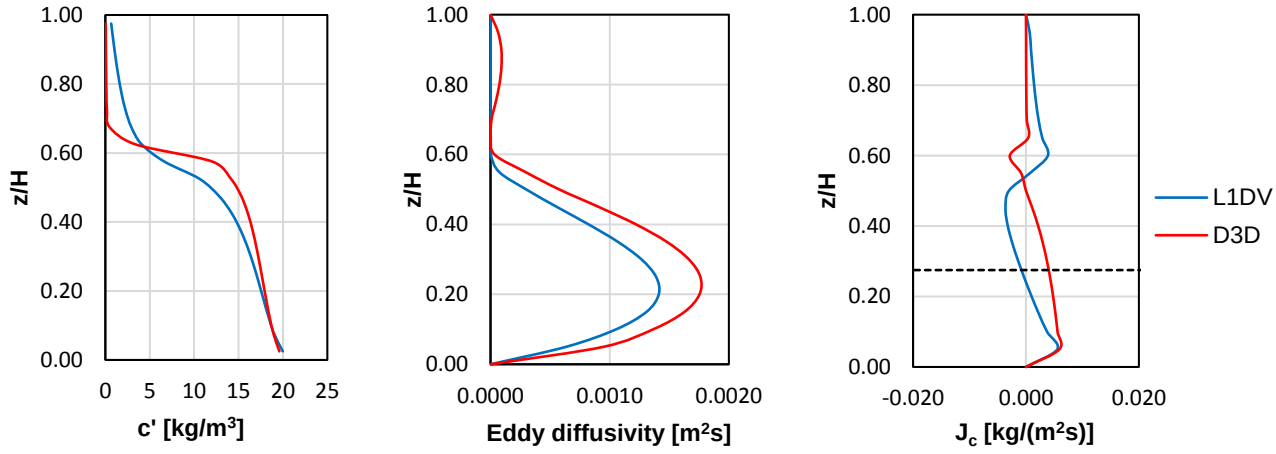

Figure 4-52. Eddy diffusivity and net vertical sediment flux (positive downwards) profiles at x=75 m

At x=75 m, turbulent mixing dominated between z/H=0.275 and z/H=0.55 in the Lagrangian 1DV model. The mass of sediment transported to the upper layer (above z/H=0.55) seemed to be close to an equilibrium with the amount of sediment transported downwards from that layer. No sediment

seemed to be transported to the region of lower velocities, below the dashed line. Then, u_c was close to the point where it stopped decreasing.

Meanwhile, in the Delft3D model, settling dominated just above the dashed line, which means that sediment was still being sent from the region of higher velocities to the region of lower velocities, producing a decrease in u_c. This could explain why a significant difference in u_c arose.

The results suggest that when the initial turbulent mixing is significantly higher in the Lagrangian 1DV model, the point where u_c stops decreasing will be closer to the source for the Lagrangian 1DV model. At this point, settling will still dominate in the region of high velocity in the Delft3D model, just above the dashed line, causing a decrease in u_c.

4.3.7 Summary and additional comments

Six different cases of non-uniform flow in a channel were modelled. Non-uniform flow was generated by defining a concentration profile different from the equilibrium concentration profile. Three different initial concentration profile shapes were tested in uncoupled and coupled models to identify and understand the origin of the differences between the Lagrangian 1DV approach and the Eulerian 2DV approach. The uncoupled models presented almost the same results in both models. The coupled models showed differences in the concentration profiles and the concentration-weighted velocity.

The interpretation of the results of the previous sections is valid for the cases in which the differences in the baroclinic term of the momentum equation are not high enough to produce differences in velocity between the models. If differences in the baroclinic term generate important differences in velocity, the interpretation may not be valid.

The results of the experiments with coupled models (type ST-C) suggested that the origin of the differences between the Lagrangian 1DV model and the Delft3D model in u_c and in the horizontal concentration gradient rely on the expression of the advective transport term of the sediment transport equation. In the Lagrangian 1DV model, sediment is transported longitudinally at a velocity u_c at all levels, while the Delft3D model uses the velocity at every particular level.

The following sketch represents the mechanism that originated the differences in the case of the vertically uniform and linear initial concentration profiles.

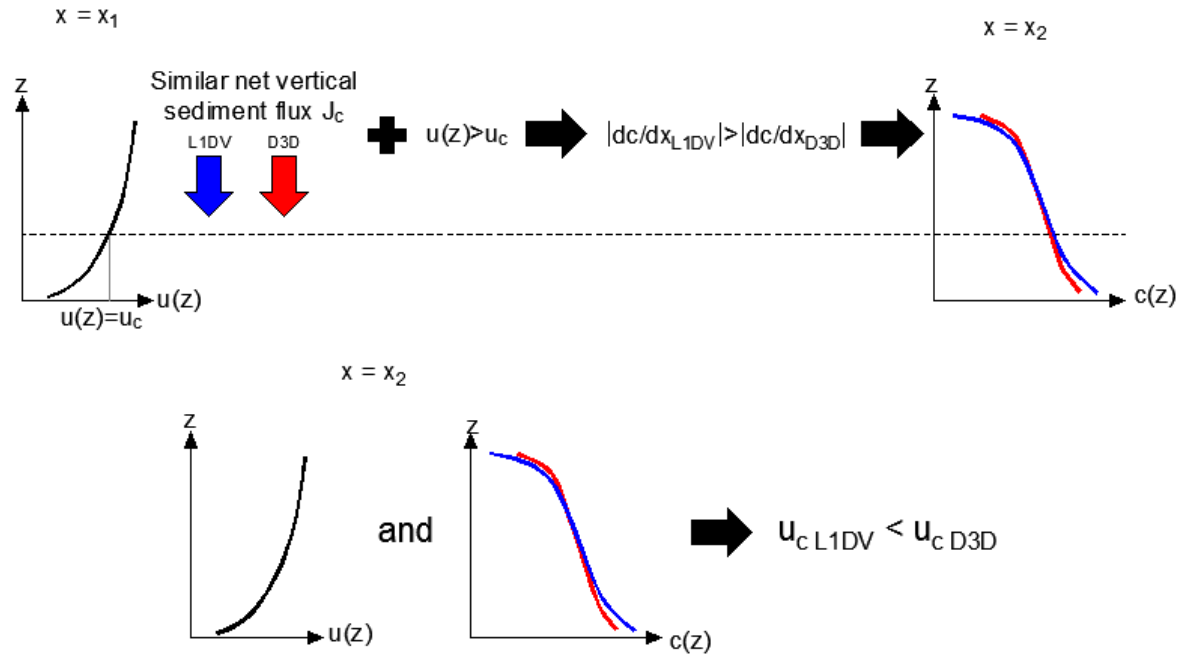

Figure 4-53. Sketch of the process that originates differences in u_c between the models (vertically uniform and linear initial concentration profiles)

When the net vertical sediment flux is similar between the models at a certain station ($x=x_1$) in the region where $u > u_c$, the horizontal concentration gradient is larger for the Lagrangian 1DV model in that region. When the net vertical sediment flux is downwards directed (dominated by settling), more sediment is sent to the region of lower velocities ($u < u_c$) in the Lagrangian 1DV model. Then, at a downstream station ($x=x_2$), u_c is lower for the Lagrangian 1DV model. As mentioned before, the sketch is valid when the difference between the models in the baroclinic term of the momentum equation is not high enough to produce important differences in velocity.

A similar situation to the previous sketch may occur at the bottom layer of turbidity currents. Velocity profiles for turbidity currents reported in literature by Sloff (1994) and De Cesare (2004) are similar to a hybrid profile (Figure 4-54), with a bottom layer (densest layer) described by a logarithmic function, as suggested by De Cesare (2004).

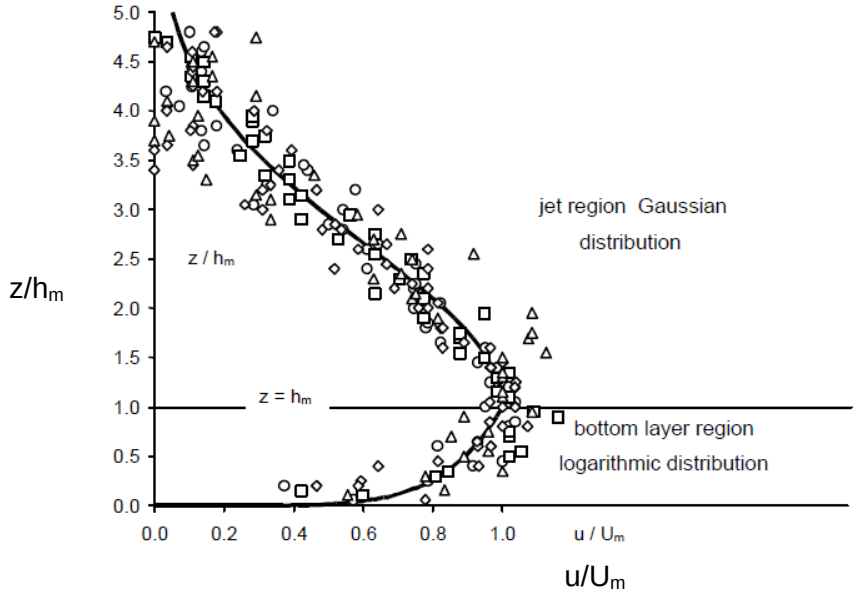

Figure 4-54. Measured velocities for turbidity currents (De Cesare, 2004)

Then, at the bottom layer, the situation may be similar to the case of Experiment ST-C for vertically uniform and linear initial concentration profiles. The velocity profile is close to logarithmic. Due to turbulence damping and high concentration, settling flux is likely to dominate.

Assuming a constant concentration from $z/h_m = 0$ to $z/h_m = 5$ (h_m is the distance from the bed to the level at which the velocity is maximum), the u_c value would be in the order of 0.7 U_m (where U_m is the maximum velocity). This means that u would be larger than u_c at most of the bottom layer. Following the same reasoning of Figure 4-53, $\partial c/\partial x_{\,L1DV}$ would be larger than $\partial c/\partial x_{\,D3D}$ in a region dominated by settling (Figure 4-55). Then, $\partial c/\partial x_{\,L1DV}$ would be more negative, transporting more sediment towards the lowest part of the bottom layer (where velocity is lower).

It can be hypothesized that this mechanism would produce a lower u_c in the Lagrangian 1DV model than in the Delft3D model in a ST-C model, or a higher deposition rate in the Lagrangian 1DV model for a STD-C model. This hypothesis will be analyzed in the following set of experiments.

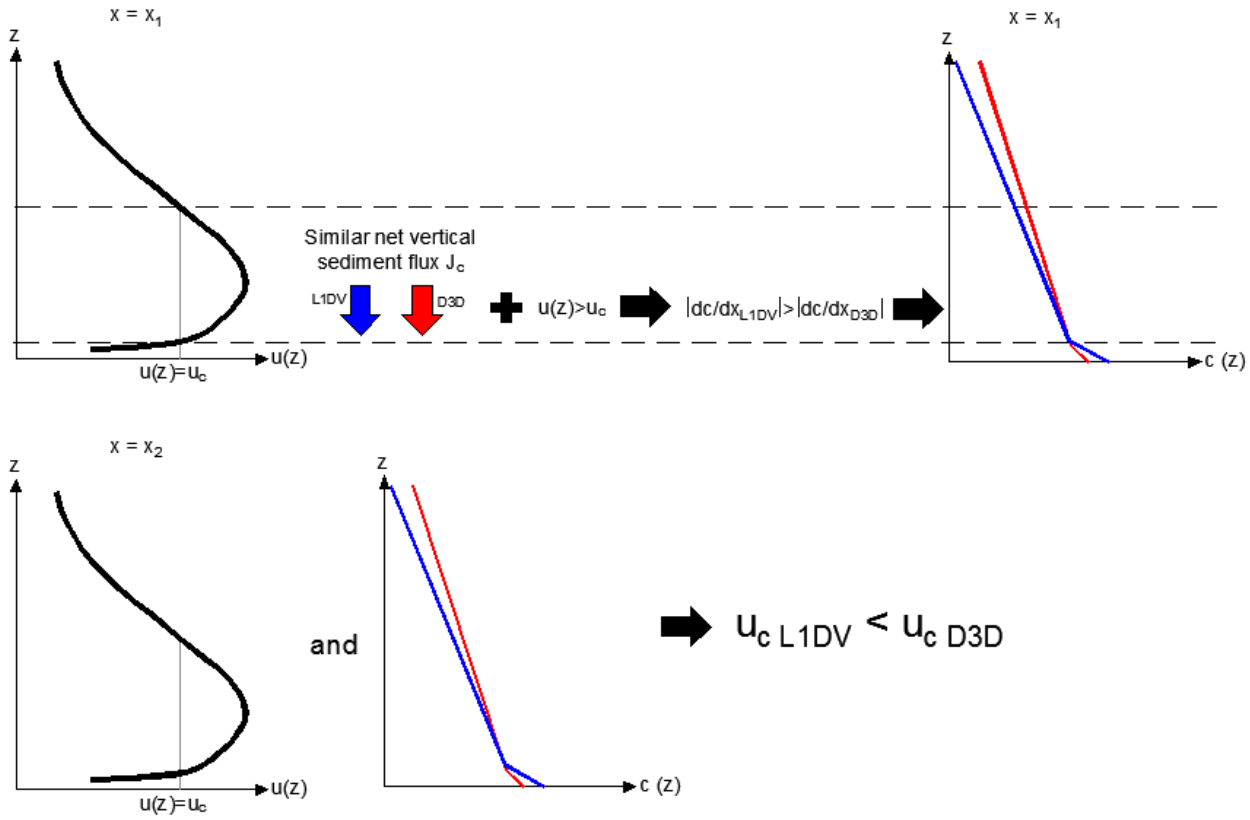

Figure 4-55. Sketch of the hypothesis for the process that generates differences in u_c between the models for turbidity currents

4.4 Experiments Set 3: Based on Run 13 of Parker et al. (1987)

This section firstly describes and summarizes the setup and results of Run 13 of the experiments by Parker et al. (1987). The setup of this run was the basis for two numerical experiments using the Lagrangian 1DV model and the Delft3D model:

- Experiment ST-C: a conservative turbidity current (no erosion or deposition)
- Experiment STD-C: including deposition (no erosion)

As in the previous sets of experiments, the Delft3D model is assumed to be a more realistic representation of sediment transport.

The objective of the Experiment ST-C was to compare the results and interpret the differences in velocity, concentration, and concentration-weighted velocity u_c of the Delft3D model and the Lagrangian 1DV model for a conservative turbidity current.

The objective of the STD-C models was to compare the results of the Delft3D model and the Lagrangian 1DV model for a depositing turbidity current. A description and comparison of the results for Experiment STD-C are presented. The results of the STD-C models for velocity and concentration were compared also with experimental data from Run 13 by Parker et al. (1987).

Erosion was not included in the analysis because the formulation is different between models. However, the experiments by Parker et al. (1987) were done over an erodible bed. This is a limitation of the experiments that should be considered when comparing the data from Run 13 to the results of the models.

4.4.1 Description of the Experiments by Parker et al. (1987)

Experimental setup

Parker et al. (1987) performed experiments on turbidity currents over an erodible bed. Non-cohesive silt (silica flour) flowed as a turbidity current over a downsloping bed of similar material (Figure 4-56).

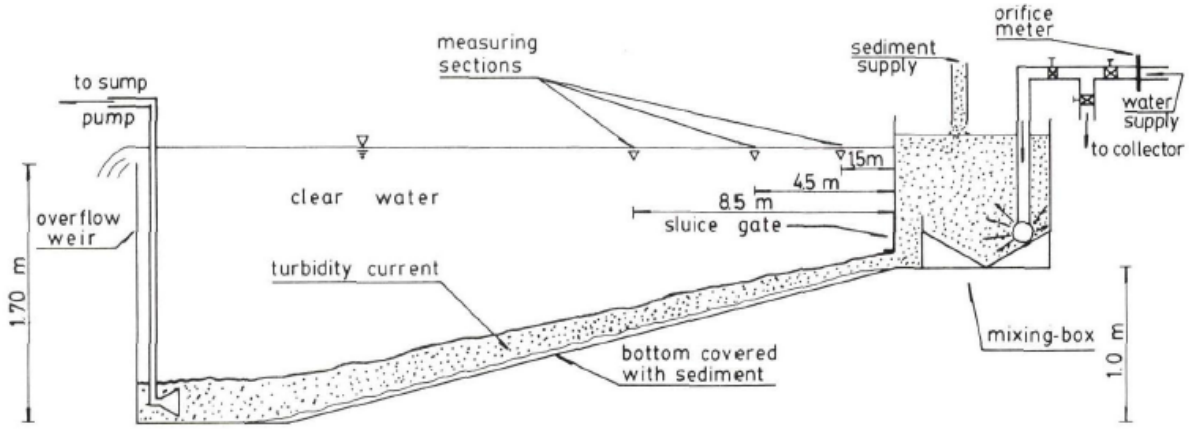

Figure 4-56. Experimental setup (Parker et al., 1987)

The flume for the experiment had a width b of 0.70 m, a varying depth H from 0.70 m at the sediment inlet (where the water-sediment mixture was discharged from a tank) to 1.70 m at the downstream end of the slope.

In total, 24 runs were performed. Tests were done for two different grain sizes (d_{50} = 30 μm and d_{50} = 60 μm), two different slopes (s = 5% and s = 8%) and different inlet conditions, varying: the initial mean velocity at the inlet U_0 (0.15 m/s to 0.27 m/s), the sluice opening h_0 (0.08 m to 0.15 m), and the volumetric concentration at the inlet C_0 (from 0.15% to 0.01%). The nomenclature above corresponds to the original report (Parker et al., 1987). Only supercritical turbidity currents were considered (initial overall Richardson number Ri_0 smaller than 1).

Silica flour particles were mixed with Mississippi River water in a headbox. The mixture was discharged through a sluice gate of adjustable height h_0. Detailed measurements of the velocity and concentration profiles were taken at 1.5 m, 4.5 m and 8.5 m from the inlet for 20 of the 24 runs.

Description of Run 13

Detailed measurements of the velocity and concentration profiles at 1.5 m, 4.5 m and 8.5 m from the inlet were presented by Parker et al. (1987) for Run 13. The parameters of Run 13 are shown in Table 4-3. These parameters were used for the numerical experiments ST-C and STD-C.

Table 4-3. Parameters of Run 13 (Parker et al., 1987)

Parameter	Value
ρ_s [kg/m^3]	2650
d_{50} [μm]	30
d_{90} [μm]	50
Average velocity at the inlet U_0 [m/s]	0.27
Inlet height h_0 [m]	0.08
Water discharge through the inlet Q_{w0} [m^3/s]	0.015
Sediment discharge through the inlet Q_{s0} [kg/s]	0.165
Average volumetric concentration at the inlet C_0 [%]	0.41
Average mass concentration at the inlet [kg/m^3]	10.9
Bed slope [-]	0.05

The turbidity current generated in Run 13 was characterized by Parker et al. (1987) as accelerating because the layer-averaged velocity of the turbidity current U increased from x=1.5 m to x=8.5 m

(where x is the distance from the inlet). It was also described as depositing because the mass flux decreased from x=1.5 m to x=8.5 m. The measurements of velocity and concentration for Run 13 were digitized and are presented in Figure 4-57.

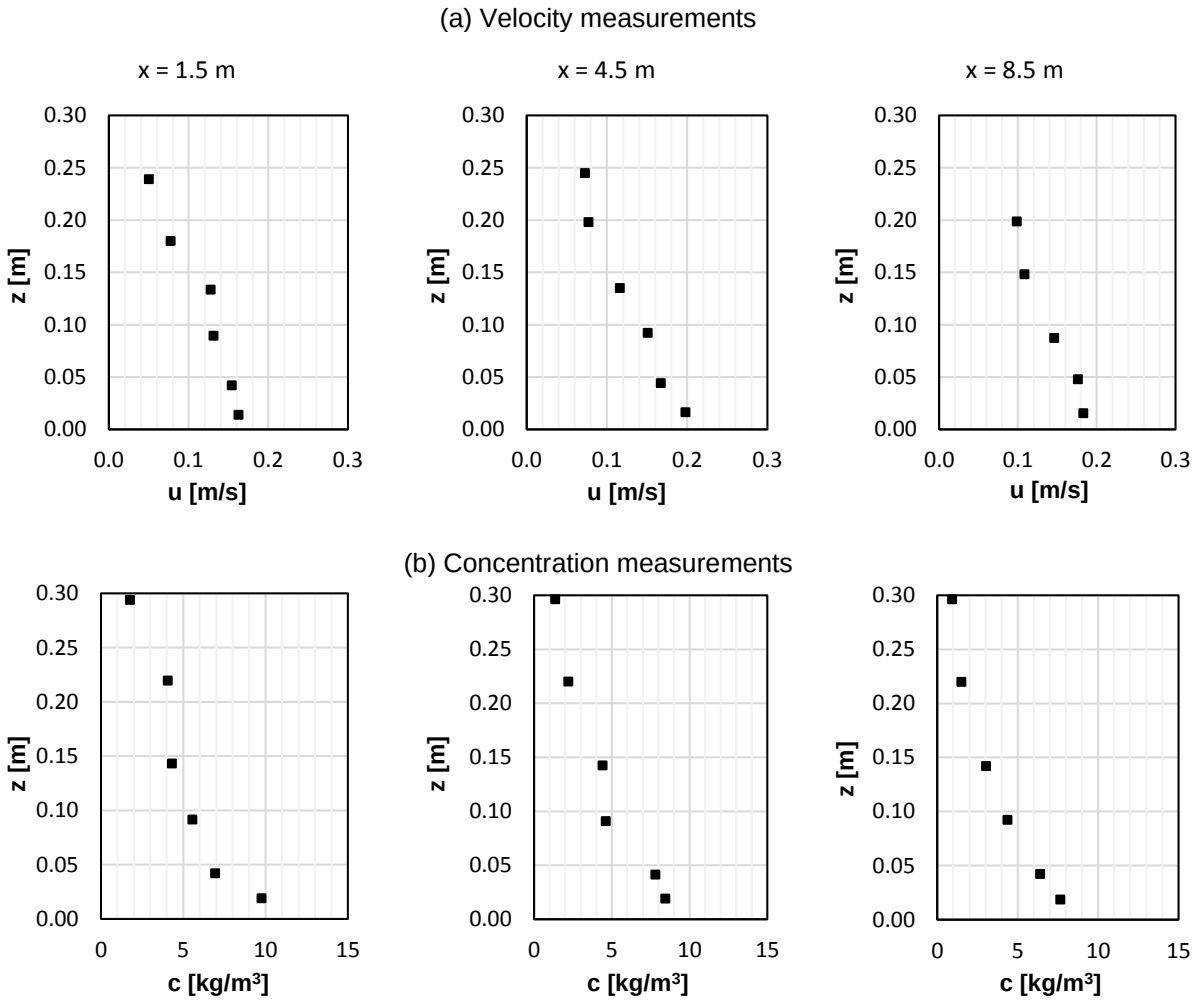

Figure 4-57. (a) Velocity and (b) concentration measurements from Run 13 by Parker et al. (1987)

4.4.2 Experiment ST-C

This numerical experiment was done with coupled models. In this case, deposition was not considered, to simulate a conservative turbidity current. Deposition is included in the next section (Experiment STD-C).

Setup of the models

In the Lagrangian 1DV model, from the parameters of Run 13 (Table 4-3), the average initial concentration c_{fl} was defined as 10.9 kg/m^3 over a height h_{fl} of 0.08 m. The average slurry velocity u_{fl} corresponded to 0.27 m/s.

The discharge was assumed to be constant along the flume, and equal to the water discharge at the inlet Q_{w0} (0.015 m^3/s). To estimate $\bar{u}$ in the Lagrangian 1DV model, it was required to define the water depth H. The water depth was variable in the experimental setup of Run 13 (Figure 4-56). On the other hand, by definition, the water depth H is constant in the Lagrangian 1DV model. The average depth from x=0 to x=10 m (H = 0.95 m) was used in the Lagrangian 1DV model to simulate the first 10 m from the inlet. For a depth H of 0.95 m, a channel width b of 0.70 m and Q_{w0} of 0.015 m^3/s, $\bar{u}$ ($= Q_{w0}/bH$) was approximated as 0.023 m/s.

The roughness length z_0 was approximated as (Van Rijn, 1984):

$$z_0 = k_s/30$$

Where k_s is the effective roughness height of Nikuradse. The value of k_s can be approximated as $2d_{90}$ to $5d_{90}$ (Van Rijn, 1984). Using a value of $3d_{90}$ (d_{90} from Table 4-3), z_0 was estimated as 5 x 10^{-6} m.

Deltares (2019) performed a validation of the Lagrangian 1DV model with the experimental data of Run 13 of Parker et al. (1987). The roughness length z_0, the grain size, the ambient flow velocity and the initial u_{fl}, c_{fl} and h_{fl} were defined as in the validation of Deltares (2019). A double logarithmic initial velocity profile and a block-shaped initial concentration profile were selected for the validation. Consistently with that selection, the same initial profile shapes were selected for this set of numerical experiments. The main difference is that Deltares (2019) considered the erosion process.

In this case, the initial profiles correction to keep the same initial mass and mass flux as defined in the input file of the Lagrangian 1DV model (further explained in Set 2 of experiments) did not generate a change in $\bar{u}$. Then, the velocity and concentration profiles at the upstream boundary of the Delft3D model were defined to match the initial profiles of the Lagrangian 1DV model at x=0 m.

As a final remark, the Delft3D model considered the depth variation of Run 13, as shown in Figure 4-56. A constant water level was defined at the downstream boundary. The backwater curve was not significant due to the small magnitude of $\bar{u}$.

Results

Velocity

The velocity profiles were plotted at x=0.5 m, x=1.5 m, x=4.5 m, and x=8.5 m (Figure 4-58). The latter three stations correspond to the measurement stations of Parker et al. (1987) for Run 13.

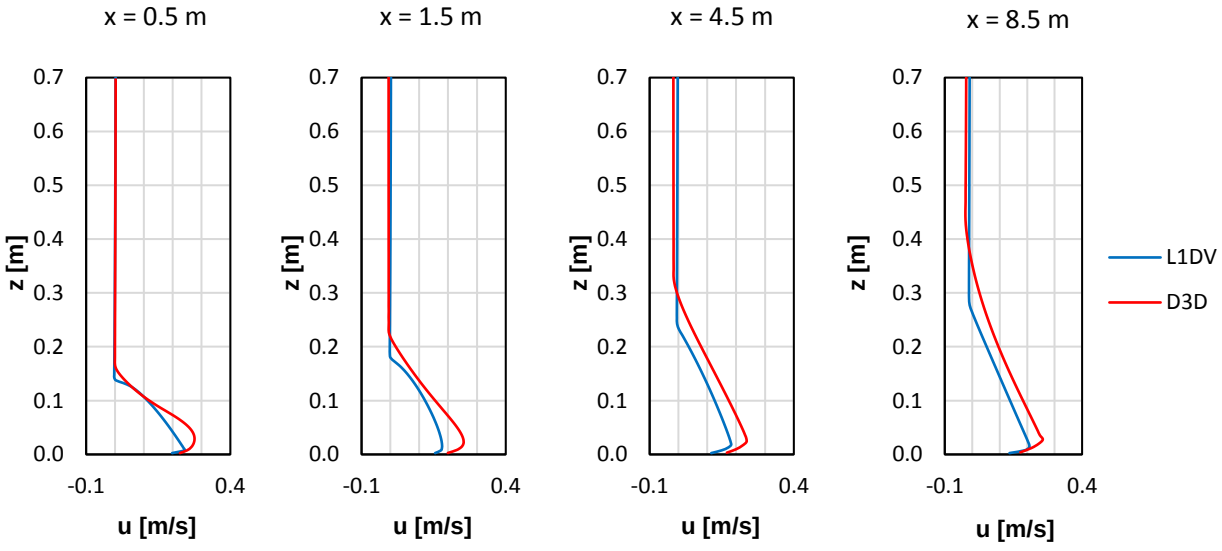

Figure 4-58. Velocity profiles for Experiment ST-C

The Delft3D model showed higher velocities for the turbidity current than the Lagrangian 1DV model. The velocity profiles also indicate that the thickness of the turbidity current in the Delft3D model increased more than in the Lagrangian 1DV model.

At x=4.5 m and x=8.5 m, both models showed small negative velocities above the turbidity current. The negative velocities were in the order of 1 cm/s, which is below 10% of the initial average slurry velocity of 0.27 m/s (for a ratio of initial turbidity current height h_{fl} over the depth of approximately 0.1 in both models). The negative velocities were slightly larger for the Delft3D model.

Concentration

The resulting concentration distribution in the 2DV field is shown in Figure 4-59, for the first 10 m from the source and below z=0.30 m. The concentration below the 10 kg/m^3 contour is larger than 10 kg/m^3, but the contours are not shown in the figure due to their closeness and the resolution of the figure. The values of concentration below the 10 kg/m^3 contour can be analyzed in the concentration profiles (Figure 4-60).

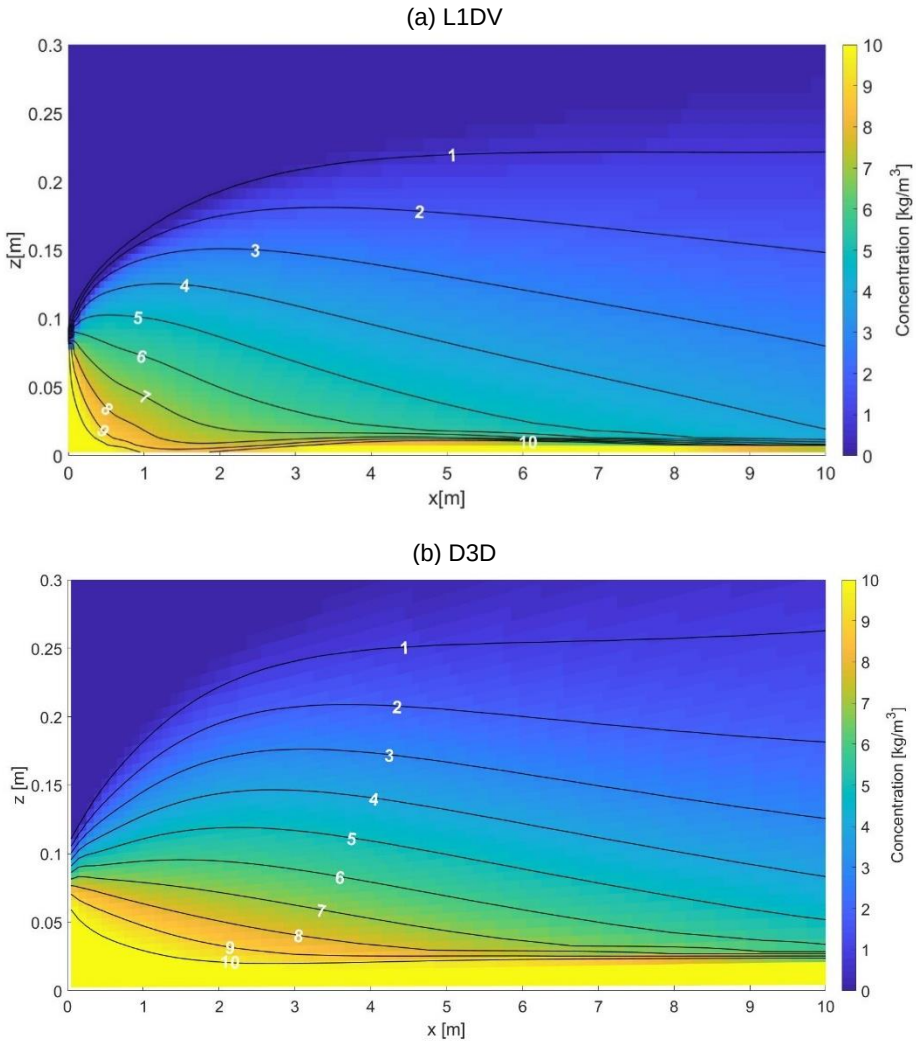

Figure 4-59. Concentration distribution for Experiment ST-C

It can be observed that the horizontal concentration gradient $\partial c/\partial x$ below the z=0.08 m (inlet height) was larger (more negative) for the Lagrangian 1DV model close to the source. This result is influenced by the increase of the sediment load in the Delft3D model along the channel, which can be better observed in Figure 4-60. The sediment load is constant along x for the Lagrangian 1DV model.

In both models, settling seemed to dominate downstream from x ≈ 3 m. The concentration profiles were plotted at x=0.5 m, x=1.5 m, x=4.5 m, and x=8.5 m. The latter three stations correspond to the measurement stations of Parker et al. (1987) for Run 13.

The concentration profiles were plotted in Figure 4-60. The concentration was higher for the Delft3D model at every station. The sediment load in the Delft3D model increased from an initial value of 0.87 kg/m^2 at x=0 to 1.34 kg/m^2 at x=4.5 m. Downstream from x=4.5 m, the sediment load decreased to 1.26 kg/m^2 at x=8.5 m.

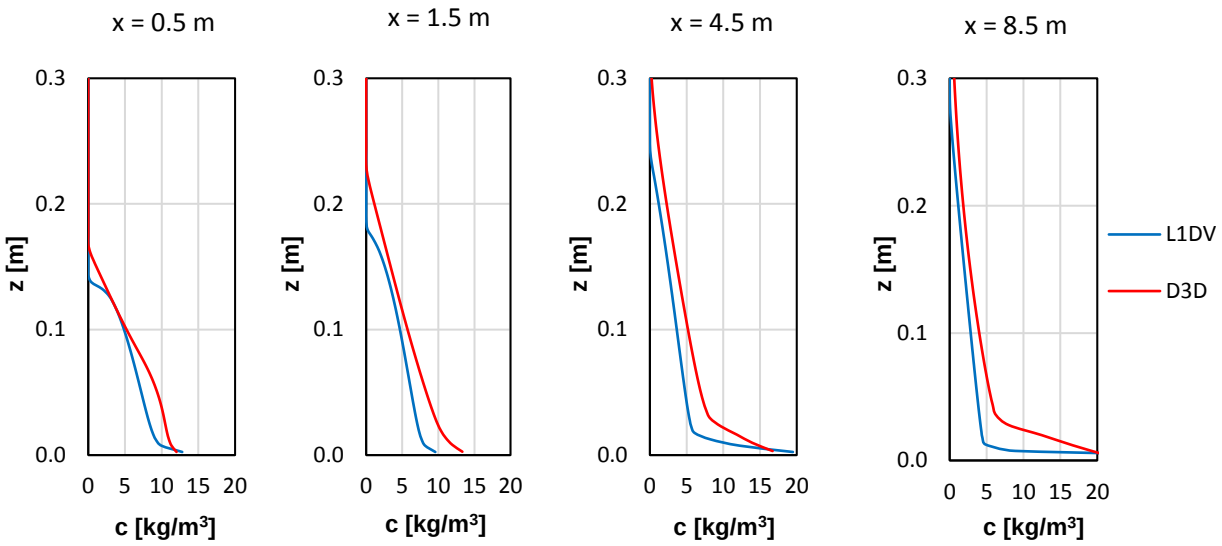

Figure 4-60. Concentration profiles for Experiment ST-C

Mass flux

The mass flux was constant along the channel for the Delft3D model and equal to the initial mass flux of 0.23 kg/s/m (there was no deposition or erosion in this numerical experiment). In the Lagrangian 1DV model the mass flux decreased from 0.23 kg/s/m at x=0 m to 0.11 kg/s/m at x=3.5 m. Then, the mass flux increased to 0.13 kg/s/m at x=8.5 m.

Variation of u_c along the channel

Figure 4-61 shows the variation of the ratio u_c/u_{c0} along the first 10 m from the source (left), where u_{c0} is the concentration-weighted velocity at x=0 m (same for both models). To have a more extended overview of the variation of u_c, an extended version of the same ST-C model was run (40 m long).

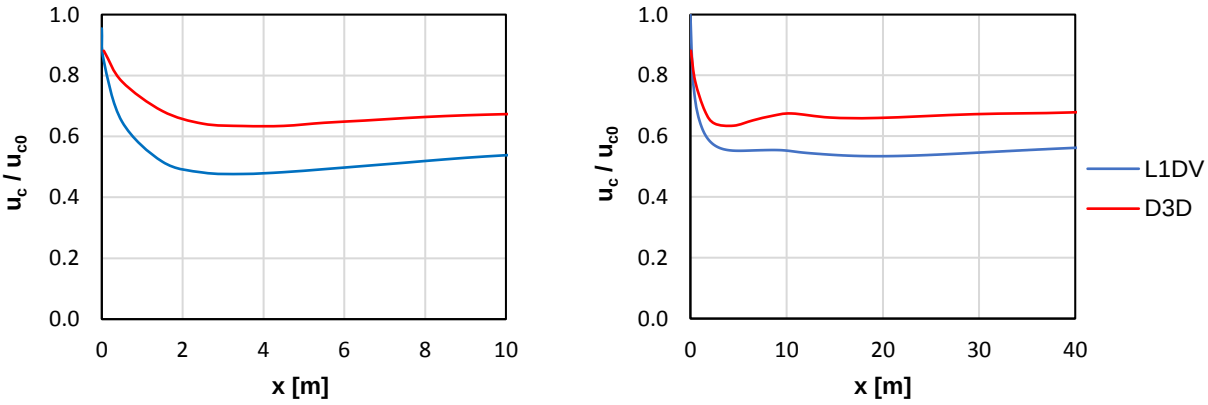

Figure 4-61. Variation of u_c/u_{c0} with the distance from the source for Experiment ST-C from x=0 m to x=10 m (left) and from x=0 to x=40 m (right)

In the Lagrangian 1DV model, the mass flux decreased along the first 3.5 m from the inlet and the sediment load remained constant (by definition). Then, a decrease in u_c occurred along that reach. From x=3.5 m to x=10 m, the mass flux increased, as well as u_c. Overall, downstream from x=10 m, u_c/u_{c0} remained fairly constant. There was a small decrease in u_c from x=10 m to x=20 m and a small increase from x=20 m to x=40 m.

In the Delft3D model, the sediment load increased along the first 3.5 m from the source and the mass flux remained constant (stationary), causing a decrease in u_c. From x=3.5 m to x=10 m, the sediment

load decreased, which was reflected on an increase in u_c. Downstream from x=10 m, u_c/u_{c0} remained fairly constant.

The main observations are that:

- Both models presented a similar behavior when comparing du_c/dx (negative from x=0 m to x=3.5 m, positive from x=3.5 m to x = 10 m, and fairly constant downstream from x=10 m).
- The magnitude of $u_c$was lower for the Lagrangian 1DV model. Averaging u_c over the distance (first 40 m), the result for the Lagrangian 1DV model (0.15 m/s) was 16% lower than the average for the Delft3D model (0.18 m/s) along the first 40 m.

In this case, differently from the numerical experiments of Set 2, the models did not approximate to the same u_c value, when u_c became nearly constant. This could be because the depth of the models differs. The Lagrangian 1DV model seems to approach to a uniform condition that corresponds to a constant depth and a constant depth-averaged velocity. On the other hand, the Delft3D model does not strictly reach a uniform condition due to the variation of the depth along the channel, which affects the magnitude of the depth-averaged velocity and, consequently, the velocity and concentration profiles.

Interpretation of the results for u_c

For the analyzed stationary condition in the Delft3D model (2DV approach), the deceleration of the sediment mass (decrease in u_c) was clearly related to an increase in sediment load. This was observed from x = 0 to x = 4.5 m. While u_c decreased, the sediment load increased significantly (53% from x=0 to x=4.5 m).

In the results of Run 13 of Parker et al. (1987) from Figure 4-57, the concentration measurements also suggest an increase of sediment load at x=4.5 m. Based on the measured concentration, the sediment load approximated to 1.1 kg/m^2 at x=4.5 m, while the initial sediment load was 0.87 kg/m^2.

An explanation for the observed variation of the sediment load both in the Delft3D model and the measurements by Parker et al. (1987) could be that:

- The sediment mass is released with a certain initial velocity
- The mass initially decelerates according to the flow conditions and geometric characteristics
- Initial deceleration causes a reduction in the mass flux
- To be able to sustain a constant mass flux when flow becomes stationary, the concentration over the water column should increase, therefore increasing the sediment load.

The increase of the sediment load is evidenced in a larger concentration in the Delft3D model than in the Lagrangian 1DV model, as previously shown in Figure 4-60. Larger concentration generated a larger baroclinic forcing in the Delft3D model.

For example, due to higher concentration, the average of the baroclinic term in the momentum equation in the region of higher velocities and concentration was 20% higher in the Delft3D model at x=2.5 m. This explains the higher acceleration that produced higher velocities in the Delft3D model (Figure 4-58). Higher velocities in the region of higher concentration produced higher values of u_c in the Delft3D model.

In the previous set of experiments (Set 2 in Section 4.3), a hypothesis was proposed to explain the differences in u_c between the models. However, this hypothesis did not take into account that for a larger baroclinic forcing, as in this case, the change in the velocity profiles is significant when the concentration profile changes.

The baroclinic term in the momentum equation became more important in this set of experiments. The difference in concentration between the models also produced differences in the velocity profiles.

The magnitude of the baroclinic pressure gradient at a level z in the Delft3D model can be expressed as:

$$\left(\frac{dp}{dx}\right)_{BC} = g\left(1 - \frac{\rho_w}{\rho_s}\right)\int_z^\zeta \frac{\partial c}{\partial x} dz'$$

The horizontal concentration gradient is expressed as:

$$\frac{\partial c}{\partial x} = \frac{-w}{u}\frac{\partial c}{\partial z} + \frac{1}{u}\frac{\partial J_c}{\partial z}$$

Then, the integral of the concentration gradient can be estimated as:

$$\int_z^\zeta \frac{\partial c}{\partial x} dz' = \int_z^\zeta \frac{-w}{u}\frac{\partial c}{\partial z'} dz' + \int_z^\zeta \frac{1}{u}\frac{\partial J_c}{\partial z'} dz' \quad (4.11)$$

In the Lagrangian 1DV model, with $u = u_c$ and $-w/u_c = tan\,\beta$ (where β is the bed slope angle), and assuming there are no fluxes through the water surface, the integral of the horizontal concentration gradient can be expressed as:

$$\int_z^\zeta \frac{\partial c}{\partial x} dz' = -c(z) \cdot tan\,\beta - \frac{1}{u_c} J_c(z) \quad (4.12)$$

The first term on the RHS in Equation (4.12) depends both on the bed slope and the concentration. This term is analogous to the first term on the RHS of Equation (4.11). It was negligible in Set 2 of experiments due to a very small bed slope. This permitted to explain the differences in u_c between the models based on the differences in the second term on the RHS.

For the case of Parker et al. (1987), the first term on the RHS was one order of magnitude larger than the second term. Then, the difference in the second term between the models were not as important as in Set 2 of Experiments to explain the difference between the models.

4.4.3 Experiment STD-C

This numerical experiment was done with coupled models, now including deposition. The results of the models were compared with the measurements by Parker et al. (1987).

Description

The input parameters of the models were the same as in Experiment ST-C, except for the parameters related to deposition. The Partheniades-Krone formulation was selected for deposition in both models. To ensure full deposition, a very high critical shear stress for deposition ($\tau_{cr,d}$ = 1000 Pa) was used.

As in experiment ST-C, the initial profiles correction to keep the same initial mass and mass flux as defined in the input file did not generate a change in $\bar{u}$. Then, the velocity and concentration profiles at the upstream boundary of the Delft3D model were defined to match the initial profiles of the Lagrangian 1DV model at x=0 m.

Results

Velocity

The velocity profiles were plotted at x=1.5 m, x=4.5 m, and x=8.5 m (Figure 4-62). The measurements by Parker et al. (1987) for Run 13 were also plotted. The accuracy of the velocity measurements was reported as ± 1 cm/s (Parker et al., 1987).

There was a good qualitative agreement with the measured velocities by Parker et al. (1987). At x=1.5 m, the velocities of the Lagrangian 1DV model showed closer results below z=0.10 m. At x=4.5 m, the measured values were between the results of both models. The measured velocities were slightly higher than the velocities calculated by the Lagrangian 1DV model and lower than the velocities estimated by the Delft3D model. The same situation was found at x=8.5 m.

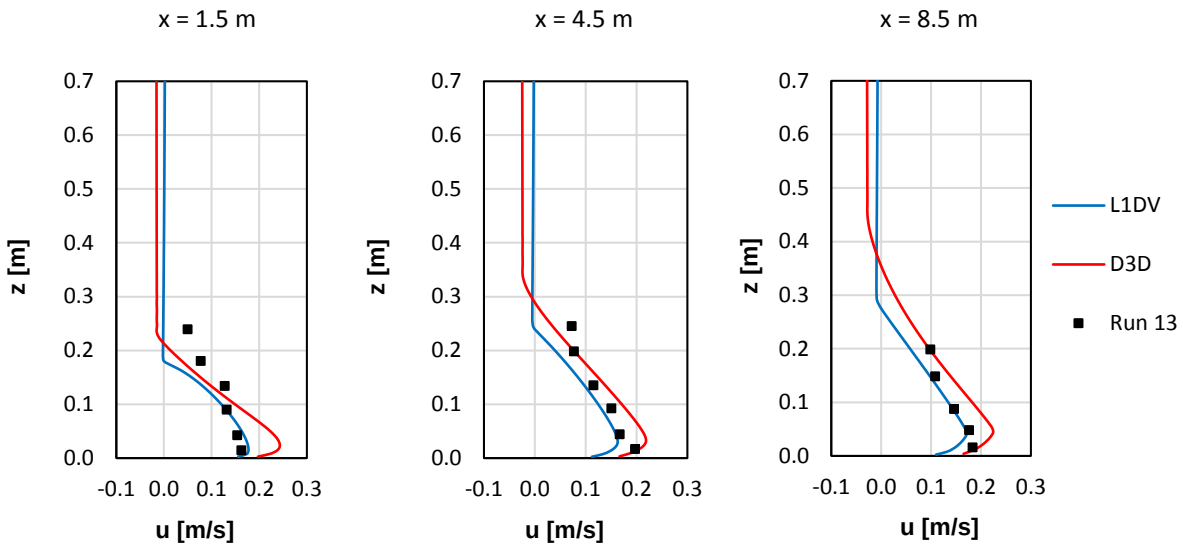

Figure 4-62. Velocity profiles for Experiment STD-C

At x=1.5 m and x=4.5 m, above the turbidity current (z > 0.20 m), the velocity was underestimated by both models. The Lagrangian 1DV model estimated approximately zero velocity, while the Delft3D model showed a negative velocity. Meanwhile, the measurements showed a significant (positive) velocity of approximately 0.05 m/s. Deltares (2019) indicate that the measured velocity above the turbidity current in Run 13 suggests the occurrence of an ambient flow velocity, which could be generated due to the drag of water by the turbidity current. This phenomenon was not captured by the models.

In general, the velocity was slightly underestimated by the Lagrangian 1DV model and slightly overestimated by the Delft3D model. As in Experiment ST-C, the velocity of the turbidity current was higher in the Delft3D model than in the Lagrangian 1DV model at all the stations.

Concentration

The resulting concentration distribution in the 2DV field is shown in Figure 4-63, for the first 10 m from the source. It can be observed that the horizontal concentration gradient $\partial c/\partial x$ below the z=0.08 m (inlet height) was larger (more negative) for the Lagrangian 1DV model close to the source. This was also observed in the numerical experiment ST-C.

The observed concentration distribution was influenced again by the increase of the sediment load in the Delft3D model along x. The concentration profiles were plotted at x=1.5 m, x=4.5 m, and x=8.5 m (Figure 4-64). These stations correspond to the measurement stations for Run 13.

Both models showed a good qualitative agreement with the measurements. The Delft3D model performed better especially at x=4.5 m and x=8.5 m.

The concentration was higher for the Delft3D model than for the Lagrangian 1DV model at every station, which is consistent with the increase of sediment load. In the Lagrangian 1DV model, the sediment load decreased from 0.87 kg/m^2 at the inlet to 0.58 kg/m^2 at x=8.5 m (33% decrease). In the Delft3D model, the sediment load increased to 1.23 kg/m^2 at x=2.5 m and, then, decreased to 1.01 kg/m^2 at x=8.5 m. The calculated sediment load in the Delft3D model was consistent with the sediment load that can be estimated with the measured concentration by Parker et al. (1987), which indicates longitudinal mass accumulation for the first 10 m.

The concentration from the Delft3D model was closer to the measured points, especially at x=4.5 m and x=8.5 m. At x=1.5 m, a significant concentration was measured above z=0.20 m (above the turbidity current). This can be a result of the formation of an eddy close to the inlet, transporting sediment to the upper levels. This phenomenon was not represented by the models.

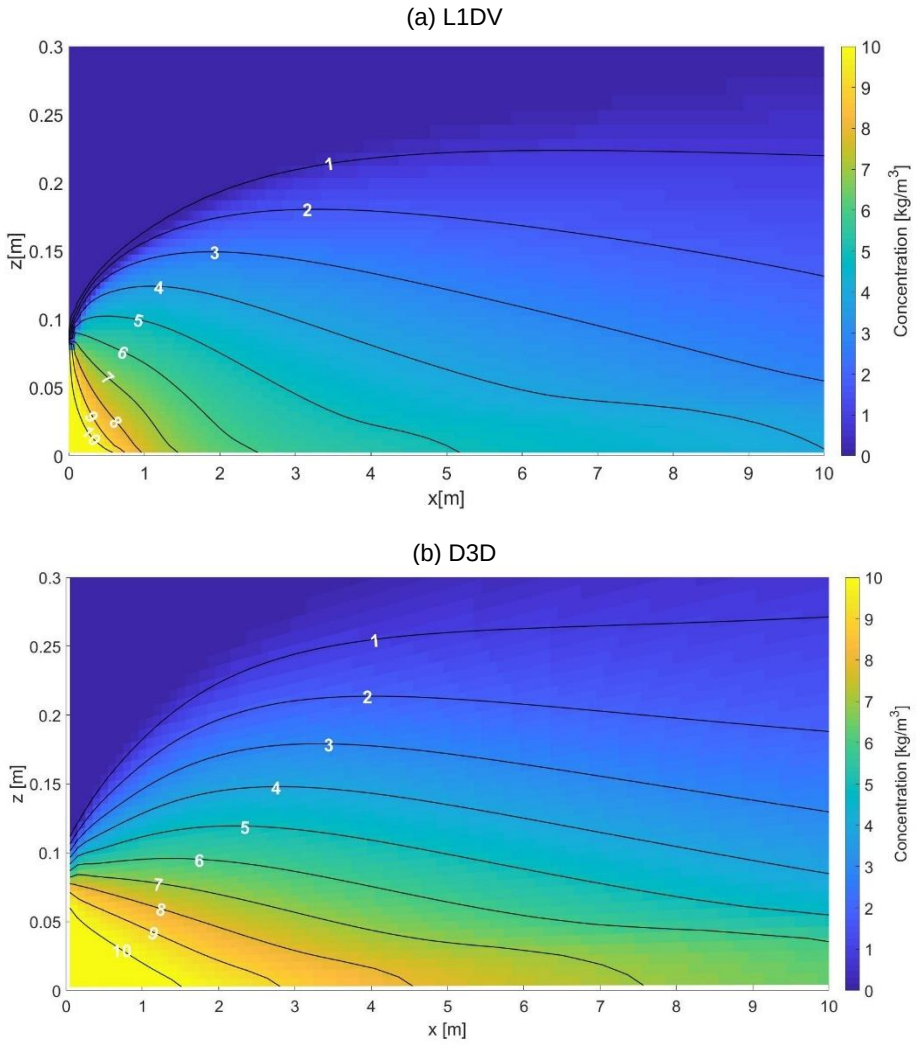

Figure 4-63. Concentration distribution for Experiment STD-C

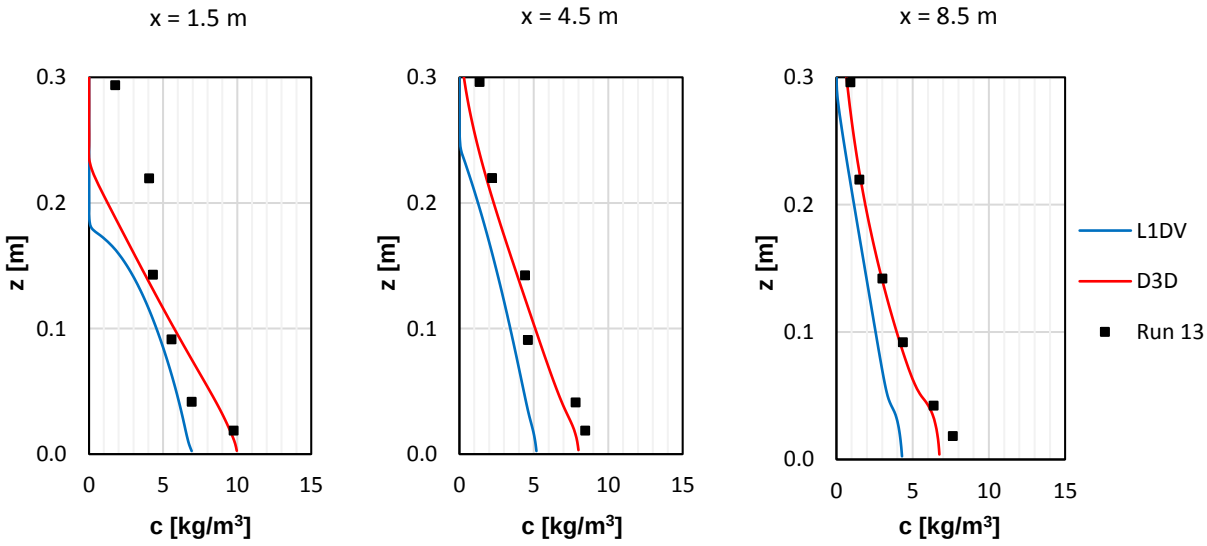

Figure 4-64. Concentration profiles for Experiment STD-C

Mass flux

In both models, the mass flux decreased along the channel due to net deposition, which was the same trend obtained by Parker et al. (1987). In the Delft3D model, the mass flux decreased from the initial value of 0.23 kg/s/m to 0.16 kg/s/m at x=8.5 m. In the Lagrangian 1DV model, the mass flux decreased more, down to 0.07 kg/s/m. The lower mass flux in the Lagrangian 1DV model is related to a lower sediment load and a lower velocity of the turbidity current as shown in Figure 4-62 and Figure 4-63.

Variation of u_c along the channel

Figure 4-65 shows the variation of the ratio u_c/u_{c0} along the first 10 m from the source (left), where u_{c0} is the concentration-weighted velocity at x=0 m. To have a more extended overview, u_c was also calculated for the first 40 m (right). The dashed lines show the result for Experiment ST-C (no deposition) as a reference.

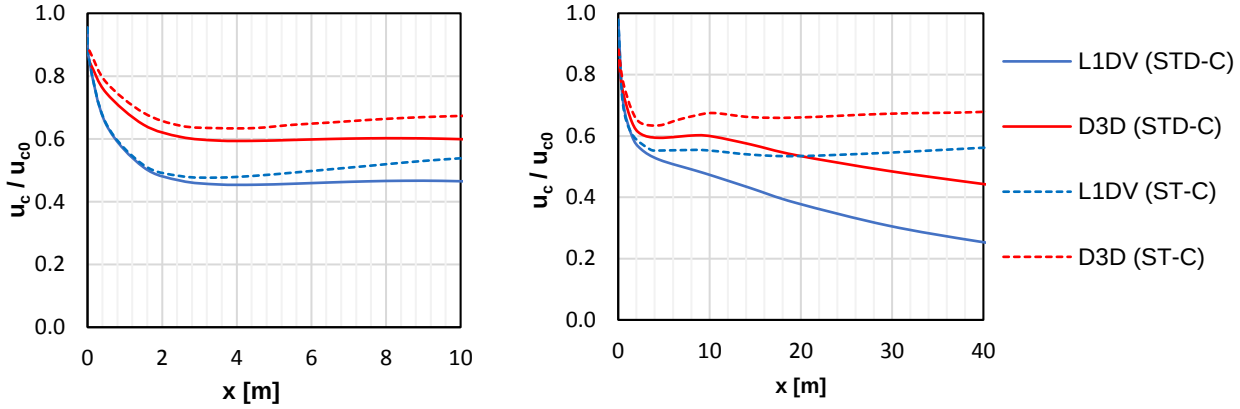

Figure 4-65. Variation of the u_c/u_{c0} with the distance from the source for Experiment STD-C from x=0 m to x=10 m (left) and from x=0 to x=40 m (right)

In the Lagrangian 1DV model, for the first 10 m (left), the mass flux decreased along the first 3.5 m from the inlet and the sediment load also decreased, because there was net deposition. A decrease in u_c occurred along that reach, which means that the reduction of mass flux was more important than the reduction of sediment load. From x=3.5 m to approximately x=10 m, u_c remained fairly constant (for H = 0.95 m). Downstream from x=10 m (right), u_c/u_{c0} started to decrease again.

The value of u_c/u_{c0} was higher for the Delft3D model than the Lagrangian 1DV model, along the analyzed reach. The difference in u_c between the models was smaller than 0.2 u_{c0} (smaller than 0.05 m/s). Averaging u_c over the first 40 m, the result for the Lagrangian 1DV model (0.12 m/s) was 20% lower than the average for the Delft3D model (0.15 m/s). The difference in u_c between the models did not increase significantly when including the deposition process.

Sedimentation

The deposition rate $D\ (= w_s c_b)$ in kg/m^2/s was calculated the Delft3D model. This value remains constant at a certain position x for a stationary solution. It was compared to the deposition rate of the Lagrangian 1DV model. The results are shown in the Figure 4-66.

The deposition rate was larger for the Delft3D model. This means that more material was deposited in the Delft3D model. However, this does not mean that the length of the sedimentation footprint was shorter in the Delft3D model, because the Delft3D model had a higher sediment load at every station in the analyzed reach.

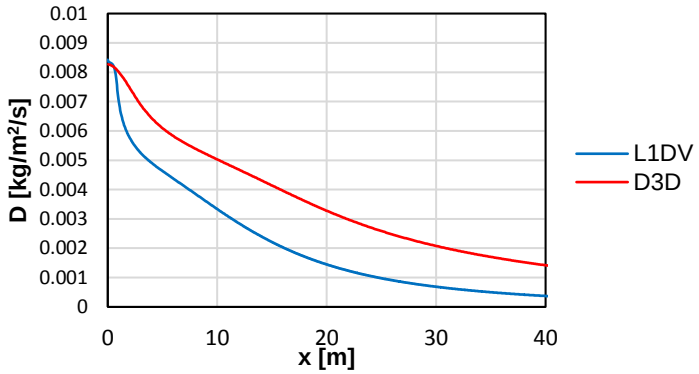

Figure 4-66. Deposition rate for Experiment STD-C.

The variation of the sediment load (Figure 4-67) indicates that sediment mass was further transported in Delft3D model.

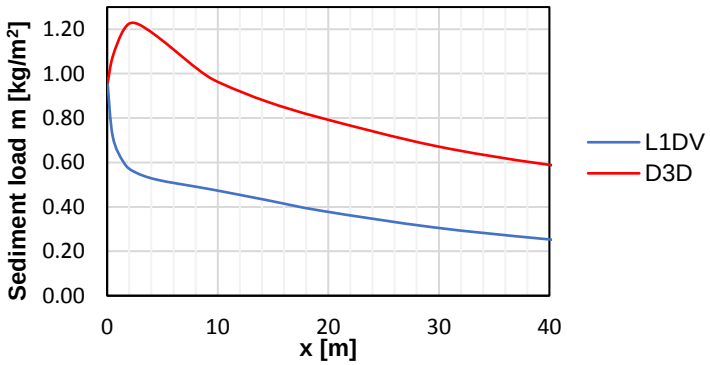

Figure 4-67. Sediment load for Experiment STD-C.

Interpretation of results for u_c

Deposition produces a loss of sediment mass in the region where velocities and concentration are higher. The reduction of mass generates a decrease in the driving force of the turbidity current, thereby decreasing u_c. This was consistent in both models.

4.5 Experiments Set 4: Based on Run 2 Van Kessel and Kranenburg (1996)

This section first describes and summarizes the setup and results of Run 2 of the experiments by van Kessel and Kranenburg (1996). The setup of this run was the basis for two numerical experiments using the Lagrangian 1DV model and the Delft3D model:

- Experiment ST-C: a conservative turbidity current (no erosion or deposition)
- Experiment STD-C: including deposition (no erosion)

The results of the STD-C models for velocity and concentration were compared also with experimental data from Run 2 by van Kessel and Kranenburg (1996).

As in the previous section, erosion was not included in the analysis because the formulation is different between models. In the case of Run 2, this is reasonable as the bed was not erodible.

4.5.1 Description of the Experiments by Van Kessel and Kranenburg (1996)

Experimental setup

Van Kessel and Kranenburg (1987) performed experiments on gravity currents of fluid mud on a sloped plane. The flume for the experiment had a length of 13.75 m, a width of 0.50 m and a depth of

0.72 m at the end of the sloping bed. Two sloping bottoms were available: a slope of 2.35% along 8.75 m and a slope of 5.41% along 8.35 m (Figure 4-68).

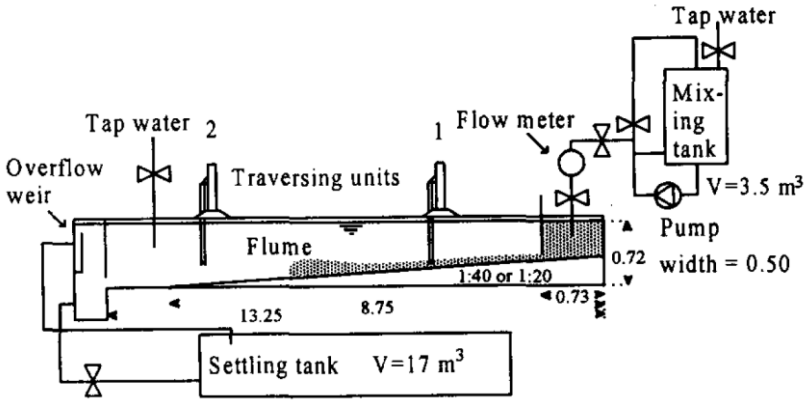

Figure 4-68. Experimental setup (van Kessel and Kranenburg, 1996)

A mixture of china clay and tap water was prepared in a tank and discharged at flow rates of approximately 0.004 m^3/s through an inlet of height h_0 of 0.05 m. A density current was generated for 300 to 600 seconds until the supply of suspension from the tank was nearly depleted. In total, 15 runs were performed combining: initial bulk densities from 1050 kg/m^3 to 1230 kg/m^3 (mass concentration from 81 kg/m^3 to 374 kg/m^3, respectively), bed slopes of 2.35% and 5.41%, inflow rates of 0.004 m^3/s and 0.007 m^3/s, and inlet heights of 5 cm, 6 cm and 7 cm.

Detailed measurements of the velocity and concentration profiles were given at 1.27 m and 5.43 m from the inlet. Due to accuracy limitations, the measurements of the concentration started at 2 cm above the bottom. Sidewall effects were considered of minor importance due to the small height to width ratio of the gravity current (around 0.1). Measurements started at a moment when the flow was considered to be steady.

Description of Run 2

Run 2 produced a turbulent gravity current. This was an important requirement of the selected run because the Lagrangian 1DV model and the Delft3D model are for turbulent flow. The average initial concentration at the inlet of 166 kg/m^3 was in the order of magnitude of WID-induced turbidity currents (from 50 kg/m^3 to 200 kg/m^3 as reported in Section 2.2.3). The parameters of Run 2 are shown in Table 4-4. These parameters were used to set up Experiments ST-C and STD-C.

Table 4-4. Parameters of Run 2 (van Kessel and Kranenburg, 1996)

Parameter	Value
ρ_s [kg/m^3]	2593
Settling velocity w_s [m/s]	$< 10^{-4}$
Drag coefficient for high effective Reynolds number [-]	0.0035
Average velocity at the inlet U_0 [m/s]	0.18
Inlet height h_0 [m]	0.045
Mixture discharge through the inlet Q_{m0} [m^3/s]	0.004
Average mass concentration at the inlet [kg/m^3]	166
Bed slope [-]	0.0235

Deposition was very small due to the small effective settling velocity. In fact, the deposition process was neglected by van Kessel and Kranenburg in their analysis. The measurements of velocity and concentration were provided by van Kessel (personal communication, 2019) and are presented in Figure 4-69.

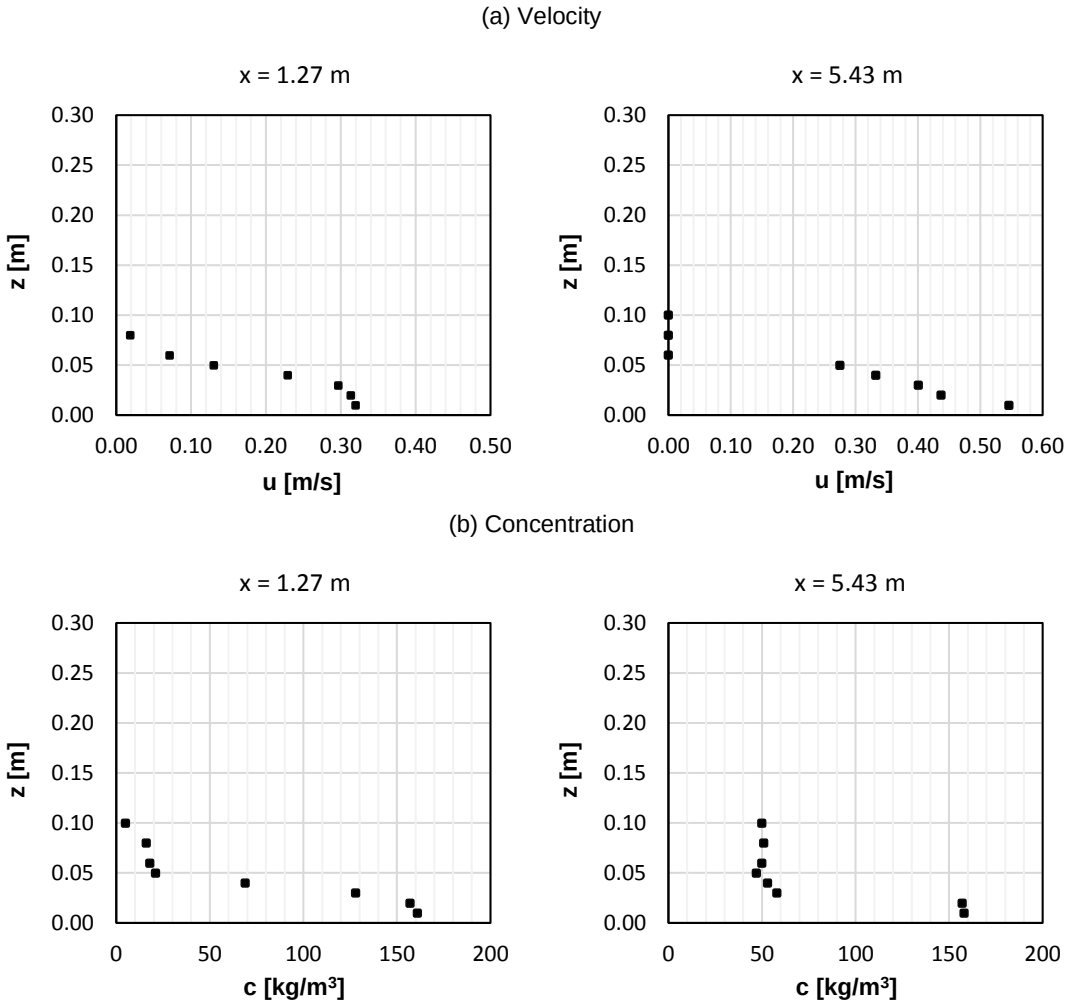

Figure 4-69. (a) Velocity and (b) concentration measurements from Run 2 by van Kessel and Kranenburg (1996)

The velocity profile at x = 1.27 m (close to the sediment source) is similar to a hyperbolic tangent function (as in the initial hybrid velocity profile available in the Lagrangian 1DV model). The shape of the profile at 5.43 m is not that clear. The difference in velocity shows that there was a significant acceleration of the turbidity current along the slope.

The concentration profile at x=5.43 m shows a strong stratification. The particular shape of the profile at that station suggests the existence of two different layers: the lowest with a concentration in the order of 150 kg/m^3 and the upper one with a concentration in the order of 50 kg/m^3.

4.5.2 Experiment ST-C

This numerical experiment was done with coupled models. In this first experiment, deposition was not considered, to simulate a conservative turbidity current. Deposition is included later in Experiment STD-C.

Setup of the models

In the Lagrangian 1DV model, from the parameters of Run 2 (Table 4-4), the average initial concentration c_{fl} was defined as 166 kg/m^3 over a height h_{fl} of 0.045 m. The average slurry velocity u_{fl} corresponded to 0.18 m/s.

The mixture discharge was assumed to be constant along the flume, and equal to the mixture discharge at the inlet Q_{m0} (0.004 m^3/s). To estimate $\bar{u}$ for the Lagrangian 1Dv model, it was required to approximate the water depth H. The water depth was variable in the experimental setup of Run 2 (Figure 4-68). On the other hand, by definition, the water depth H is constant in the Lagrangian 1DV

model. The average depth from x=0 to x=10 m (H = 0.65 m) was used in the Lagrangian 1DV model to simulate the first 10 m from the inlet. For a depth H of 0.65 m, a channel width b of 0.50 m and Q_{m0} of 0.004 m^3/s, $\bar{u}$ ($= Q_{m0}/bH$) was approximated as 0.012 m/s.

The approximate value of the drag coefficient c_D (=0.0035) corresponds to a Chézy coefficient of 53 ($\mathrm{C} = \sqrt{g/c_D}$). The structural dry density was defined as 300 kg/m^3. This parameter was used for calibration and gave better results when comparing the concentration measurements to the results of Experiment STD-C.

Based on the shape of the profiles at x=1.27 m, a hybrid initial velocity profile (hyperbolic tangent function at the upper part of the profile). For Run 2, the block-shaped concentration profile provided the best results when compared with the measurements.

In this case, the initial profiles correction to keep the same initial mass and mass flux as defined in the input file (further explained in Set 2 of experiments) did not generate a change in $\bar{u}$. Then, the velocity and concentration profiles at the upstream boundary of the Delft3D model were defined to match the initial profiles of the Lagrangian 1DV model at x=0 m.

The Delft3D model considered the depth variation of Run 2, as shown in Figure 4-68. A constant water level was defined at the downstream boundary. The backwater curve was not significant due to the small $\bar{u}$.

Results

Velocity

The velocity profiles were plotted at x=0.5 m, x=1.25 m, x=5.45 m and x=9.45 m (Figure 4-70). The second and third stations correspond to the closest stations to the measurement stations of van Kessel and Kranenburg (1996).

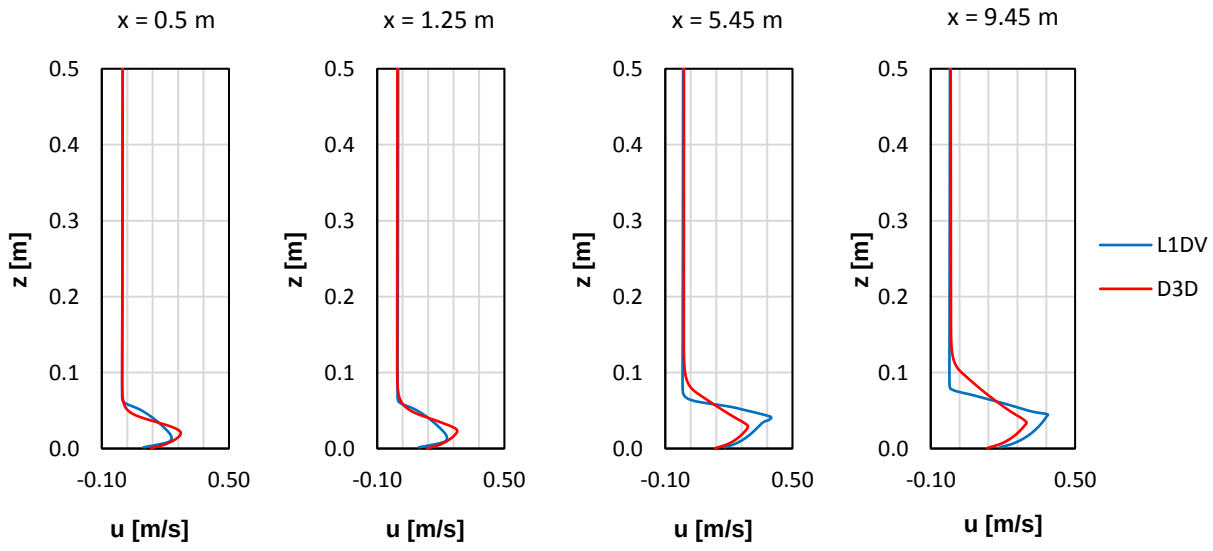

Figure 4-70. Velocity profiles for Experiment ST-C

From x=0.5 m to x=9.45 m, the average velocity of the turbidity current (approximated as the average of the positive velocities) increased in both models. The increase in the average velocity was larger in the Lagrangian 1DV model.

Both models showed small negative velocities in the same order of magnitude above the turbidity current. The negative velocities were in the order of 1 cm/s, which is below 10% of the initial average slurry velocity of 0.18 m/s. The ratio of initial turbidity current height h_{fl} over the depth H was approximately 0.1 in both models.

The Delft3D model showed a higher maximum velocity than the Lagrangian 1DV model at the first two stations. At x=5.45 m and x=9.45 m, the maximum velocity was higher for the Lagrangian 1DV model. The thickness of the turbidity current was larger for the Delft3D model at the latter two stations.

Concentration

The resulting concentration distribution in the 2DV field is shown in Figure 4-71, for the first 10 m from the source from z=0 m to z=0.10 m. The wiggles of the contours of the Delft3D model concentration distribution are likely due to interpolation between the center of the cells (they do not seem like a reasonable physical feature). The stability of the concentration profiles was checked in the Delft3D model at different times where flow seemed stationary. No signs of instability were observed.

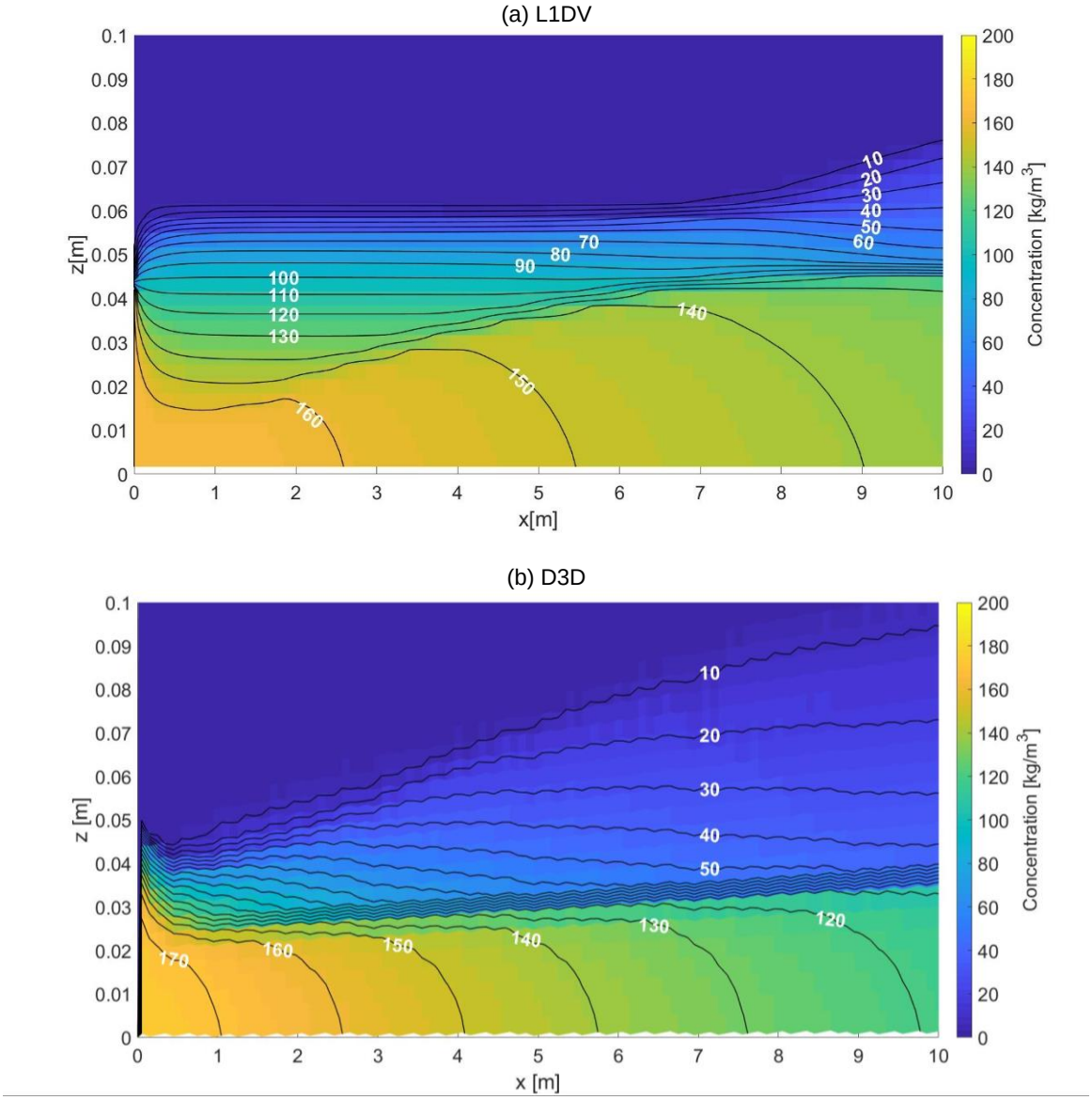

Figure 4-71. Concentration distribution for Experiment ST-C

It can be observed that the horizontal concentration gradient $\partial c/\partial x$ below z=0.045 m (inlet height) was larger (more negative) for the Delft3D model. Settling dominated in the first 1 m in the Delft3D model. Mixing increased downstream.

Initial mixing was higher for the Lagrangian 1DV model. In the first meter from the inlet, the concentration was approximately 100 kg/m^3 at the inlet height (z=0.045 m), while the Delft3D model showed a concentration of approximately 20 kg/m^3.

Opposite to the situation of Run 13 in Parker et al. (1987), the observed concentration distribution is influenced by the decrease of the sediment load in the Delft3D model along the slope. The sediment load in the Delft3D model decreased from an initial value of 7.5 kg/m^2 at x=0 to 6.1 kg/m^2 at x=3.5 m. Downstream from x=3.5 m, the sediment load remained fairly constant.

The concentration profiles were plotted at x=0.5 m, x=1.25 m, x=5.45 m, and x=9.45 m.

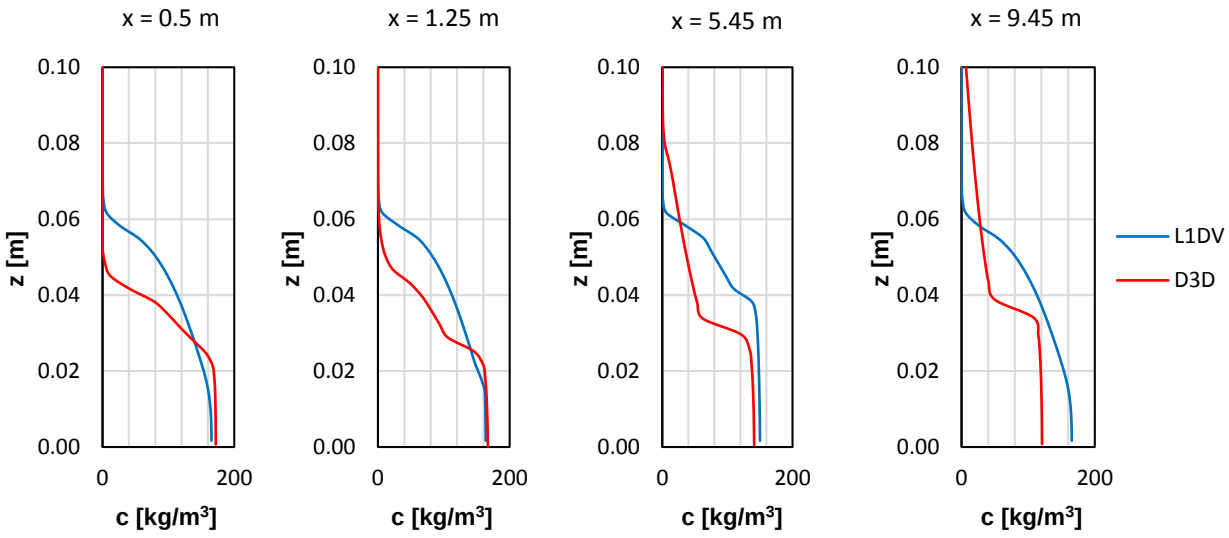

Figure 4-72. Concentration profiles for Experiment ST-C

The near-bed concentration was similar for both models at the first three stations and close to the initial concentration of 166 kg/m^3. At x=5.45 m and x=9.45 m, concentration was higher for the Delft3D model above z>0.6 m, showing the increase of the turbidity current thickness previously suggested by the velocity profiles. In general, the concentration and the sediment load were larger for the Lagrangian 1DV model at the analyzed reach.

Sediment mass flux

The mass flux was constant along the channel for the Delft3D model and equal to the initial mass flux of 1.34 kg/s/m (there was no deposition or erosion in this numerical experiment to decrease or increase the mass flux). In the Lagrangian 1DV model the mass flux increased from 1.34 kg/s/m at x=0 m to 2.30 kg/s/m at x=7.5 m. From x=7.5 m to x=10 m, it slightly decreased to 2.20 kg/s/m.

Variation of u_c along the channel

Figure 4-73 shows the variation of the ratio u_c/u_{c0} along the first 10 m from the source (left), where u_{c0} is the concentration-weighted velocity at x=0 m (same for both models). To have a more extended overview, $u_c$was also calculated in an extended model for the first 40 m in an extended model (right).

As it was mentioned, the sediment mass flux in the Lagrangian 1DV model increased along the first 7.5 m from the inlet, and the sediment load remained constant, by definition. Then, an increase in u_c occurred along that reach. From x=7.5 m to x=10 m, the mass flux slightly decreased, as well as u_c. Downstream from x=10 m (right), u_c/u_{c0} increased from 1.48 to 1.55 (small acceleration).

In the Delft3D model, the sediment load decreased along the first 3.5 m from the source, and the mass flux remained constant, producing an increase in u_c. Downstream from x=3.5 m, the sediment load remained fairly constant, which was reflected on an approximately constant value for u_c/u_{c0} (between 1.21 and 1.25).

The main observations are that:

- Both models presented a similar behavior when comparing du_c/dx, with a phase of acceleration of the sediment mass that ended in a relatively constant value for the ratio u_c/u_{c0}, larger than 1.

- The magnitude of $u_c$was higher for the Lagrangian 1DV model. Averaging u_c over the distance (first 40 m), the result for the Lagrangian 1DV model (0.26 m/s) was 18% higher than the average for the Delft3D model (0.22 m/s).

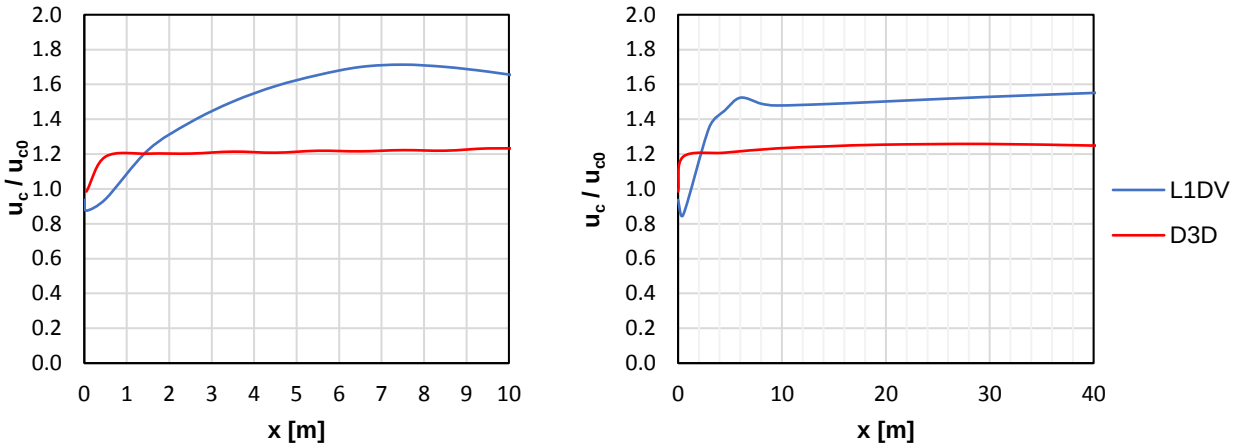

Figure 4-73. Variation of u_c/u_{c0} with the distance from the source for Experiment ST-C from x=0 m to x=10 m (left) and from x=0 to x=40 m (right)

As in Experiments Set 3, based on Parker et al. (1987), the results did not seem to approximate to the same u_c value, when u_c became relatively constant. This could be because the definition of the depth of the models differs. The Lagrangian 1DV model seems to approach to a uniform condition that corresponds to a constant depth and a constant depth-averaged velocity. On the other hand, the Delft3D model does not strictly reach a uniform condition due to the variation of the depth along the channel, which affects the magnitude of the depth-averaged velocity and, consequently, the velocity and concentration profiles.

Interpretation of the results for u_c

The results for u_c in this experiment were the opposite of the results of Experiment ST-C for Run 13 of Parker et al. (1987), in terms of which model showed a higher u_c. In the case of the Experiment ST-C for Run 13, the Delft3D model presented a higher u_c value. In the case of Experiment ST-C for Run 2 of van Kessel and Kranenburg (1996), the Lagrangian 1DV model showed a higher u_c value.

A similar reasoning as for Experiment ST-C for Run 13 of Parker et al. (1987) was followed to find a possible explanation of the observed result. Instead of a decrease in u_c (as seen in Run 13), in Run 2 of van Kessel and Kranenburg (1996), an increase of u_c was observed. For the stationary condition in the Delft3D model, the acceleration of the sediment mass (increase in u_c) was clearly related to a decrease in the sediment load. This was observed from x = 0 to x = 7.5 m in the Delft3D model. While u_c increased, the sediment load decreased significantly from 7.5 kg/m^2 at x=0 to 6.1 kg/m^2 at x=7.5 m (18% decrease). Downstream, the sediment load and u_c remained relatively constant.

Analyzing the data from Figure 4-69, the measured concentration profiles also suggest a decrease of the sediment load from 7.5 kg/m^2 at x=0 to approximately 6.0 kg/m^2 at x=1.27 m, and to approximately 7.2 kg/m^2 at x=5.43 m.

A possible explanation for the observed variation of the sediment load both in the Delft3D model and the measurements could be that:

- The sediment mass is released at a certain initial velocity (in this case, 0.18 m/s)
- The mass initially accelerates, according to the flow conditions and geometric characteristics
- Initial acceleration causes an increase in the mass flux
- To be able to sustain a constant mass flux when flow becomes stationary, the concentration over the water column should decrease, therefore reducing the sediment load.

The decrease of the sediment load is evidenced in lower concentration in the Delft3D model than in the Lagrangian 1DV model, as previously shown in Figure 4-72. Lower concentration generated a smaller baroclinic forcing in the Delft3D model.

The average of the baroclinic term of the momentum equation in the region of higher velocities and concentration was estimated at x=7.5 m, where u_c was 29% higher in the Lagrangian 1DV model. It was verified that this average was higher for the Lagrangian 1DV model. This explains the higher acceleration that produced higher velocities in the Delft3D model (Figure 4-70). Higher velocities in the region of higher concentration produced higher values of u_c in the Delft3D model.

In the previous set of experiments (Set 2 in Section 4.3), a hypothesis was proposed to explain the differences in u_c between the models. However, this hypothesis did not take into account that for a larger baroclinic forcing, as in this case, the change in the velocity profiles is significant when the concentration profile changes. The baroclinic forcing became more important in this set of experiments due to a higher bed slope and larger concentration. Then, the differences in concentration between the models produced differences in the velocity profiles.

In the Delft3D model, the integral of the concentration gradient can be written as:

$$\int_z^\zeta \frac{\partial c}{\partial x} dz' = \int_z^\zeta \frac{-w}{u} \frac{\partial c}{\partial z'} dz' + \int_z^\zeta \frac{1}{u} \frac{\partial J_c}{\partial z'} dz'$$

In the Lagrangian 1DV model, with $u = u_c$ and $-w/u_c = tan\,\beta$ (where β is the bed slope angle), and assuming there are no fluxes through the water surface, the integral of the horizontal concentration gradient can be expressed as:

$$\int_z^\zeta \frac{\partial c}{\partial x} dz' = -c(z) \cdot tan\,\beta - \frac{1}{u_c} J_c(z)$$

The first term on the RHS in Equation (4.12) depends both on the bed slope and the concentration. This term is analogous to the first term on the RHS of Equation (4.11). It was negligible in Set 2 of experiments due to a very small bed slope, which permitted to explain the differences in u_c between the models based only on the differences in the concentration profiles.

4.5.3 Experiment STD-C

This numerical experiment was done with coupled models, now including deposition. The results of the models for velocity and concentration were compared with the measurements by Van Kessel and Kranenburg (1996).

Description

The input parameters of the models were the same as in Experiment ST-C, except for the parameters related to deposition. The Partheniades and Krone formulation was selected for deposition in both models. Full deposition was assumed. Then, a very high critical shear stress for deposition ($\tau_{cr,d}$ = 1000 Pa) was used.

As in experiment ST-C, the initial profiles correction of the Lagrangian 1DV model to keep the same initial mass and mass flux as defined in the input file did not generate a change in $\bar{u}$. Then, the velocity and concentration profiles at the upstream boundary of the Delft3D model were defined to match the initial profiles of the Lagrangian 1DV model at x=0 m.

Results

Velocity

The velocity profiles were plotted at x=1.25 m, x=5.45 m, and x=9.45 m. The changes with respect to the Experiment ST-C were very small because the deposition rate was very small (in the order of 10^{-}

[4] kg/m^2/s). The measurements by Van Kessel and Kranenburg (1996) at x=1.27 m and x=5.43 m for Run 2 were also plotted at x=1.25 m and x=5.45 m, respectively.

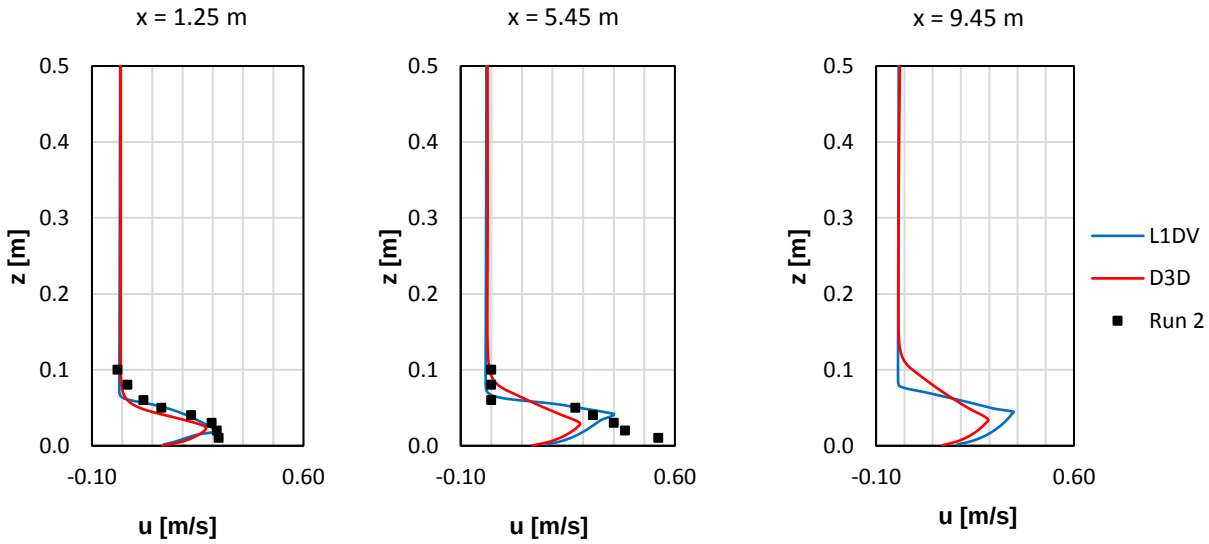

Figure 4-74. Velocity profiles for Experiment STD-C

At x=1.25 m, there was good agreement of the results of both models with the measured velocities. The results for the Lagrangian 1DV model were closer to the measured values. Both models estimated accurately an upstream directed velocity at z=0.10 m.

At x=5.45 m, both models underestimated the velocity at the lower part of the profile (below z=0.05 m). The results Lagrangian 1DV model agreed better with the measurements above z=0.05 m. The measured velocity of zero above z=0.06 m and, consequently, the turbidity current thickness were better reproduced by the Lagrangian 1DV model.

At both stations, the maximum velocity was located at a higher level for the numerical models. This result suggests that the selected drag coefficient (translated into a Chezy coefficient) was higher than in the laboratory flume.

In general, as in Experiment ST-C, the Lagrangian 1DV model estimated higher velocities below z=0.06 m (region of high concentration) than the Delft3D model. The velocity measurements are more in line with the Lagrangian 1DV model results.

Concentration

The resulting concentration distribution in the 2DV field is presented in Figure 4-75, for the first 10 m from the source. Again, the stability of the concentration profiles was checked in the Delft3D model at different times where flow seemed stationary. No signs of instability were observed. The wiggles could be a consequence of interpolation between the center of the grid cells.

The change of the concentration distribution was very small compared to Experiment ST-C. For example, a near-bed concentration (at the lowest grid cell) of 140 kg/m^3 occurred at x=8.84 m for Experiment STD-C in the Lagrangian 1DV model. In Experiment ST-C, this concentration occurred only a few centimeters downstream at x=9.02 m. In the Delft3D model, the same near-bed concentration (140 kg/m^3) occurred at x=5.65 m for Experiment STD-C and at x=5.75 m for Experiment ST-C.

The horizontal concentration gradient $\partial c / \partial x$ near the bed (below z=0.02 m) was larger (more negative) for the Delft3D model. Considering that the deposition rate was very small in both models, the difference is likely to be an effect of the general decrease of the sediment load in the Delft3D model along the slope.

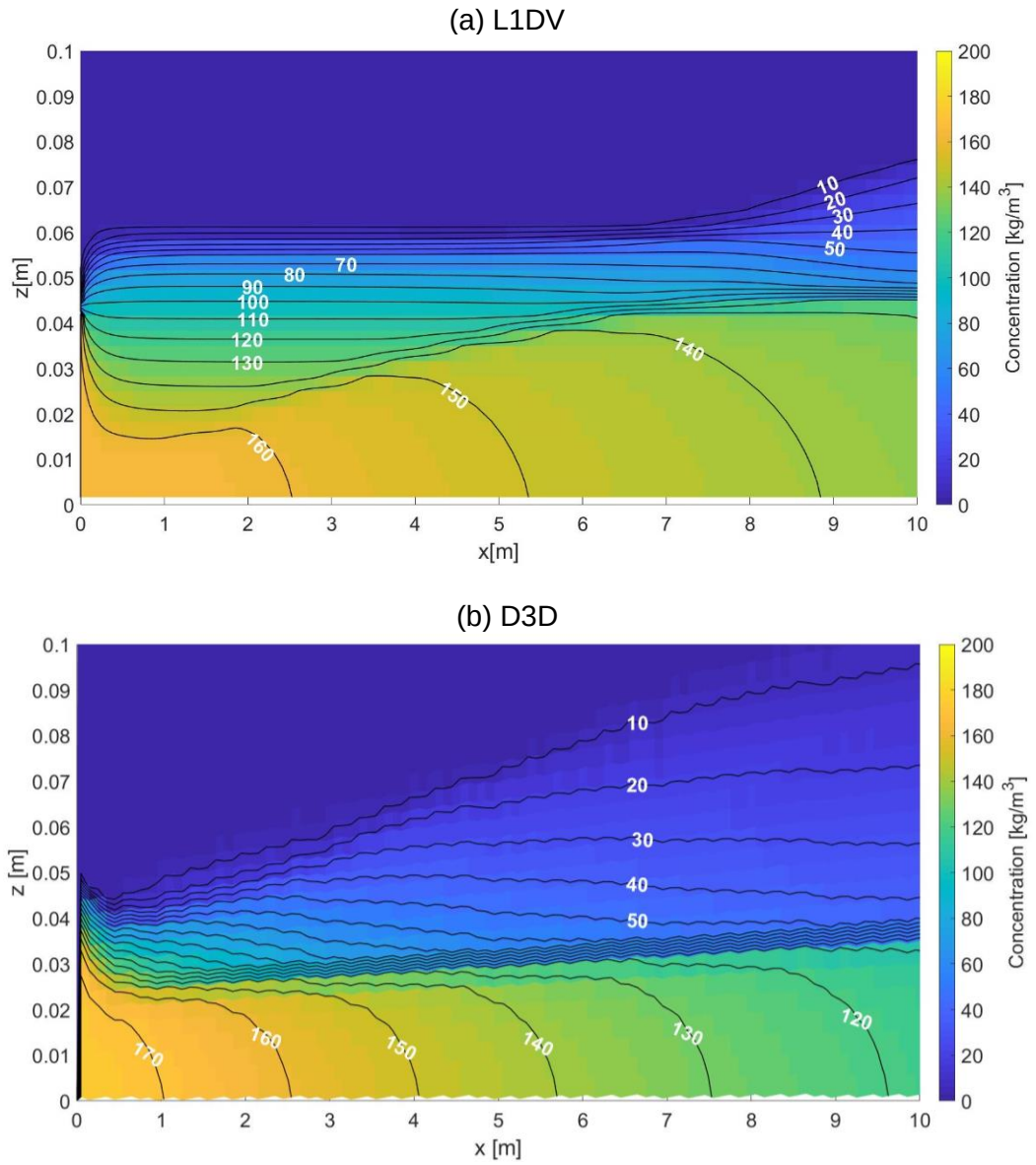

Figure 4-75. Concentration distribution for Experiment STD-C

The concentration profiles were plotted at x=1.25 m, x=5.45 m, and x=9.45 m. The measurements by Van Kessel and Kranenburg (1996) at x=1.27 m and x=5.43 m for Run 2 were also plotted at x=1.25 m and x=5.45 m, respectively.

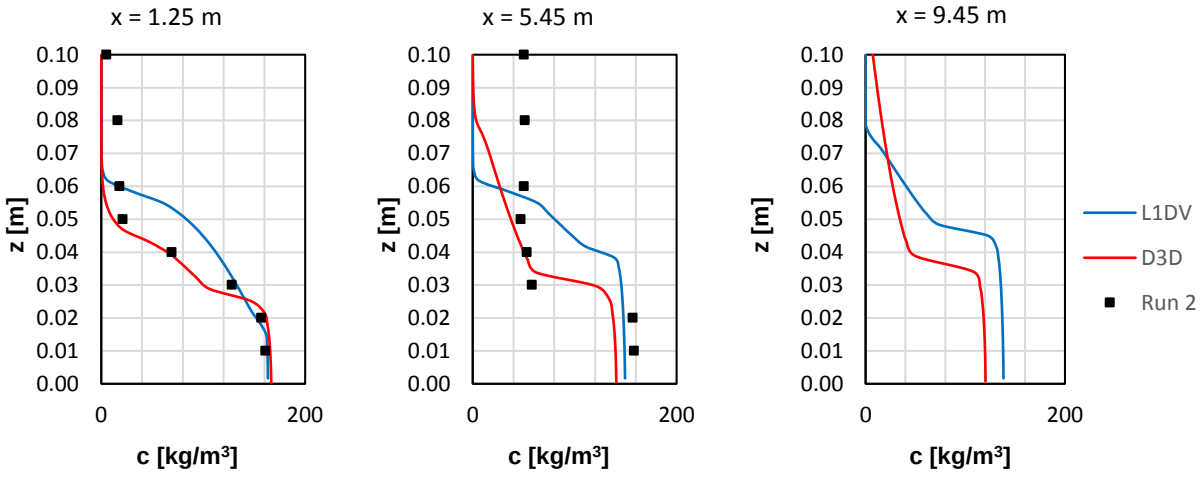

Figure 4-76. Concentration profiles for Experiment STD-C

In general, the concentration below z=0.06 m was lower for the Delft3D model than for the Lagrangian 1DV model. The change in the concentration profiles was very small compared to Experiment ST-C.

The measured concentration was closer to the profiles estimated by the Delft3D model. The Delft3D model accurately estimated the concentration and concentration gradient below z=0.06 m. At x=5.45 m, the measured concentration above z=0.06 m and below z=0.10 m was high (above 40 kg/m^3) and fairly constant, which was not expected and not reproduced by the models.

Mass flux

The variation trend was approximately the same as for Experiment ST-C as the deposition rate was very small in the analyzed reach.

Variation of u_c along the channel

Figure 4-77 shows the variation of the ratio u_c/u_{c0} along the first 10 m from the source (left) and along the first 40 m (right). To estimate the variation of u_c/u_{c0} along the first 40 m in the Lagrangian 1DV model, the depth was modified to 1.44 m (average depth of the Delft3D model along that reach) and the depth-averaged velocity was set accordingly to 0.005 m/s for this depth.

The dashed lines show the previously presented results for Experiment ST-C (no deposition) as a reference.

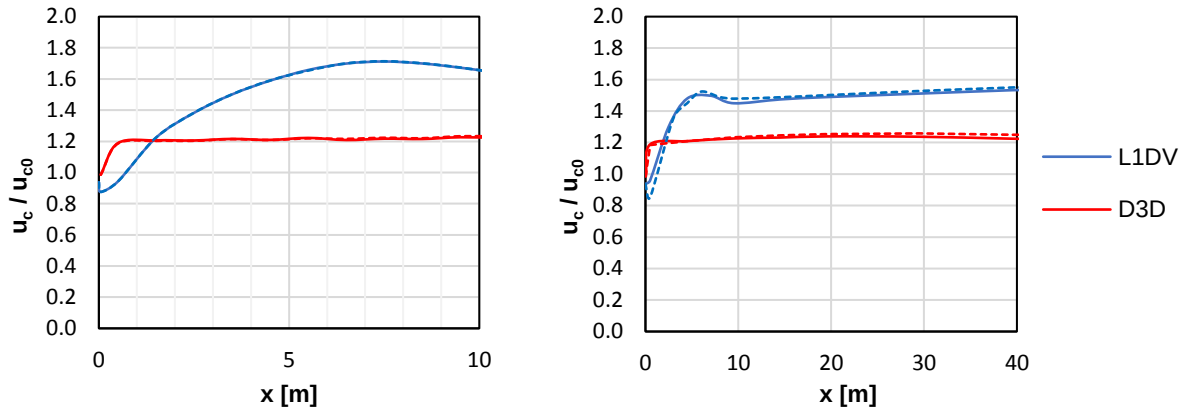

Figure 4-77. Variation of the u_c/u_{c0} with the distance from the source for Experiment STD-C from x=0 m to x=10 m (left) and from x=0 to x=40 m (right)

The difference in the magnitude of u_c/u_{c0} compared to the results of Experiment ST-C was negligible. Again, the value of u_c/u_{c0} was lower for the Delft3D model than the Lagrangian 1DV model, along the analyzed reach (except for the first meter). Averaging u_c over the distance (first 40 m), the result for the Lagrangian 1DV model (0.26 m/s) was 18% higher than the average for the Delft3D model (0.22 m/s) along the first 40 m.

Sedimentation

The deposition rate $D\ (= w_s c_b)$ in kg/m^2/s was calculated for the Delft3D model. This value remains constant at a certain position x, when the flow is stationary. It was compared to the deposition rate of the Lagrangian 1DV model. The results are shown in Figure 4-78.

The deposition rate was larger for the Lagrangian 1DV model. The variation of the sediment load (Figure 4-79) suggests that the transport distance may be longer in the Lagrangian 1DV model. However, the analysis of a longer reach is required to confirm it, as the decrease in the sediment load was very small in the analyzed length.

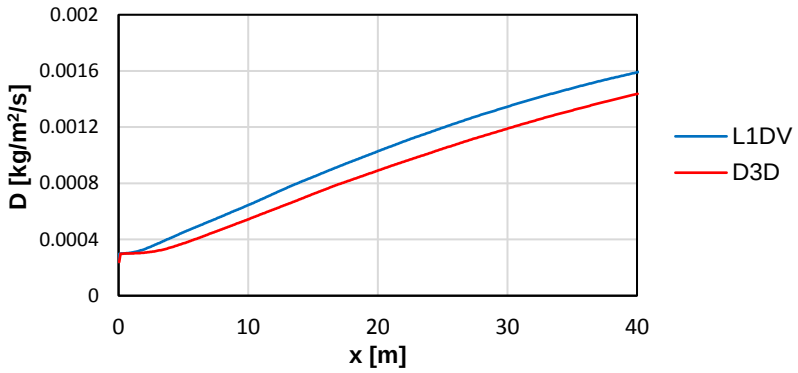

Figure 4-78. Deposition rate for Experiment STD-C.

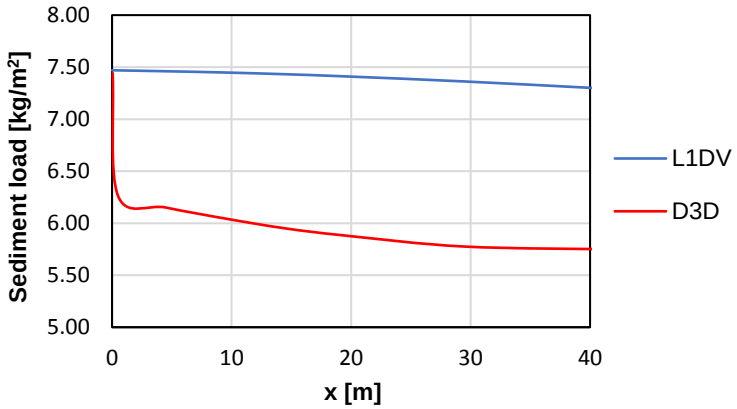

Figure 4-79. Sediment load variation for Experiment STD-C.

Interpretation of results for u_c

For this experiment, the deposition rate was very small. The sediment load only decreased by 2.5% in the first 40 m. The change in the sediment load and the concentration due to deposition did not produce a significant change in the baroclinic term of the momentum equation, along the analyzed length in any of the models. Therefore, the result for u_c was almost the same as in Experiment ST-C.

5 Discussion

This chapter includes a reflection on the validity of the L1DV approach for sediment transport modelling, the relevance and uncertainty of the modelled processes, and possible practical implications of its assumptions when modelling a WID-induced turbidity current.

5.1 Validity of the Lagrangian 1DV approach compared to a 2DV approach

5.1.1 Uniform and non-uniform conditions

The Lagrangian 1DV approach was first compared to the 2DV approach in uniform flow conditions. As presented in Chapter 3, the Lagrangian 1DV model is based on the 1DV Point Model to solve the processes in the water column. One of the main assumptions of the 1DV Point Model is uniformity in the Eulerian reference frame. It is assumed that uniformity in the Eulerian reference frame corresponds to stationarity in the Lagrangian frame of reference. Then, by satisfying the uniformity assumption in the Delft3D model (2DV approach), it was expected that the difference between the Lagrangian 1DV model and the Delft3D model was not significant. Experiments Set 1 (Section 4.2) was executed to verify this.

The results of Experiments Set 1 agreed with the expected result. For the first experiment (Experiment ST-UC, with no erosion or deposition), there were no significant differences between the models at a station of the channel where both the velocity and the concentration were uniform (at a distance of 1000 m from the sediment source, in this case). Both models performed in good agreement with the analytical solution, producing the expected logarithmic profile for velocity and Rouse profile for the concentration. This experiment already indicated that the settling and turbulent diffusive fluxes were consistently estimated by the Lagrangian 1DV model and the Delft3D model.

The models of Experiments Set 1 were first run in their uncoupled (UC) version. Therefore, sediment concentration did not influence the density of the fluid, and the solution of the sediment transport equation had no effect on the solution of the momentum equation. In a second stage, with the same geometrical setup and initial conditions (upstream boundary conditions in Delft3D), the Lagrangian 1DV and the Delft3D models were run in the coupled (C) version. This was done to test their performance when linking the solution of the momentum and sediment transport equations through the baroclinic term. The concentration of the models was very low (1 kg/m^3) and, consequently, very small density differences did not lead to significant differences between the results for velocity and concentration in the Lagrangian 1DV model and the Delft3D model. The difference was not significant comparing to the uncoupled version of the models.

Experiments Set 1 confirmed the validity of the Lagrangian 1DV approach for uniform flow, and that the formulations for settling and turbulent mixing produced almost the same results in the Lagrangian 1DV model and the Delft3D model for uniform conditions and very low concentration. This confirmation was necessary to advance to Experiments Set 2, where the behaviour of the models was examined in non-uniform conditions and the concentration was increased (significant baroclinic pressure gradient).

Experiments Set 2 analyzed if non-uniform conditions lead to differences between the models or not. It consisted of six experiments: three different initial concentration profiles (upstream boundary concentration profiles in the Delft3D model) and two types of models (uncoupled and coupled). The initial depth-averaged concentration was increased from 1 kg/m^3 (Experiments Set 1) to 10 kg/m^3. The length of the modelled channel in Delft3D model (1000 m) permitted to observe both a non-uniform flow stage (closer to the source) and the uniform flow stage downstream. Erosion and deposition were not considered.

The concentration-weighted velocity u_c was compared between the Lagrangian 1DV and the Delft3D models first for the uniform flow regime. For the Delft3D model, u_c was also defined as the ratio

between the mass flux and the sediment load in the Delft3D model. Table 5-1 summarizes the obtained u_c values, as a reference for discussion. The value of u_c of the Delft3D model was assumed as the reference to calculate the difference in u_c between the models.

Table 5-1. Concentration-weighted velocity u_c for uniform flow regime (Experiments Set 2).

Experiment	u_c [m/s]		Difference in u_c [%]
	Lagrangian 1DV	Delft3D	
ST-UC (vertically uniform initial profile)	0.993	0.994	-0.10%
ST-C (vertically uniform initial profile)	0.986	0.990	-0.40%
ST-UC (linear initial profile)	0.993	0.994	-0.10%
ST-C (linear initial profile)	0.988	0.990	-0.20%
ST-UC (block-shaped initial profile)	0.993	0.994	-0.10%
ST-C (block-shaped initial profile)	0.988	0.990	-0.20%

The value of u_c is constant along the channel for uniform flow. The variation of u_c along the channel can be observed in Figure 5-1, as a complement Table 5-1.

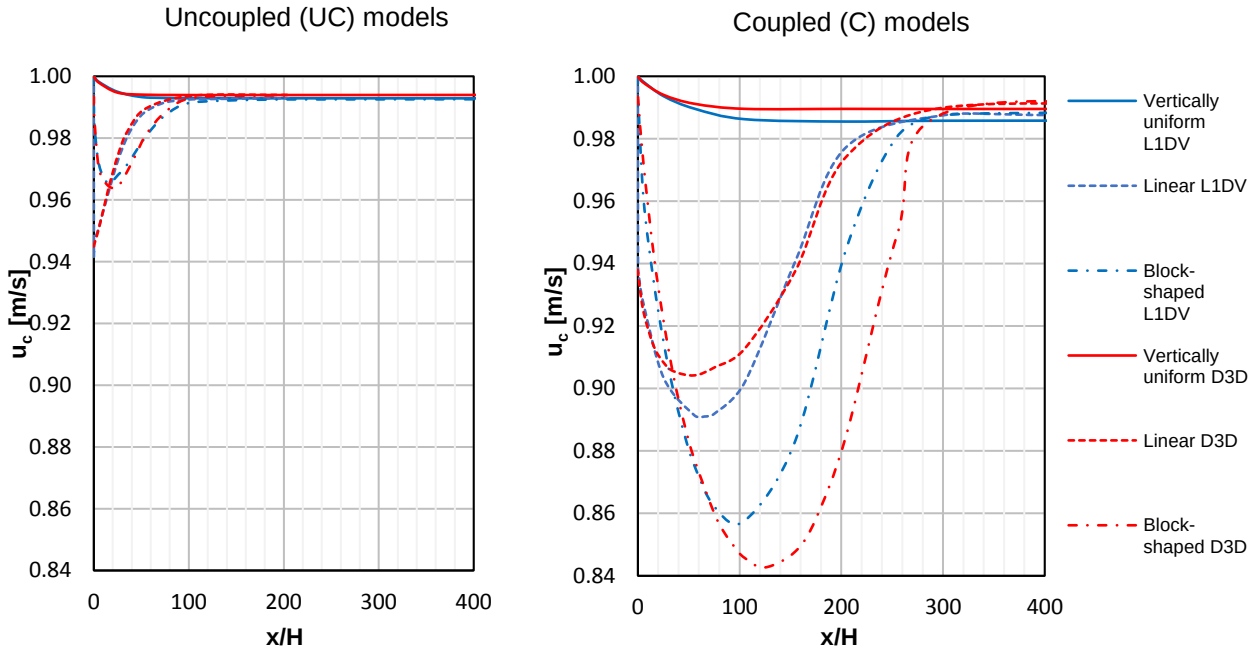

Figure 5-1. Variation of the concentration-weighted velocity along the channel for uncoupled models (Experiments Set 2)

For uniform flow, the difference in u_c between the Lagrangian 1DV model and the Delft3D model for the uncoupled models (labeled as "-UC") was -0.1% (u_c was slightly lower for the Lagrangian 1DV model). As seen in Figure 5-1, independently of the initial profile shape, the Lagrangian 1DV model and the Delft3D model converged to almost the same value of u_c for the uncoupled models, which is the theoretical u_c value for the combination of a Rouse profile and a logarithmic velocity profile (approximately 0.994 m/s). Obtaining the same values of u_c for uniform flow showed again (as it was shown in Experiments Set 1) that the differences in the results of the formulations of the vertical processes between the Lagrangian 1DV model and the Delft3D model were minimal for uncoupled models, even downstream from a reach of non-uniform flow regime.

For coupled models (right graph of Figure 5-1), the difference in u_c between the Lagrangian 1DV model and the Delft3D model for uniform flow was 0.40% for the case of the vertically uniform initial profile and 0.20% for the other two types of initial profiles. Independently of the initial profile shape, the Lagrangian 1DV model and the Delft3D model converged to almost the same value of u_c. Hence,

the differences in the results of the formulations for the vertical processes showed to be minimal also for coupled models, with an initial depth-averaged concentration of 10 kg/m^3.

Experiment ST-C with a vertically uniform initial profile reported a slightly lower value for u_c at the uniform flow stage (0.986 m/s) which may be explained by the fact that a lower z_0 was used for this experiment (different from the other experiments, but the same value in the Lagrangian 1DV model and the Delft3D model for that specific experiment).

Regarding non-uniform flow, the analysis is done separately for uncoupled models and for coupled models. Uncoupled models (for each particular profile) showed almost the same values for u_c along the channel in the Lagrangian 1DV model and the Delft3D model (left graph of Figure 5-1). This indicates that turbulent mixing and settling (vertical processes) do not generate differences between the models, even in non-uniform conditions, if there are no significant density differences.

The adaptation length (defined here as the required length to adapt from initial non-uniform conditions to uniform flow) was compared between the uncoupled models for the different cases of initial concentration profiles. The downstream end of the adaptation length can be visually determined from the left graph of Figure 5-1, at the station where u_c becomes constant. Table 5-2 summarizes the results for the adaptation length from Section 4.3, as a reference for discussion.

Table 5-2. Adaptation length for the uncoupled models (Experiments Set 2).

Experiment	Adaptation length [m]	
	Lagrangian 1DV	Delft3D
ST-UC (vertically uniform initial profile)	70	70
ST-UC (linear initial profile)	130	130
ST-UC (block-shaped initial profile)	160	160

In general terms, the adaptation length of the Lagrangian 1DV model and the Delft3D model were similar, for each specific profile. The block-shaped initial profile provided the longest adaptation length (approximately 20% longer than the adaptation length for the linear initial profile). This is explained below because it also happened for the coupled models.

Differences in u_c between the Lagrangian 1DV model and the Delft3D model arose for non-uniform flow when the density differences were significant, because of the feedback on the baroclinic part of the pressure gradient (feedback between the momentum equation and the sediment transport equation). Table 5-3 indicates the maximum difference in u_c along the adaptation length for each experiment of Set 2 with coupled models. The value of u_c of the Delft3D model was used as a reference to compute the maximum differences with the Lagrangian 1DV model.

Table 5-3. Maximum difference in u_c and adaptation length for coupled models (Experiments Set 2).

	Maximum difference in uc [%]	Adaptation length[m]	
		L1DV	D3D
ST-C (vertically uniform initial profile)	-0.4%	150	130
ST-C (linear initial profile)	-1.6%	300	300
ST-C (block-shaped initial profile)	6.8%	350	375

The adaptation length was approximately twice as long compared to the uncoupled models, for each of the profiles. This was expected because, in uncoupled models, changes in velocity are not because of changes in concentration (there is no density difference and, therefore, no baroclinic pressure gradient). In coupled models, concentration and velocity changes are linked, which makes adaptation to uniform flow a more complex process.

The trend of the adaptation length for coupled models (Table 5-3) was the same as for the uncoupled models. The block-shaped profile showed the longest adaptation length. Apart from the difference in the initial concentration profile, the initial velocity profile for that experiment was considerably different from the profile for uniform flow. Then, it is reasonable that the adaptation length for the block-shaped profile was the longest. Additionally, for that profile, a significant difference was observed between

the Lagrangian 1DV model and the Delft3D model in the initial turbulence conditions and their development near to the source. The Lagrangian 1DV model estimated a higher eddy diffusivity at the upper part of the water column, while Delft3D had higher diffusivity at the slurry layer. This situation limited the analysis of the differences between the models. It is not known to what extent the differences in u_c that were observed in the Experiment ST-C for the block-shaped profile reflect the difference between the turbulence initial conditions, and to which extent they reflect the difference between the Lagrangian approach and the 2DV approach. However, it is known that both of them have an influence on the model outcome.

The linear initial profile and the vertically uniform initial profile produced small differences in u_c between the models. The block-shaped initial profile yielded a longer adaptation length (17% longer in the Lagrangian 1DV model and 25% longer in the Delft3D model than the linear profile). Hence, the difference in u_c remained for a longer distance.

Comparing to the 2DV approach, the block-shaped profile showed a larger difference between the Lagrangian 1DV model and the Delft3D model. The linear profile showed considerably smaller differences. Then, it is likely that it produces closer results to the 2DV situation.

According to Deltares (2019), a model with a linear initial concentration profile with the center of mass at the same height as the center of mass of the block-shaped profile would be more appropriate for comparison. The limitation again is that the initial turbulent conditions would be different between the Lagrangian 1DV model and the Delft3D model, as it was observed for the case of the block-shaped profile.

The results of the coupled experiments of Experiments Set 2 suggest that the origin of the differences between the Lagrangian 1DV model and the Delft3D model in u_c and in the horizontal concentration gradient rely on the expression of the advective transport term of the sediment transport equation.

In the Lagrangian 1DV model, sediment is transported longitudinally at a velocity u_c at all levels, while the Delft3D model uses the velocity at every particular level. This means that, when the profile of the net vertical sediment flux is similar in both models (settling and turbulent mixing are in the same order of magnitude in both models), the horizontal concentration gradient will be larger for the Lagrangian 1DV model at the levels where $u > u_c$. This was observed in the experiments with the vertically uniform and the linear initial profiles. At the upper part of the water column, where $u > u_c$, $\partial c/\partial x$ was larger for the Lagrangian 1DV model. In the reach of the channel where the differences in u_c originated, settling was dominant at the upper part of the water column. Hence, $\partial c/\partial x$ was more negative in the upper part of the water column. Then, for a certain horizontal distance, more sediment was directed downwards to a region of lower velocities in the Lagrangian 1DV model, yielding a lower u_c value. A sketch to explain this situation was included in Section 4.3.7 and is included below to compare it with the case of the block-shaped initial profile.

It is important to remark that, in Experiments Set 2, the differences in the baroclinic pressure gradient were not high enough to produce significant differences in the velocity profile between the models. Then, the previous explanation is valid for those conditions.

In the case of the initial block-shaped profile, the analysis was limited because the net vertical sediment flux profiles of the Lagrangian 1DV model and the Delft3D model, near the station of the channel where the differences seemed to originate, was not similar (as for the linear and vertically uniform profiles). However, the results suggest that the dominance of the turbulent diffusive flux in the Lagrangian 1DV model at the upper part of the water column (where $u > u_c$) produced a higher u_c, opposite from the relation for the cases of the initial vertically uniform and linear profiles, where u_c was lower for the Lagrangian 1DV model. The following figure shows the situation for the vertically uniform and linear initial concentration profiles (up), also shown in Figure 4-55, and the described situation for the block-shaped profile (down).

(a) For vertically uniform and linear initial concentration profiles

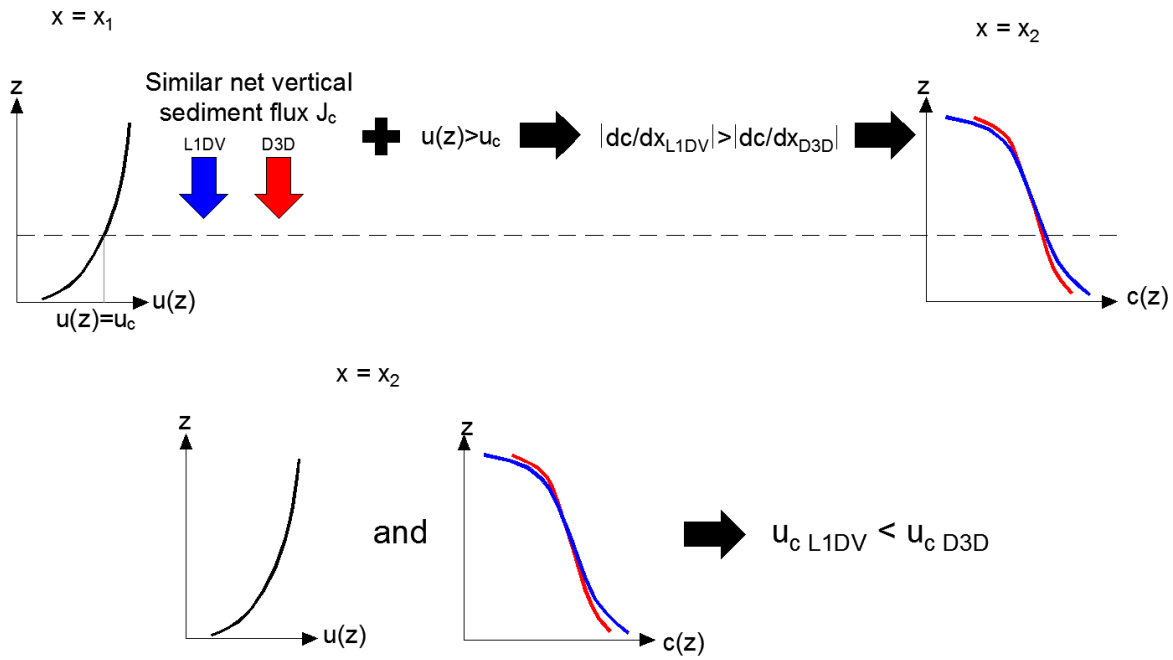

(b) For block-shaped initial concentration profile

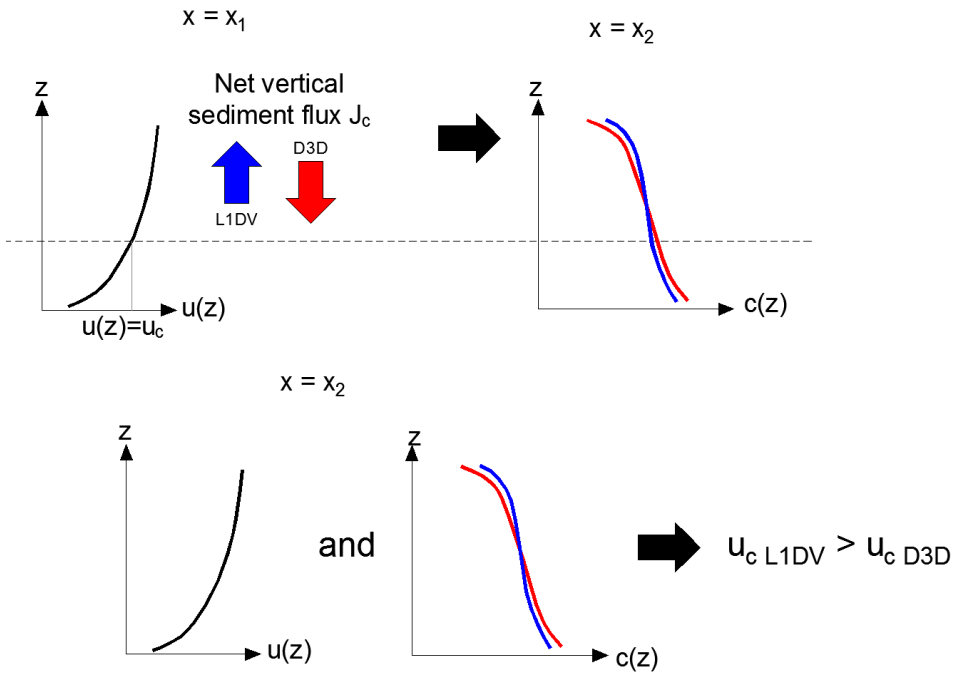

Figure 5-2. Possible explanation for the process that generates differences in u_c for (a) vertically uniform and linear initial profiles and (b) for the block-shaped initial concentration profile

In general, the results for the Lagrangian 1DV approach did not show large differences with the results of the 2DV approach for the coupled models of Experiments Set 2. This set of experiments was done with a low concentration (10 kg/m^3) compared to the order of magnitude of the concentrations present in a WID-induced turbidity current (~100 kg/m^3). This was done for two reasons: to be able to detect the effect of non-uniformity of flow on the difference between the models and to keep the depth and depth-averaged velocity of the Delft3D model constant along the channel. Trial tests in a channel with the same setup in Delft3D model, but increased concentration, showed that a large concentration in

a ~1 m depth channel in the Delft3D model reduces the near-bed velocities and the bed shear stress, and produces a significant water depth change, with the consequent change in the depth-averaged velocity and mass flux. The change of the depth along the channel and the significant depth-averaged velocity made the Delft3D model not comparable to the Lagrangian 1DV model.

5.1.2 Magnitude of the baroclinic pressure gradient and its effect on u_c

The explanation of the process that generated differences in u_c between the models in Experiments Set 2 (Figure 5-2) was based on how the concentration profile changed along the channel. In Experiments Set 2, the velocity profiles showed very small differences between the models. A hypothesis was proposed to explain how different u_c would be for a turbidity current in Section 4.3.7. This hypothesis was tested in Experiments Set 3 and Experiments Set 4, based on Run 13 of Parker et al. (1987) and Run 2 of van Kessel and Kranenburg (1996), respectively. However, the hypothesis was not able to explain the obtained results. This could be because the baroclinic term in the momentum equation was more important for Experiments Set 3 and Set 4, due to a higher bed slope and higher concentration. Therefore, different from what was observed in Experiments Set 2, the difference in the baroclinic pressure gradient between the models produced important differences in velocity for Experiments Set 3 and Experiments Set 4.

In the case of Experiments Set 3, based on Run 13 of Parker et al. (1987), u_c was lower for the Lagrangian 1DV model along the analyzed reach (first 40 m from the source). For Experiment ST-C, u_c was 24% lower at the point of maximum difference. Averaged over the distance, u_c was 16% lower. Both models presented a similar trend in the variation of u_c along the channel: a significant decrease (deceleration of the sediment mass) in the first 4.5 m from the source, followed by an increase until x=10 m to finally reach a relatively constant value downstream from x=10 m.

The deceleration of the sediment mass in the Delft3D model (decrease in u_c) was clearly related to an increase in sediment load. This was observed from x = 0 to x = 4.5 m. While u_c decreased, the sediment load increased significantly (53% from x=0 to x=4.5 m). The concentration measurements from Parker et al. (1987) also suggest an increase of sediment load at x=4.5 m. Based on the measured concentration at that station, the sediment load was approximately 1.1 kg/m^2 at x=4.5 m, while the initial sediment load was 0.87 kg/m^2.

A possible explanation for the observed variation of the sediment load both in the Delft3D model and the measurements by Parker et al. (1987) could be that the initial deceleration would cause a reduction in the mass flux. However, to be able to reach a constant mass flux when flow becomes stationary, the concentration over the water column increases, therefore increasing the sediment load. Meanwhile, the sediment load of the Lagrangian 1DV model is constant by definition.

The higher value of u_c can be explained by the observed increase of the sediment load and the concentration in the Delft3D model. Larger concentration generated a larger baroclinic forcing in the Delft3D model. The difference in the baroclinic pressure gradient between the Delft3D model and the Lagrangian 1DV model was considerable and produced higher velocities in the Delft3D model, which yielded a higher value of u_c.

The addition of the deposition process (Experiment STD-C of Experiments Set 3) did not affect considerably the differences in u_c between the models. Averaged over the distance, u_c was 20% lower for the Lagrangian 1DV model. The variation of the sediment load in these experiments indicates that the sediment mass was transported further in the Delft3D model. At x=40 m, the Delft3D model still transported 60% of the initial sediment load, while the Lagrangian 1DV model transported 26%.

Experiments Set 4, based on Run 2 of van Kessel and Kranenburg (1996), showed a higher u_c value for the Lagrangian 1DV model along the channel (the opposite of what was observed in Experiments Set 3). For Experiment ST-C, u_c was 40% higher at the point of maximum difference. Averaged over the distance (along 40 m), u_c was 18% higher.

Also opposite to the case of Experiments Set 3, there was an acceleration of the sediment mass in both models at the first meters from the source. The acceleration of the sediment mass in the Delft3D model (increase in u_c) was clearly related to a decrease in sediment load. While u_c increased, the sediment load decreased significantly from x=0 to x=7.5 m (18% decrease). Downstream, the sediment load and u_c remained relatively constant. The measured concentration profiles also suggest a decrease of the sediment load from 7.5 kg/m^2 at x=0 to approximately 6.0 kg/m^2 at x=1.27 m, and to approximately 7.2 kg/m^2 at x=5.43 m.

Following the same reasoning as for Experiment ST-C of Experiments Set 3, a possible explanation for the observed variation of the sediment load both in the Delft3D model could be that the initial acceleration would cause an increase in the velocity and in the mass flux. However, to be able to reach a constant mass flux when flow becomes stationary, the concentration over the water column should decrease, therefore decreasing the sediment load.

The lower value of u_c in the Delft3D model can be explained by the observed decrease of the sediment load and the concentration in the Delft3D model. Larger concentration in the Lagrangian 1DV model generated a larger baroclinic forcing. The difference in the baroclinic pressure gradient between the models was considerable and produced higher velocities in the Lagrangian 1DV model, which yielded a higher value of u_c.

The next sketch shows the observed process that could explain the variation of u_c in the models of Experiments Set 3 and Set 4.

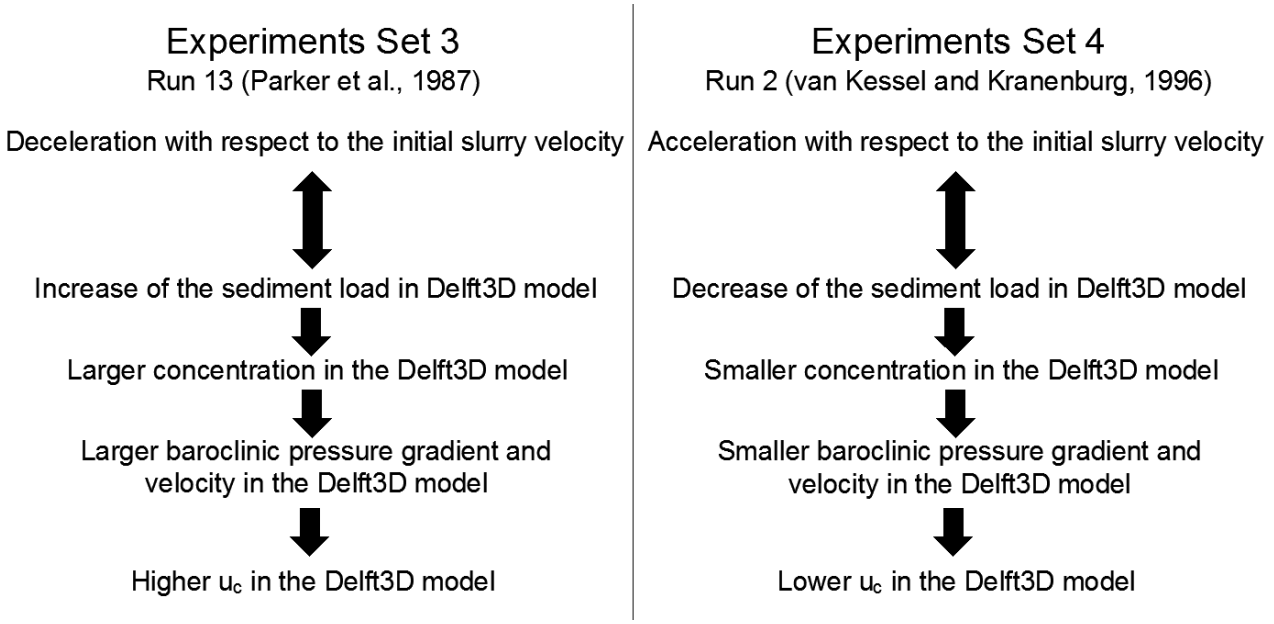

Figure 5-3. Observed relations of velocity, sediment load and concentration-weighted velocity in Experiments Set 3 and Set 4

Experiment STD-C of Experiments Set 4 included the deposition process. However, the results for u_c were practically the same as in Experiment ST-C because the deposition rate was very small. The variation of the sediment load suggests that sediment was transported further in the Lagrangian 1DV model. Nonetheless, a model analyzing a longer reach is required to confirm this.

5.2 Relevant physical processes

As it was mentioned above, the formulation of the settling and turbulent mixing processes in the water column does not produce any difference between the Lagrangian 1DV model and the Delft3D model for the uniform flow regime. In non-uniform flow, differences were observed in the initial turbulent mixing for the experiments of Set 2 with the block-shaped initial concentration profile, and for Experiments Set 3 and Set 4. These differences may be relevant for the increase of suspended sediment concentration in the water column.

About the importance of the turbulent mixing process, its relevancy is expected to decrease in a WID-induced turbidity current. For the high concentrations expected WID (in the order of 100 kg/m^3), turbulence may be damped considerably.

Erosion and deposition were identified as important processes in the theoretical framework. These processes were analyzed in detail in Experiments Set 1. The formulation for deposition produced almost the same result in both models for the provided conditions of uniform velocity along the channel. The difference was below 1% in the near-bed concentration between the models and with the analytical solution. In the last part of the Set 1 of experiments, the erosion process was studied (Experiment STE-UC) with the Partheniades-Krone formulation, which is mainly applied to cohesive sediment. There was a small difference in the bed shear stress between the models and with the theoretical value. The bed shear stress in the Delft3D model was 4% higher than the theoretical value, which was reflected in a higher erosion rate. The origin of this difference was not clear as the models were run for the same bed slope, roughness length z_0, depth H and depth-averaged velocity $\bar{u}$.

Experiments STD-UC (including deposition) and STE-UC (including erosion) from Experiments Set 1 suggested that deposition is more important than erosion in determining the concentration of the turbidity current. For the selected soil parameters, the erosion rate was in the order of 10^{-4} kg/m^2/s and the deposition rate, even for a low concentration of 1 kg/m^3, was still higher (in the order of 10^{-3} kg/m^2/s).

For a typical WID application, the near-bed concentration is in the order of 100 kg/m^3. For the range of settling velocities in WID practice (0.1 mm/s to approximately 10 mm/s), the deposition rate is in the order of 0.01 to 1 kg/m^2/s. As observed in Experiments Set 1, for a high depth-averaged velocity in the order of 1 m/s (considered here an upper limit for a typical WID-induced turbidity current), the bed shear stress was in the order of 1 Pa. For a critical shear stress for erosion $\tau_{cr,e}$ of 0.1 Pa (low) and an erosion parameter in the order of 10^{-3} kg/m^2/s (high), an upper limit of the erosion rate is in the order of 0.01 kg/m^2/s (in the order of the lower limit for deposition). This suggests that deposition is a more important process than erosion in the determination of the suspended sediment concentration profile and sedimentation due to a WID-induced turbidity current.

As a result of the relative importance of the processes, the accurate determination of the settling velocity, which defines the deposition rate, is more important for the application than a very detailed determination of the erosion parameter.

The relevance of deposition and erosion when sediment is non-cohesive sediment must also be analyzed. This was not part of the scope of this study as the main objective was the comparison of the Lagrangian 1DV and the 2DV approach, and the formulations of Delft3D-FLOW for the erosion of non-cohesive sediment are not included in the Lagrangian 1DV model.

5.3 Practical implications of the Lagrangian 1DV approach

5.3.1 Initial concentration and velocity profiles

The selection of the initial profiles is an important step in the setup of the Lagrangian 1DV model. The case of the block-shaped initial concentration profile highlighted that the initial concentration profile influences the difference in the outcome of the Lagrangian 1DV model and the Delft3D model.

It was observed that using the linear initial concentration profile provided smaller differences in the concentration-weighted velocity and the mass flux between the Lagrangian 1DV model and the Delft3D model. With the available information, this suggests that the linear profile may be a better selection than the block-shaped initial profile for the Lagrangian 1DV model. However, the result should be carefully analyzed, because the linear profile was tested with an initial velocity profile close to logarithmic and the concentration profile occupied all the water column. The eddy diffusivity matched between the Lagrangian 1DV model and the Delft3D model from the beginning. On the other hand, for the block-shaped profile, the eddy diffusivity presented important differences close to the source.

The determination of the shape of the initial velocity, concentration and turbulent kinetic energy profiles for a WID-induced turbidity current is a topic for further research.

5.3.2 Engineering questions

One of the engineering questions related to WID is to determine the extension of the sedimentation footprint, for environmental impact assessment or to know in advance how feasible is to transport the sediment to a predefined pit or storage area. The difference in the travelling distance of the turbidity current depends on the available sediment load, the deposition rate, and u_c. Experiments Set 3 and Set 4 produced differences in u_c between 16% and 20% (averaged along the analyzed reach).

Considering the differences in sediment load and u_c, the available information from Experiment STD-C based on Parker et al. (1987) showed that at x=40 m, the Delft3D model still transported 60% of the initial sediment load, while the Lagrangian 1DV model only transported 26% (less than half of what Delft3D transports). Then, the results suggest that the difference in travelling distance (in %) is larger than the difference in u_c. The magnitude of the difference in travelling distance is not possible to determine with the available information. It requires numerical modelling of the specific case. The same approach used in this report to compare the models can be applied.

The differences between the Lagrangian 1DV model and the Delft3D model may be in the order of magnitude of other sources of error when modelling. The estimation of the ambient conditions such as the flow velocity, or the characterization of sediment properties such as the settling velocity and the structural dry density could induce an error in the calculation in a similar order of magnitude of the deviation of u_c from the 2DV situation. Then, being as accurate as possible in the determination of the input parameters is an important first step for the use of the model.

The input parameters for a model of a typical case of a WID application, from literature and from the experience of Boskalis, are shown in Table 5-4.

Table 5-4. Parameters for a model of a typical WID application

Parameter	Value
Bed slope [-]	10^{-4}
Depth [m]	10
Depth-averaged velocity [m/s]	0.3
Initial turbidity current height h_{fl} [m]	0.7
Initial averaged turbidity current velocity u_{fl} [m/s]	1
Initial averaged turbidity current mass concentration c_{fl} [kg/m3]	100
Single particle settling velocity w_{s0} [mm/s]	1
Structural dry density c_{gel} [kg/m3]	600

A run of the Lagrangian 1DV model with the settings of Table 5-4, considering the Partheniades-Krone formulation for deposition and no erosion gives the variation of u_c that is shown in Figure 5-4.

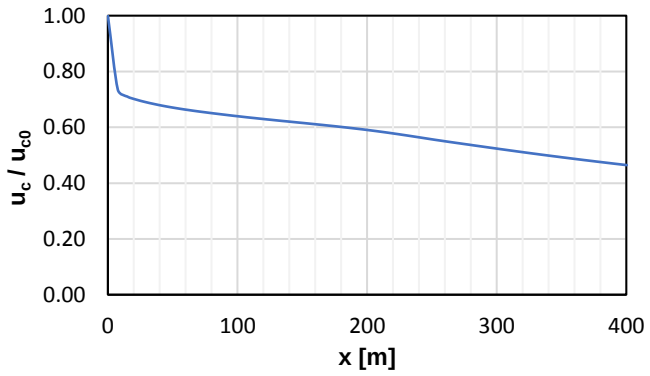

Figure 5-4. Variation of the concentration-weighted velocity for a typical WID case

The trend of variation of u_c is similar to the case of Experiments Set 3, based on Parker et al. (1987), with a significant deceleration of the sediment mass. The results of that experiment suggest that u_c would be higher for the 2DV situation and that the turbidity current would travel more distance than the one estimated with the Lagrangian 1DV model. If the calculation is for a case in which the sediment should be transported to a disposal area, the estimation may be conservative (the actual travelling distance may be longer than the required distance). If the travelling distance is restricted for environmental reasons, the calculation may be unsafe (sediment could reach a longer distance than estimated, affecting the sensitive area).

To confirm the interpretation and obtain the exact difference in u_c and the distribution of the sediment load, numerical modelling is required. The same approach of Chapter 4 for Experiments Set 3 and Set 4 can be used to compare the results of the models.

6 Conclusions and Recommendations

6.1 Conclusions

Which physical processes influence the characteristics of a WID-induced turbidity current and the associated sediment suspension in the water column?

The main involved processes can be categorized into processes in the water column and large-scale processes. The characteristics of a turbidity current are influenced by the following processes in the water column:

- (Hindered) settling,

- Turbulent mixing and stratification,

- Deposition,

- Erosion

The first three processes govern the behaviour of a WID-induced turbidity current. For typical characteristics of a WID-induced turbidity current, erosion is expected to be at least one order of magnitude smaller than deposition.

Two large-scale processes may affect the transport direction of the sediment: lateral spreading (in the transversal direction) and return flow (in the opposite longitudinal direction for large turbidity currents in relation to the depth).

Lateral spreading causes a loss of sediment mass to the sides of the turbidity current, decreasing the amount of mass moving in the longitudinal direction and, consequently, reducing the baroclinic forcing and the longitudinal distance travelled by the turbidity current. Limited information is found in literature about lateral spreading for turbidity currents to quantify its effect, especially for a WID application.

Return flow produces sediment transport at the upper part of the water column, in the opposite direction of the turbidity current. For WID, this would cause sediment to move towards the source, which means it may contribute to reduce the dispersion of the plume but it may increase the suspended sediment concentration near the source near the source. For a typical ratio between the thickness of the turbidity current (in the order of 1 m) and water depth (in the order of 10 m), the return flow is not expected to be significant. For special applications in shallower waters (depth of 3 m to 5 m), the upstream directed velocities generated by return flow may be important compared to the velocity of the turbidity current.

Which of the physical processes are included in the Lagrangian 1DV model?

Settling, turbulent mixing, deposition, and erosion are included. Morphological changes and flocculation are not in the tool, in order to keep its objective of rapid assessment. Lateral spreading is not included as a consequence of the initial conceptualization as a 2DV process. Sediment transport by return flow is not included due to the Lagrangian 1DV approach of the tool.

Considering the main assumptions of the Lagrangian 1DV approach (Section 1.3), what are the differences between the mathematical descriptions of a Lagrangian 1DV approach and a 2DV approach for WID-induced turbidity currents?

The main differences are:

1. The assumption of uniformity of the 1DV Point Model is assumed as stationarity in the Lagrangian frame of reference ($\partial/\partial\tau = 0$), which means that as the turbidity current travels at the Lagrangian velocity, the change of a physical quantity in time equals the change of the quantity in space (in the direction in which the fluid column moves).

2. The definition of the Lagrangian velocity as a concentration-weighted velocity (u_c) over the water column, expressed as the ratio between the mass flux and the sediment load. This means that water and sediment in the column are advected at the same velocity, at a certain time step.

Considering the mathematical differences of the approaches, a method was developed to compare the results: the representation in a 2DV field of the solution of the Lagrangian 1DV model equations for every position was compared to a stationary solution for a continuous release of sediment from a static source in a Eulerian 2DV model (one fluid column released every time step).

Which implications do the main assumptions of the Lagrangian 1DV approach have for sediment transport?

For the uniform flow regime, numerical experiments showed that the differences between the models in u_c and in mass flux were not significant. It was confirmed that the Lagrangian 1DV model is as valid as an Eulerian 2DV approach to represent sediment transport in uniform flow.

For uncoupled models (no effect of sediment on fluid density), no important differences were observed between the Lagrangian 1DV model and the 2DV calculation in the Delft3D model in the concentration and velocity profiles along the channel, even in non-uniform conditions. Differences in the concentration-weighted velocity u_c along the channel were below 1% for all the experiments with uncoupled models (Experiment ST-UC of Set 1 and the experiments ST-UC of Set 2). Then, the results indicate that the Lagrangian 1DV model is as valid as the Eulerian 2DV approach to represent sediment transport in non-uniform flow when density differences are negligible.

Differences between the Lagrangian 1DV model and the Delft3D model in the velocity and concentration profiles appeared when density differences became more important (i.e., in coupled models with an initial depth-averaged concentration of 10 kg/m^3). The differences in u_c for non-uniform flow were below 7% for all tested cases (coupled models of Experiments Set 2 for non-uniform flow in a channel).

The maximum difference in u_c of Experiments Set 2 occurred for the block-shaped initial concentration profile. The comparison of the vertical eddy diffusivity profiles between the Lagrangian 1DV model and the Delft3D model close to the upstream boundary of the channel indicated that part of the difference between the models was due to different formulations for the initial (upstream boundary) turbulent conditions, which created higher initial mixing in the upper part of the water column for the Lagrangian 1DV model.

The results of the coupled experiments of Experiments Set 2 suggest that the origin of the differences between the Lagrangian 1DV model and the Delft3D model in u_c and in the horizontal concentration gradient relied on the expression of the advective transport term of the sediment transport equation. In the Lagrangian 1DV model, sediment is transported longitudinally at a velocity u_c at all levels, while the Delft3D model uses the velocity at every particular level. This means that, when net vertical sediment flux profile is similar in both models (settling and turbulent mixing are in the same order of magnitude in both models at every level), the horizontal concentration gradient will be larger for the Lagrangian 1DV model at the levels where $u > u_c$.

Based on the results and analysis of the experiments of Set 2, a hypothesis was elaborated about the expected difference in u_c for a turbidity current. The hypothesis was tested in Experiments Set 3 and Set 4, based on the experiments with turbidity currents by Parker et al. (1987) and van Kessel and Kranenburg (1996).

In the case of Experiments Set 3, based on Run 13 of Parker et al. (1987), u_c was 16% lower (on average) along the analyzed reach in the Lagrangian 1DV model, for a model without deposition. Both the Lagrangian 1DV model and the Delft3D model presented a similar trend in the variation of u_c along the channel: a significant decrease (deceleration of the sediment mass) in the first meters from the source to finally reach a relatively constant value downstream from x=10 m.

The hypothesis from Experiments Set 2 was tested, in order to find an explanation for the difference in u_c. However, the hypothesis could not explain the observed results. A reason for this could be that

in Experiments Set 3, different from Set 2, the difference in the baroclinic pressure gradient between the models was high enough to produce considerable differences in velocity between the models.

An explanation of the differences between u_c was searched by analysing the variation of the sediment load in the Delft3D model. The deceleration of the sediment mass in the Delft3D model (decrease in u_c) was related to an increase in sediment load. While u_c decreased, the sediment load increased significantly. The concentration measurements from Parker et al. (1987) also suggest an increase in sediment load.

A possible explanation for the observed variation of the sediment load both in the Delft3D model and the measurements by Parker et al. (1987) could be that the initial deceleration would cause a reduction in the mass flux. However, to be able to reach a constant mass flux when flow becomes stationary, the concentration over the water column increases, therefore increasing the sediment load. Larger concentration generated a larger baroclinic pressure gradient in the Delft3D model. The difference in the baroclinic pressure gradient between the Delft3D model and the Lagrangian 1DV model was considerable and produced higher velocities in the Delft3D model, which yielded a higher value of u_c.

Experiments Set 4, based on Run 2 of van Kessel and Kranenburg (1996), showed the opposite results compared to Set 3: a higher u_c value for the Lagrangian 1DV model. Averaged over the distance (along 40 m), u_c was 18% higher for Experiment ST-C (no deposition).

Also opposite to the results of Experiments Set 3, there was acceleration of the sediment mass in both models at the first meters from the source. The acceleration of the sediment mass in the Delft3D model was clearly related to a decrease in sediment load. The measured concentration profiles also suggest a decrease of the sediment load.

Following the same reasoning as for Experiments Set 3, a possible explanation for the observed variation of the sediment load both in the Delft3D model could be that the initial acceleration would cause an increase in the velocity and in the mass flux. However, to be able to reach a constant mass flux when flow becomes stationary, the concentration over the water column should decrease, therefore decreasing the sediment load. Therefore, lower concentration in the Delft3D model generated a smaller baroclinic pressure gradient. The difference in the baroclinic pressure gradient between the models was considerable and produced lower velocities in the Delft3D model, which yielded a lower value of u_c.

The addition of the deposition process (Experiment STD-C of Experiments Set 3 and Set 4) did not affect considerably the differences in u_c between the models. The variation of the sediment load in Experiments Set 3 indicated that the sediment mass was transported further in the Delft3D model. At the downstream end of the modelled reach, the Delft3D model still transported 60% of the initial sediment load, while the Lagrangian 1DV model transported 26%.

Experiment STD-C of Experiments Set 4 included the deposition process. However, the results for u_c were practically the same as in Experiment ST-C because the deposition rate was very small.

Which implications do these differences have when the model parameters are in the range of WID application?

Regarding the initial concentration profile (Experiments Set 2), the linear profile provided a shorter adaptation length to uniform flow than the block-shaped profile. It also resulted in less difference in u_c between the Lagrangian 1DV model and the Delft3D model. This suggests that it is a better choice than the block-shaped profile. However, the result should be carefully analyzed. The eddy diffusivity for the case of the linear concentration profile matched between the Lagrangian 1DV model and the Delft3D model from the beginning. On the other hand, for the block-shaped profile, the eddy diffusivity presented important differences close to the source.

In order to investigate if the travelling distance of the turbidity current was underestimated or overestimated by the Lagrangian 1DV model, u_c was calculated for a typical case of WID, considering deposition. The trend of variation of u_c for the typical case was similar to the case of Experiments Set

3, based on Parker et al. (1987), with a deceleration of the sediment mass from the beginning. The results of the experiment based on Parker et al. (1987) indicate that u_c was higher for the 2DV approach and that the turbidity current travelled a longer distance than the one estimated with the Lagrangian 1DV model. In analogy, the same result may occur for the typical case for WID.

If the calculation of the travelling distance is for a case in which the sediment should be transported to a disposal area, the estimation may be conservative (the actual travelling distance may be longer than the required distance). If the travelling distance is restricted for environmental reasons, for example, the calculation may be unsafe (sediment could reach a longer distance than estimated, affecting the sensitive area).

To confirm the interpretation and obtain the exact difference in u_c and the distribution of the sediment load, numerical modelling is required. The same approach in Chapter 4 can be used to compare the results of the models.

6.2 Recommendations

6.2.1 Physical processes

It is recommended to study the magnitude of lateral spreading of a turbidity current with a high concentration on mild slopes. According to Choi and Garcia (2001), a limitation of these experiments is that they require large facilities especially when turbulent flow needs to be developed. The analysis of field data from previous WID applications could be an option to understand this process. Especially for WID-induced turbidity currents, it is interesting to observe if the trench that the dredger excavates generates certain confinement of the current. More knowledge about lateral spreading may be useful to decide if the magnitude of the baroclinic term in the longitudinal direction (main direction of the movement of the turbidity current) should be adjusted.

6.2.2 Initial profiles

Laboratory research can help to characterize better the transition zone between jetting and the beginning of what is considered the turbidity current. First, it can be done qualitatively to gain insight into the process and, later, quantitively when the parameters that define the process are better known. The objective would be to understand better the processes in this transition and, hopefully, to define characteristic shapes of the initial velocity, concentration, and turbulent kinetic energy profiles. The length of this transition zone should also be studied.

6.2.3 Numerical modelling

The conclusions about the travelling distance for the case with typical WID parameter settings should be confirmed with a numerical experiment, comparing the results Lagrangian 1DV approach and a 2DV calculation in Delft3D for typical WID cases.

The methodology of Experiments Set 3 and Set 4 seems convenient for the numerical experiments, starting with ST-C models with the parameters of Table 5-4 and then adding the deposition process (STD-C). If sediment is non-cohesive, a third type of model including erosion can be analyzed (erosion of non-cohesive sediment was not studied in this report).

A similar analysis could be useful to determine the difference between the models in the increase in suspended sediment concentration:

- Compare the results for u_c of the Lagrangian 1DV model and the Delft3D model.
- Relate the variation of u_c (deceleration or acceleration) with the variation of the turbidity source term in both models

- Run the Lagrangian 1DV model for other specific cases and conclude if the calculation is conservative or unsafe, based on the behavior of u_c

6.2.4 Validation with field data

It is recommended to validate the models (Delft3D model and Lagrangian 1DV model) with field data. The following aspects can be studied.

Sedimentation footprint

For this purpose, it is recommended to measure the bathymetry of the dredged area and the expected storage area before and after every dredging track and at the end of the dredging works. Flow velocity should also be measured, preferably with an ADCP device (direct measurement).

Turbidity increase

The turbidity increase can be measured with a monitoring vessel with an ADCP device, navigating behind the dredger along the dredged track.

Turbidity current concentration profiles

Concentrations can be measured from the monitoring vessel. However, if the turbidity current is too dense, bed tracking can be interrupted or fail. Then, it is recommended to complement the measurements from the vessel with measurements from bottom-mounted ADCPs.

7 Bibliography

Becker, J. (2015). Estimating source terms for far field dredge plume modelling. *Journal of Environmental Management, 149*, 282-293.

Bonnecaze, R. (1993). Particle-driven density currents. *Journal of Fluid Mechanics*, 339-369.

Bray, R. (2008). *Environmental aspects of dredging.* Leiden: Taylor & Francis/Balkema.

Choi, S., & Garcia, M. (2001). Spreading of gravity plumes on an incline. *Coastal Engineering Journal, 43*(4), 221-237.

Deltares. (2008). *Validation Document Delft3D-FLOW.* Delft.

Deltares. (2019). *Development of a numerical rapid assessment tool to simulate fate and environmental impact of fluidized sediment layers.* Delft: Deltares.

Dorrell, R., & Hogg, A. (2012). Length and Time Scales of Response of Sediment Suspensions to Changing Flow Conditions. *ASCE*, 430-439.

FAO. (2018). *Chapter 5 - Sediment transport*. Retrieved from http://www.fao.org/docrep/T0848E/t0848e-10.htm

Garcia, M. (1994). Depositional Turbidity Currents Laden with Poorly Sorted Sediment. *Journal of Hydraulic Engineering, 120*(11), 1240-1263.

GEODE. (2015). *Water Injection Dredging Guidance Document.* GEODE.

HAM-VOW. (1994). *Evaluatierapport Proef Waterinjectiebaggeren Haringvliet.* Utrecht: Rijkswaterstaat.

Hanssen. (2016). *Towards improving predictions of non-Newtonian settling slurries with Delft3D: theoretical development and validation in 1DV.* Delft: TU Delft.

Kirichek, A. e. (2018, June). *Sediment Management in the Port of Rotterdam.* Retrieved from www.mudnet.eu: https://www.mudnet.eu/test4.html

Kortmaan, H. (1994). *Waterinjectie baggeren: een vernieuwe modellering.* Delft: TU Delft.

Kranenburg, W. (2013). *Modeling sheet-flow sand transport under progressive waves.* Enschede: Gildeprint Drukkerijen.

Kranendonk, W. (2019). Conditions for the application of WID. (L. Alfaro, Interviewer)

Longo et al. (2018). Gravity currents produced by lock-release: Theory and experiments concerning the effect of a free top in non-Boussinesq systems. *Advances in water Resources*, 456-471.

Mastbergen, D. (1995). *Demostratieproeven WIB Waterinjectie Baggeren.* Delft: WL.

Middleton, G. (1993). Sediment Deposition from Turbidity Currents. *Annual Review of Earth and Planetary Sciences*, 89-114.

Oberkampf, W. (2002). Error and uncertainty in modeling and simulation. *Reliability Engineering and System Safety*, 333-357.

Parker, G. (1987). Experiments on turbidity currents over an erodible bed. *Journal of Hydraulic Research*, 123-147.

Partheniades, E. (1965, January). Erosion and deposition of cohesive soils. *Journal of Hydraulics Division, ASCE, 91*, 105-139.

PIANC. (2013). *Report 120-2013: Injection Dredging.* Brussels: PIANC MarCom.

Pietrzak, J. (2016). *An Introduction to Stratified Flows for Civil and Offshore Engineers.* Delft: TU Delft.

Rapp, B. (2017). *Microfluidics: Modelling, Mechanics and Mathematics.* Springer.

Rijkswaterstaat. (1986). *Note: GWIO-86.506: Stroom-, troebelheids- en materiaaltransportmetingen ten behoeve van een nieuwe baggermethode in de Veerhaven Kruiningen en Zij- en Buitenhaven Hansweert.* Middelburg: Rijkswaterstaat.

Siteur. (2012). *Sedimentation-velocity in jet induced flow.* Delft: TU Delft.

Sloff. (1994). *Modelling Turbidity Currents in Reservoirs.* Delft: TU Delft.

Swart, R. (2015). *Autonomous dredging of mud.* Delft: TU Delft.

Uittenbogard, R., & Winterwerp, J. (1997). *Sediment transport and fluid mud flow.* Delft: Delft Hydraulics.

Ungarish, M. (2009). *An Introduction to Gravity Currents and Intrusions.* Israel: CRC Press.

USACE. (1987). *Confined disposal of dredged material.* Washington: USACE.

USACE. (1993). *Water Injection Dredging Demonstration on the Upper Mississippi River.* Mississippi: US Army Engineer Waterways Experiment Station.

USACE. (2017). *Water Injection Dredging.* Retrieved from USACE Digital Library: https://usace.contentdm.oclc.org/digital/collection/p266001coll1/id/4291/

Van der Schrieck, G. (2015). *Dredging Technology - Lecture notes.* Delft: TU Delft.

Van Eekelen, E. (2007). *Experimental research on dynamic dredge overflow plumes.* Delft: TU Delft.

Van Kessel , T., & Kranenburg, C. (1996). Gravity Current of Fluid Mud on Sloping Bed. *Journal of Hydraulic Engineering*, 710-717.

Van Kessel, T. (1997). *Generation and transport of subaqueous fluid mud layers.* Delft: TU Delft.

Van Rijn, L. (1994). *Principles of Sediment Transport in Rivers, Estuaries and Coastal Seas.* Amsterdam: Aqua Publications.

Van Rijn, L. (2017). *Water Injection Dredging.* Retrieved from https://www.leovanrijn-sediment.com/papers/Waterinjectiondredging.pdf

Verweij, J. (1997). *Waterinjectiebaggeren: modellering van afstroming.* Delft: TU Delft.

Wilson, D. (2007). Water Injection Dredging in U.S. Waterways: History and Expectations. *WODCON XVIII*, (pp. 397-412). Florida.

Winterwerp, J. (2002). Far-field impact of water injection dredging in the Crouch. *Water & Maritime Engineering*(4), pp. 285-296.

Winterwerp, J. (2019, August 9). Transformation from Eulerian to Lagrangian coordinates. (L. Alfaro, Interviewer)

Winterwerp, J., & Van Kesteren, W. (2004). *Introduction to the Physics of Cohesive Sediment in the Marine Environment.* Amsterdam: Elsevier.

Appendices

Appendix A: Derivation of the equations of the 2DV approach

A.1. Mass conservation equation

The 3D mass conservation equation for an infinitesimal control volume in its general form (Navier-Stokes) reads as follows:

$$\frac{\partial \rho}{\partial t} + \frac{\partial(\rho_b u)}{\partial x} + \frac{\partial(\rho_b v)}{\partial y} + \frac{\partial(\rho_b w)}{\partial z} = 0 \tag{A.1}$$

Where ρ_b is the density of the fluid. Applying the product rule, this can be expressed as:

$$\frac{\partial \rho_b}{\partial t} + u\frac{\partial \rho_b}{\partial x} + v\frac{\partial \rho_b}{\partial y} + w\frac{\partial \rho_b}{\partial z} + \rho_b\frac{\partial u}{\partial x} + \rho_b\frac{\partial v}{\partial y} + \rho_b\frac{\partial w}{\partial z} = 0$$

The first four terms correspond to the material time derivative of the density, which for an ***incompressible fluid*** equals zero. Then:

$$\frac{\partial u}{\partial x} + \frac{\partial v}{\partial y} + \frac{\partial w}{\partial z} = 0$$

Skipping the terms in the y-direction for the 2DV approach:

$$\frac{\partial u}{\partial x} + \frac{\partial w}{\partial z} = 0 \tag{A.2}$$

A.2. Momentum Equation

Navier-Stokes Momentum Equation

From Newton's second law, the rate of change of momentum of an element equals the applied force. Being $\boldsymbol{V}$ the velocity vector, this can be expressed as:

$$\boldsymbol{F} = dx\,dy\,dz\,\frac{D(\rho_b \boldsymbol{V})}{Dt}$$

$$\boldsymbol{F} = dx\,dy\,dz\left[\frac{\partial}{\partial t}(\rho_b \boldsymbol{V}) + \frac{\partial}{\partial x}(\rho_b \boldsymbol{V})\cdot\frac{dx}{dt} + \frac{\partial}{\partial y}(\rho_b \boldsymbol{V})\cdot\frac{dy}{dt} + \frac{\partial}{\partial z}(\rho_b \boldsymbol{V})\cdot\frac{dz}{dt}\right]$$

$$\boldsymbol{F} = dx\,dy\,dz\left[\frac{\partial}{\partial t}(\rho_b \boldsymbol{V}) + u\frac{\partial}{\partial x}(\rho_b \boldsymbol{V}) + v\frac{\partial}{\partial y}(\rho_b \boldsymbol{V})\cdot\frac{dy}{dt} + w\frac{\partial}{\partial z}(\rho_b \boldsymbol{V})\right]$$

The term in brackets can be written as:

$$\boldsymbol{V}\left[\frac{\partial \rho_b}{\partial t} + u\frac{\partial \rho_b}{\partial x} + v\frac{\partial \rho_b}{\partial y} + w\frac{\partial \rho_b}{\partial z}\right] + \rho_b\left(\frac{\partial \boldsymbol{V}}{\partial t} + u\frac{\partial \boldsymbol{V}}{\partial x} + v\frac{\partial \boldsymbol{V}}{\partial y} + w\frac{\partial \boldsymbol{V}}{\partial z}\right)$$

The term in brackets corresponds to the mass conservation equation (equals zero). Then:

$$\boldsymbol{F} = \rho_b\left(\frac{\partial \boldsymbol{V}}{\partial t} + u\frac{\partial \boldsymbol{V}}{\partial x} + v\frac{\partial \boldsymbol{V}}{\partial y} + w\frac{\partial \boldsymbol{V}}{\partial z}\right)dx\,dy\,dz \tag{A.3}$$

There are two types of applied forces: body forces and surface forces. Body forces result from external fields such as gravity. Surface forces are produced by stresses on the sides of the element, which in a fluid are due to pressure p and viscous (shear) stresses τ_{ij}, which arise from velocity gradients. For every direction and adding the body force in z-direction ($= -\rho_b g\ dx\ dy\ dz$):

$$\boldsymbol{F_x} = \left(-\frac{\partial p}{\partial x} + \frac{\partial \tau_{xx}}{\partial x} + \frac{\partial \tau_{yx}}{\partial y} + \frac{\partial \tau_{zx}}{\partial z}\right) dx\ dy\ dz \tag{A.4}$$

$$\boldsymbol{F_y} = \left(-\frac{\partial p}{\partial y} + \frac{\partial \tau_{xy}}{\partial x} + \frac{\partial \tau_{yy}}{\partial y} + \frac{\partial \tau_{zy}}{\partial z}\right) dx\ dy\ dz$$

$$\boldsymbol{F_z} = \left(\frac{\partial p}{\partial z} + \frac{\partial \tau_{xz}}{\partial x} + \frac{\partial \tau_{yz}}{\partial y} + \frac{\partial \tau_{zz}}{\partial z} - \rho_b g\right) dx\ dy\ dz$$

Then, combining (A.3) and (A.4) the differential momentum equation is:

$$-\frac{\partial p}{\partial x} + \frac{\partial \tau_{xx}}{\partial x} + \frac{\partial \tau_{yx}}{\partial y} + \frac{\partial \tau_{zx}}{\partial z} = \rho_b \left(\frac{\partial u}{\partial t} + u\frac{\partial u}{\partial x} + v\frac{\partial u}{\partial y} + w\frac{\partial u}{\partial z}\right) \tag{A.5}$$

$$-\frac{\partial p}{\partial y} + \frac{\partial \tau_{xy}}{\partial x} + \frac{\partial \tau_{yy}}{\partial y} + \frac{\partial \tau_{zy}}{\partial z} = \rho_b \left(\frac{\partial v}{\partial t} + u\frac{\partial v}{\partial x} + v\frac{\partial v}{\partial y} + w\frac{\partial v}{\partial z}\right)$$

$$-\frac{\partial p}{\partial z} + \frac{\partial \tau_{xz}}{\partial x} + \frac{\partial \tau_{yz}}{\partial y} + \frac{\partial \tau_{zz}}{\partial z} - \rho g = \rho_b \left(\frac{\partial w}{\partial t} + u\frac{\partial w}{\partial x} + v\frac{\partial w}{\partial y} + w\frac{\partial w}{\partial z}\right)$$

Momentum equations for incompressible fluid (2DV case)

Skipping the terms in the y-direction:

$$-\frac{\partial p}{\partial x} + \frac{\partial \tau_{xx}}{\partial x} + \frac{\partial \tau_{zx}}{\partial z} = \rho_b \left(\frac{\partial u}{\partial t} + u\frac{\partial u}{\partial x} + w\frac{\partial u}{\partial z}\right) \tag{A.6}$$

$$-\frac{\partial p}{\partial z} + \frac{\partial \tau_{xz}}{\partial x} + \frac{\partial \tau_{zz}}{\partial z} - \rho g = \rho_b \left(\frac{\partial w}{\partial t} + u\frac{\partial w}{\partial x} + w\frac{\partial w}{\partial z}\right)$$

Momentum equations for incompressible and Newtonian fluid (2DV case)

For a **Newtonian fluid**, viscous stresses are proportional to the strain rate and a coefficient of viscosity. The following relations can be derived geometrically for infinitesimal deformations:

$$\tau_{xx} = 2\mu\frac{\partial u}{\partial x};\ \tau_{zz} = 2\mu\frac{\partial w}{\partial z};$$

$$\tau_{xz} = \tau_{zx} = \mu\left(\frac{\partial u}{\partial z} + \frac{\partial w}{\partial x}\right)$$

Substitution in the momentum equation (A.6) in the x-direction yields:

$$-\frac{\partial p}{\partial x} + 2\frac{\partial}{\partial x}\left(\mu\frac{\partial u}{\partial x}\right) + \frac{\partial}{\partial z}\left(\mu\frac{\partial u}{\partial z}\right) + \frac{\partial}{\partial z}\left(\mu\frac{\partial w}{\partial x}\right) = \rho_b \left(\frac{\partial u}{\partial t} + u\frac{\partial u}{\partial x} + w\frac{\partial u}{\partial z}\right)$$

Rearranging:

$$-\frac{\partial p}{\partial x} + \frac{\partial}{\partial x}\left(\mu\frac{\partial u}{\partial x}\right) + \frac{\partial}{\partial x}\left(\mu\frac{\partial u}{\partial x}\right) + \frac{\partial}{\partial z}\left(\mu\frac{\partial u}{\partial z}\right) + \frac{\partial}{\partial z}\left(\mu\frac{\partial w}{\partial x}\right) = \rho_b \left(\frac{\partial u}{\partial t} + u\frac{\partial u}{\partial x} + w\frac{\partial u}{\partial z}\right)$$

$$-\frac{\partial p}{\partial x} + \frac{\partial}{\partial x}\left(\mu\frac{\partial u}{\partial x}\right) + \frac{\partial}{\partial x}\left[\mu\left(\frac{\partial u}{\partial x} + \frac{\partial w}{\partial z}\right)\right] + \frac{\partial}{\partial z}\left(\mu\frac{\partial u}{\partial z}\right) = \rho_b \left(\frac{\partial u}{\partial t} + u\frac{\partial u}{\partial x} + w\frac{\partial u}{\partial z}\right)$$

The terms in square brackets equal zero due to continuity. Then:

$$-\frac{\partial p}{\partial x}+\frac{\partial}{\partial x}\left(\mu\frac{\partial u}{\partial x}\right)+\frac{\partial}{\partial z}\left(\mu\frac{\partial u}{\partial z}\right)=\rho_b\left(\frac{\partial u}{\partial t}+u\frac{\partial u}{\partial x}+w\frac{\partial u}{\partial z}\right)$$

The momentum equation in z-direction (following the same procedure) yields:

$$-\frac{\partial p}{\partial z}+\frac{\partial}{\partial x}\left(\mu\frac{\partial w}{\partial x}\right)+\frac{\partial}{\partial z}\left(\mu\frac{\partial w}{\partial z}\right)-\rho_b g=\rho_b\left(\frac{\partial w}{\partial t}+u\frac{\partial w}{\partial x}+w\frac{\partial w}{\partial z}\right)$$

Applying the **Boussinesq approximation** (density variation taken into account only for body forces), then:

$$-\frac{\partial p}{\partial x}+\frac{\partial}{\partial x}\left(\mu\frac{\partial u}{\partial x}\right)+\frac{\partial}{\partial z}\left(\mu\frac{\partial u}{\partial z}\right)=\rho_w\left(\frac{\partial u}{\partial t}+u\frac{\partial u}{\partial x}+w\frac{\partial u}{\partial z}\right) \quad \text{(A.7)}$$

$$-\frac{\partial p}{\partial z}+\frac{\partial}{\partial x}\left(\mu\frac{\partial w}{\partial x}\right)+\frac{\partial}{\partial z}\left(\mu\frac{\partial w}{\partial z}\right)-\rho_b g=\rho_w\left(\frac{\partial w}{\partial t}+u\frac{\partial w}{\partial x}+w\frac{\partial w}{\partial z}\right)$$

Momentum equations for incompressible and Newtonian fluid in shallow waters (2DV case)

For external flow, the depth is assumed to be much smaller than the horizontal length scale so that the shallow water assumption is valid.

For internal flow (stratification), according to Bonnecaze et al. (1993), soon after release, the current has a length much greater than its depth and it is valid to apply the shallow-water approximation. This is not valid for the front of a turbidity current. However, the model is focused on the stationary state of the body of the turbidity current.

In this context, the vertical accelerations are small compared to the gravitational acceleration and are not taken into account. For this condition, the momentum equation in the vertical direction is reduced to:

$$\frac{\partial p}{\partial z}=-\rho_b g \Rightarrow p=p_{atm}+g\int_z^{\xi}\rho_b\,dz \quad \text{(A.8)}$$

This result is used later for the definition of the horizontal pressure gradient.

RANS momentum equations for incompressible and Newtonian fluid (2DV case)

Velocity, pressure and density can be decomposed into a mean and a fluctuating part. For example, the horizontal velocity can be expressed as:

$$u=\bar{u}+u'$$

Where $\bar{u}$ is the time-averaged horizontal velocity (related to the large scale flow) and u' refers to the fluctuation (small scale turbulence). Applying the Reynolds decomposition to the momentum equation in the x-direction gives:

$$-\frac{1}{\rho_w}\frac{\partial(\bar{p}+p')}{\partial x}+\nu\left(\frac{\partial^2(\bar{u}+u')}{\partial x^2}+\frac{\partial^2(\bar{u}+u')}{\partial z^2}\right)=\frac{\partial(\bar{u}+u')}{\partial t}+(\bar{u}+u')\frac{\partial(\bar{u}+u')}{\partial x}+(\bar{w}+w')\frac{\partial(\bar{u}+u')}{\partial z}$$

Time-averaging every term (density and viscosity fluctuations are omitted):

1. $\dfrac{1}{\rho_w}\overline{\dfrac{\partial(\bar{p}+p')}{\partial x}}=\dfrac{\partial\bar{p}}{\partial x}+\dfrac{\partial\overline{p'}}{\partial x}=\dfrac{\partial\bar{p}}{\partial x}$

2. $\overline{\left(\dfrac{\partial^2(\bar{u}+u')}{\partial x^2}+\dfrac{\partial^2(\bar{u}+u')}{\partial z^2}\right)}=\dfrac{\partial^2\bar{u}}{\partial x^2}+\dfrac{\partial^2\overline{u'}}{\partial x^2}+\dfrac{\partial^2\bar{u}}{\partial z^2}+\dfrac{\partial^2\overline{u'}}{\partial z^2}=\dfrac{\partial^2\bar{u}}{\partial x^2}+\dfrac{\partial^2\bar{u}}{\partial z^2}$

3. $\overline{\frac{\partial(\bar{u}+u')}{\partial t}} = \frac{\partial \bar{u}}{\partial t} + \frac{\partial \overline{u'}}{\partial t} = \frac{\partial \bar{u}}{\partial t}$

4. $\overline{(\bar{u}+u')\frac{\partial(\bar{u}+u')}{\partial x}} = \overline{\bar{u}\frac{\partial \bar{u}}{\partial x}} + \overline{\bar{u}\frac{\partial u'}{\partial x}} + \overline{u'\frac{\partial \bar{u}}{\partial x}} + \overline{u'\frac{\partial u'}{\partial x}} = \bar{u}\frac{\partial \bar{u}}{\partial x} + \overline{u'\frac{\partial u'}{\partial x}}$

5. $\overline{(\bar{w}+w')\frac{\partial(\bar{u}+u')}{\partial z}} = \bar{w}\frac{\partial \bar{u}}{\partial z} + \overline{w'\frac{\partial u'}{\partial z}}$

Replacing the terms with the resulting expressions:

$$-\frac{1}{\rho_w}\frac{\partial \bar{p}}{\partial x} + \nu\left(\frac{\partial^2 \bar{u}}{\partial x^2} + \frac{\partial^2 \bar{u}}{\partial z^2}\right) = \frac{\partial \bar{u}}{\partial t} + \bar{u}\frac{\partial \bar{u}}{\partial x} + \bar{w}\frac{\partial \bar{u}}{\partial z} + \overline{u'\frac{\partial u'}{\partial x}} + \overline{w'\frac{\partial u'}{\partial z}}$$

Adding the continuity equation for fluctuations (which equals zero):

$$-\frac{1}{\rho_w}\frac{\partial \bar{p}}{\partial x} + \nu\left(\frac{\partial^2 \bar{u}}{\partial x^2} + \frac{\partial^2 \bar{u}}{\partial z^2}\right) = \frac{\partial \bar{u}}{\partial t} + \bar{u}\frac{\partial \bar{u}}{\partial x} + \bar{w}\frac{\partial \bar{u}}{\partial z} + \overline{u'\frac{\partial u'}{\partial x}} + \overline{w'\frac{\partial u'}{\partial z}} + \overline{u'\left(\frac{\partial u'}{\partial x} + \frac{\partial w'}{\partial z}\right)}$$

The last four terms of the RHS can be rewritten as:

$$\overline{u'\frac{\partial u'}{\partial x}} + \overline{w'\frac{\partial u'}{\partial z}} + \overline{u'\frac{\partial u'}{\partial x}} + \overline{u'\frac{\partial w'}{\partial z}} = \overline{\frac{\partial u'u'}{\partial x}} + \overline{\frac{\partial w'u'}{\partial z}}$$

Then, the Reynolds averaged momentum equation for x-direction becomes:

$$-\frac{1}{\rho_w}\frac{\partial \bar{p}}{\partial x} + \nu\left(\frac{\partial^2 \bar{u}}{\partial x^2} + \frac{\partial^2 \bar{u}}{\partial z^2}\right) = \frac{\partial \bar{u}}{\partial t} + \bar{u}\frac{\partial \bar{u}}{\partial x} + \bar{w}\frac{\partial \bar{u}}{\partial z} + \overline{\frac{\partial u'u'}{\partial x}} + \overline{\frac{\partial w'u'}{\partial z}}$$

Even knowing that the last two terms in the RHS are convective terms, they are usually modelled as viscous terms. Rewriting the previous equation and dropping the time-averaged notation for simplicity:

$$-\frac{1}{\rho_w}\frac{\partial p}{\partial x} + \frac{\partial}{\partial x}\left(\nu\frac{\partial u}{\partial x}\right) + \frac{\partial}{\partial z}\left(\nu\frac{\partial u}{\partial z}\right) = \frac{\partial u}{\partial t} + u\frac{\partial u}{\partial x} + w\frac{\partial u}{\partial z} + \frac{1}{\rho_w}\frac{\partial}{\partial x}(\rho_w u'u') + \frac{1}{\rho_w}\frac{\partial}{\partial z}(\rho_w w'u')$$

The terms $-\rho u'u'$ and $-\rho u'w'$ are called Reynolds turbulent stresses (they are interpreted as shear stresses):

$$\tau''_{xx} = -\rho_0 u'u'$$
$$\tau''_{xz} = -\rho_0 u'w'$$

In a turbulence model, analogously to the case of molecular viscosity, these stresses can be expressed as:

$$\tau''_{xx} = 2\rho_w \upsilon_h \frac{\partial u}{\partial x};\ \tau''_{zz} = 2\rho_w \upsilon_T \frac{\partial w}{\partial z};$$
$$\tau''_{xz} = \tau''_{zx} = \rho_w \upsilon_T \frac{\partial u}{\partial z} + \rho_w \upsilon_h \frac{\partial w}{\partial x}$$

Where υ_h and υ_T are the eddy viscosity coefficients in the horizontal and vertical direction, respectively. Proceeding in the same way as for molecular viscosity, the momentum equation becomes:

$$-\frac{1}{\rho_w}\frac{\partial p}{\partial x} + \frac{\partial}{\partial x}\left(\upsilon\frac{\partial u}{\partial x}\right) + \frac{\partial}{\partial x}\left(\upsilon_h\frac{\partial u}{\partial x}\right) + \frac{\partial}{\partial z}\left(\upsilon\frac{\partial u}{\partial z}\right) + \frac{\partial}{\partial z}\left(\upsilon_T\frac{\partial u}{\partial z}\right) = \frac{\partial u}{\partial t} + u\frac{\partial u}{\partial x} + w\frac{\partial u}{\partial z} \qquad \text{(A.9)}$$

Using the Leibniz rule, the horizontal pressure gradient can be expressed as:

$$\frac{\partial p}{\partial x} = \frac{\partial p_{atm}}{\partial x} + \rho_w(x) g \frac{\partial \xi}{\partial x} + g\int_z^{\xi} \frac{\partial \rho_b(x,z)}{\partial x}\, dz$$

The first term on the RHS can be neglected (atmospheric pressure variation is not expected for the spatial scale of WID operations). The second term on the RHS corresponds to the barotropic forcing and the third term to the baroclinic forcing. It is assumed that the horizontal density gradient in the case of a turbidity current is caused by sediment concentration differences (no salinity or temperature gradients are considered). Including the expression for the horizontal pressure gradient, the momentum equation in the horizontal direction can be expressed as:

$$-g\frac{\partial \xi}{\partial x}-\frac{g}{\rho_w}\int_z^{\xi}\frac{\partial \rho_b}{\partial x}\,dz+\frac{\partial}{\partial x}\left(\upsilon\frac{\partial u}{\partial x}\right)+\frac{\partial}{\partial x}\left(\upsilon_h\frac{\partial u}{\partial x}\right)+\frac{\partial}{\partial z}\left(\upsilon\frac{\partial u}{\partial z}\right)+\frac{\partial}{\partial z}\left(\upsilon_T\frac{\partial u}{\partial z}\right)=\frac{\partial u}{\partial t}+u\frac{\partial u}{\partial x}+w\frac{\partial u}{\partial z}$$

Considering that the product of the viscosity and the horizontal velocity gradient is small, then:

$$\frac{\partial u}{\partial t}+u\frac{\partial u}{\partial x}+w\frac{\partial u}{\partial z}+g\frac{\partial \zeta}{\partial x}+\frac{g}{\rho_w}\int_z^{\xi}\frac{\partial \rho_b}{\partial x}\,dz=\frac{\partial}{\partial z}\left[(\upsilon+\upsilon_T)\frac{\partial u}{\partial z}\right] \qquad \text{(A.10)}$$

Appendix B: The 1DV Point Model

The following overview of the 1DV Point Model is based on the description of the model by Uittenbogaard and Winterwerp (1997) and Winterwerp (1999). A more detailed description of the model can be found at these references.

Momentum equation

The equation for u (a single horizontal velocity component) reads:

$$\frac{\partial u}{\partial t}+\frac{1}{\rho_b}\frac{\partial p}{\partial x}=\frac{\partial}{\partial z}\left\{(\nu+\nu_T)\frac{\partial u}{\partial z}\right\} \tag{B.1}$$

Equation B.1. applies to uniform flow. The vertical eddy viscosity (ν_T) is obtained from the k-ϵ model. The pressure term is adjusted to maintain a predefined and time dependent depth-averaged velocity:

$$\frac{1}{\rho_b}\frac{\partial p}{\partial x}=\frac{\tau_s-\tau_b}{\rho_b H}-\frac{\bar{u}(t)-U_{ref}(t)}{T_{rel}} \tag{B.2}$$

Where $\bar{u}(t)$ is the computed depth-averaged flow velocity, U_{ref} is the desired depth-averaged velocity, T_{rel} is the relaxation time (usually taken as twice the time step), τ_s is the horizontal component of the bed shear stress exerted on the free water surface and τ_b is the bed shear stress. The bed shear stress depends on the near-bed velocity through a quadratic friction law that satisfies a log-law:

$$\tau_b=\rho_b|u_*|u_*;\ u_*=\frac{\kappa u(z_{bc}+0.5\Delta z_b)}{\ln(1+0.5\Delta z_b/z_{bc})} \tag{B.3}$$

Where: κ is the von Karman constant, z_{bc} is the apparent roughness length and $u(z_{bc}+0.5\Delta z_b)$ is the near-bed velocity, defined at the center of the computational bed layer with thickness Δz_b.

Mass balance for suspended sediment

The advection-diffusion equation for various sediment fractions (i) is written as:

$$\frac{\partial c^{(i)}}{\partial t}-\frac{\partial {w_s}^{(i)}c^{(i)}}{\partial z}=\frac{\partial}{\partial z}\left\{\left({D_s}^{(i)}+{\Gamma_T}^{(i)}\right)\frac{\partial c^{(i)}}{\partial z}\right\}+E^{(i)}-D^{(i)} \tag{B.4}$$

Where $c^{(i)}$ is the sediment mass concentration for fraction (i), D_s is the molecular diffusion coefficient for sediment, w_s is the effective settling velocity of the sediment suspension, w_{s0} is the settling velocity of the individual particle and Γ_T is the eddy diffusivity. For the Lagrangian 1DV model, the molecular diffusion coefficient D_s is neglected. The diffusive and advective fluxes at the bed and the water surface are zero, as boundary conditions. The erosion and deposition mass fluxes are defined as source and sink terms at the bed. The erosion and deposition fluxes follow the Partheniades-Krone (Partheniades, 1965) formulation:

$$E^{(i)}=MS\left(\frac{\tau_b}{\tau_{cr,e}}-1\right);\ D^{(i)}={w_s}^{(i)}{c_b}^{(i)}S\left(1-\frac{\tau_b}{\tau_{cr,d}}\right);\ {c_b}^{(i)}=c^{(i)}(0.5\Delta z_b,t) \tag{B.5}$$

Step function: $S(\theta)=\theta$ if $\theta>0$; $S(\theta)=0$ if $\theta=0$

Appendix C: Equations of the Lagrangian 1DV model

Momentum and advection-diffusion equations

The following derivation of the momentum and advection-diffusion equations of the Lagrangian 1DV model was provided by Winterwerp (personal communication, August 9, 2019).

Following the transformation rules and the definition of the concentration-weighted velocity of Equations (3.8) and (3.9), the momentum equation of the 1DV Point Model can be expressed in Lagrangian coordinates as:

$$u_c \frac{\partial u}{\partial \xi} + \frac{1}{\rho_b}\frac{\partial p}{\partial \xi} = \frac{\partial}{\partial z}\left\{(\nu + \nu_T)\frac{\partial u}{\partial z}\right\} \tag{C.1}$$

This implies that stationary conditions in the Lagrangian reference frame are equivalent to uniform conditions in the 1DV Point Model (Eulerian).

The longitudinal pressure gradient $\partial p/\partial \xi$ follows from Equation B.4, but now including the vertical velocity w (not present in the 1DV Point Model):

$$\frac{\partial c}{\partial t} - \frac{\partial (w - w_s)c}{\partial z} = \frac{\partial}{\partial z}\left\{\Gamma_T \frac{\partial c}{\partial z}\right\} \tag{C.2}$$

Assuming that the turbidity current is thin and travels approximately parallel to the bed, with bed slope β, then:

$$tan\,\beta = -w/u_c \tag{C.3}$$

Then, the vertical mass balance can be expressed in Lagrangian coordinates (stationary) as:

$$u_c \frac{\partial c}{\partial \xi} - u_c\, tan\,\beta \frac{\partial c}{\partial z} = \frac{\partial}{\partial z}\left\{w_s c + \Gamma_T \frac{\partial c}{\partial z}\right\} \tag{C.4}$$

Defining $\rho_b = \rho_w + \alpha c$, then $\partial \rho_b/\partial \xi = \alpha\, \partial c/\partial \xi$ and the longitudinal density gradient is expressed as:

$$\frac{\partial \rho_b}{\partial \xi} = \alpha\ tan\,\beta \frac{\partial c}{\partial z} + \frac{\alpha}{u_c}\frac{\partial}{\partial z}\left\{w_s c + \Gamma_T \frac{\partial c}{\partial z}\right\} \tag{C.5}$$

The baroclinic part of the pressure gradient can then be expressed as:

$$\frac{g}{\rho_b}\int_z^\zeta \frac{\partial \rho_b}{\partial \xi}\, dz' = \frac{g}{\rho_b}\int_z^\zeta \left[\alpha\ tan\,\beta \frac{\partial c}{\partial z} + \frac{\alpha}{u_c}\frac{\partial}{\partial z}\left\{w_s c + \Gamma_T \frac{\partial c}{\partial z}\right\}\right] dz' \tag{C.6}$$

Considering the same boundary conditions of the 1DV Point Model (sediment fluxes are zero through the bed and the water surface), then:

$$\frac{g}{\rho_b}\int_z^\zeta \frac{\partial \rho_b}{\partial \xi}\, dz' = -\frac{\alpha\, g\ tan\,\beta\, c}{\rho_b} - \frac{\alpha g}{\rho_b u_c}\frac{\partial}{\partial z}\left\{w_s c + \Gamma_T \frac{\partial c}{\partial z}\right\} \tag{C.7}$$

The barotropic part is the same as in the 1DV Point Model (RHS of Equation B.2.):

$$\frac{\partial \zeta}{\partial \xi} = \frac{\tau_s - \tau_b}{\rho_b H} - \frac{\bar{u}(t) - U_{ref}(t)}{T_{rel}} \tag{C.8}$$

Substituting into the momentum equation (C.1) with the pressure gradient, as the sum of the barotropic and baroclinic parts, yields:

$$u_c \frac{\partial u}{\partial \xi} + \frac{\tau_s - \tau_b}{\rho_b H} + \frac{U_{ref}(t) - \bar{u}(t)}{T_{rel}} - \left[\frac{\alpha\ g\ \ tan\,\beta\ c}{\rho_b} + \frac{\alpha g}{\rho_b u_c}\frac{\partial}{\partial z}\left\{w_s c + \Gamma_T \frac{\partial c}{\partial z}\right\}\right] = \frac{\partial}{\partial z}\left\{(\nu + \nu_T)\frac{\partial u}{\partial z}\right\} \quad \text{(C.9)}$$

Transforming back into the Eulerian reference frame of the 1DV Point Model, the momentum equation is written as:

$$\frac{\partial u}{\partial t} + \frac{\tau_s - \tau_b}{\rho_b H} + \frac{U_{ref}(t) - \bar{u}(t)}{T_{rel}} - \left[\frac{\alpha\ g\ \ tan\,\beta\ c}{\rho_b} + \frac{\alpha g}{\rho_b u_c}\frac{\partial}{\partial z}\left\{w_s c + \Gamma_T \frac{\partial c}{\partial z}\right\}\right] = \frac{\partial}{\partial z}\left\{(\nu + \nu_T)\frac{\partial u}{\partial z}\right\} \quad \text{(C.10)}$$

The advection-diffusion equation (C.2) is now expressed as:

$$\frac{\partial c}{\partial t} - \left[u_c\, tan\,\beta \frac{\partial c}{\partial z}\right] - \frac{\partial w_s c}{\partial z} = \frac{\partial}{\partial z}\left\{\Gamma_c \frac{\partial c}{\partial z}\right\} \quad \text{(C.11)}$$

Processes in the water column and formulations

Hindered settling

The Lagrangian 1DV model uses the formulation of Richardson and Zaki to consider hindered settling:

$$w_s = w_{s,0}(1 - \phi_s)^n \quad \text{(C.12)}$$

The suggested values for n by Deltares (2019) are 4 for mud and 5 for sand. Delft3D-FLOW uses n=5. The volumetric concentration ϕ_s is the ratio between the mass concentration and the gelling concentration c_{gel}.

Erosion and deposition

For mud, the formulations of Partheniades-Krone are used, as in the 1DV Point Model.

For sand, two options are available: “no erosion” and a reference concentration formula as proposed by Zyserman and Fredsoe (1994). The “no erosion” consists of zero erosion and full deposition ($D = w_s c_b$).

The reference concentration formulation of Zyserman and Fredsoe defines a concentration at the lowest cell:

$$c_b = \frac{A(\theta' - 0.045)^n}{1 + \frac{A}{c_m}(\theta' - 0.045)^n} \quad \text{(C.13)}$$

Where c_b is the reference concentration, and A, N, and c_b are fitting parameters with values of 0.331, 1.75 and 0.46, respectively.